

## **ABSTRACT**

BOY, RAMÍZ. Formation of Biofibers and Biofilms from Blends of Polysaccharides and Proteins. (Under the direction of Richard Kotek).

Fibers and films that are sustainable and biodegradable can be engineered from a combination of polysaccharide and protein. In a binary polymeric blend, the compatibility of these polymers is influenced by the characteristics of each polymer in the employed solvent system as well as processing conditions. Therefore, effective solvents are chosen to directly dissolve both components at the optimum conditions.

In the first study, the blends of chitosan and soy protein was cast using acetic and formic acid as solvents to produce films. It was found that blend films from acetic acid gave higher hydrophobicity, better internal blend miscibility, and better tensile properties than blend films from formic acid. The interaction between the two biopolymers was confirmed by chemical and thermal analysis, indicating their compatibility. Moreover, increasing chitosan content increased the tensile strength and the absorptive properties.

In other studies, ethylenediamine and potassium thiocyanate (ED/KSCN), was chosen to directly dissolve cellulose with proteins, including soy protein, collagen, and keratin, at the optimum conditions. This process ensures fast dissolution at 90°C within 2-4 hours with no temperature cycling. In addition, the solvent is nondegrading to the polymers and no stabilizer is necessary. By regulating solution composition of the blends, a variety of novel cellulose - high protein content solutions were converted into mainly fibers as well as films to examine the properties of the resultant polymer compositions.

The chemical and x-ray analysis of cellulose/soy protein blend fibers confirms the formation of the interaction through mainly secondary bonding. Increasing protein content provided slightly higher thermal stability to the fibers. The electron microscopy images of the

fibers showed homogeneous dispersion of the protein without phase separation. The percent crystallinity and the tensile data revealed that the best compatibility occurred with 20% soy protein ratio and the fiber had the same birefringence as the control fiber. Furthermore, blending cellulose with protein imparted faster biodegradation to the fibers.

The chemical and thermal analysis of cellulose/collagen fiber revealed an intermolecular interaction between cellulose and the protein and improved thermal stability, respectively. The electron microscopy images mostly exhibited fibrillar morphology with no visible phase separation, indicating compatibility between the two phases. Furthermore, the fibers containing higher cellulose content showed higher crystallinity, tensile, and birefringence properties of the composite fibers.

Thermal analysis of cellulose/keratin fibers confirmed the substantial blending of the two polymers. The electron microscopy images did not exhibit two phase morphology indicating compatible blends. The X-ray diffraction of blend fibers became more distinct with more protein content due most likely to the enlarging network of intermolecular interaction between the polymer phases. While the modulus and the tenacity diminished, the elongation of the fibers improved with an increasing keratin ratio.

Uniform and strong cellulose/soy protein films were produced using the ED/KSCN solvent system. Gamma irradiation was applied to the film forming solutions to stabilize the molecular network structure of the blend films. The interaction between cellulose and soy protein, exhibited by chemical analysis, was rearranged after exposure to the irradiation. The thermal analysis revealed insignificant changes in the thermal stability. The irradiation up to 10 kGy led to higher elongation at in the resulting film. Moreover, the transparency of the film somewhat decreased. However, the water absorption capacity significantly decreased.

© Copyright 2016 Ramiz Boy

All Rights Reserved

Formation of Biofibers and Biofilms from Blends of Polysaccharides and Proteins

by  
Ramiz Boy

A dissertation submitted to the Graduate Faculty of  
North Carolina State University  
in partial fulfillment of the  
requirements for the degree of  
Doctor of Philosophy

Fiber and Polymer Science

Raleigh, North Carolina

2016

APPROVED BY:

---

Dr. Richard Kotek  
Committee Chair

---

Dr. Samuel M. Hudson

---

Dr. Mohamed Bourham

---

Dr. Thomas Theyson

## **DEDICATION**

*To my beloved wife Özge, my precious daughter, Mira İdil, and my wonderful parents*

*Mürşidiye and Yüksel.*

## **BIOGRAPHY**

Ramiz Boy was born on October 11, 1984 in Aydın, Turkey. He graduated from Uludağ University, Turkey, department of Textile Engineering with a minor degree in Mechanical Engineering in 2007. After graduation, he started working as a process engineer at the indigo dying department of ISKO Denim where he was awarded with a scholarship from Republic of Turkey Ministry of National Education supporting his graduate study in the U.S.A. He attended English Language Institute at University of Delaware. In 2011, he received his Master degree in Polymer and Fiber Engineering at Auburn University where he did research on the development of polysaccharide based materials. He continued his research at North Carolina State University to pursue a Ph.D. degree in Fiber and Polymer Science. He has been doing internship at Oak Ridge National Laboratory since February 2015. Ramiz has been married to Özge and they have an adorable daughter, Mira.

## ACKNOWLEDGMENTS

First, I would like to express my gratitude to my advisor, Prof. Richard Kotek, for all his guidance and patience during my Ph.D. research. His supervision led me to improve myself in different research areas besides my dissertation topic. Without his support, my academic career would not have come to this point.

I am grateful to my dissertation committee including Prof Samuel Hudson, Prof. Mohamed Bourham, and Prof. Thomas Theyson. I would like to thank Dr. Hudson for his technical support and his time to explain the experimental procedure. His insight and knowledge helped me to overcome research obstacles. Dr. Bourham generously provided assistance for the irradiation study. Dr. Theyson also kindly contributed to my research on soy protein studies. I am indebted to each of them to complete this thesis.

I would like to give a special thanks to Dr. Amit Naskar for allowing me to use test instruments. He has been encouraging and supportive during my internship.

I would like to acknowledge the financial support from Republic of Turkey Ministry of Education.

I appreciate the help from laboratory managers; Tri Vu, Judy D. Elson, William Barnes, and Birgit Anderson.

I would like to also thank my colleagues and friends; Ganesh Narayanan, Cagatay Karan, Halil I. Akyildiz, Ozkan Yildiz, Murat Yokus for supporting me during my PhD work.

Last but not the least, I am most thankful to my wife for sharing the endeavor to earn my academic career. Our daughter has been a perfect gift to my simple life. In addition, I am much obligated to my parents for their selfless and constant support.

## TABLE OF CONTENTS

LIST OF TABLES .....	xi
LIST OF FIGURES .....	xii
<b>Chapter 1 Formation of Cellulose and Protein Blend Biofibers.....</b>	<b>1</b>
1.1 Introduction .....	1
1.1.1 Cellulose.....	2
1.1.2 Proteins.....	7
1.2 Viscose Process .....	12
1.3 Cuprammonium Process .....	21
1.4 Lithium Chloride and <i>N,N</i> -Dimethylacetamide .....	24
1.5 <i>N</i> -Methylmorpholine <i>N</i> -Oxide and Water.....	30
1.6 Aqueous Alkali and Aqueous Alkali/Urea.....	35
1.7 Ionic Liquids .....	42
1.8 Cellulose Derivatives/Protein Blend Fibers .....	46
1.9 Concluding Remarks .....	50
1.10 References .....	50
<b>Chapter 2 Properties of Chitosan/Soy Protein Blended Films with Added Plasticizing Agent as a Function of Solvent Type at Acidic pH .....</b>	<b>66</b>
2.1 Introduction .....	66
2.2 Materials and Methods.....	68

2.2.1 Materials.....	68
2.2.2 Preparation of Films.....	69
2.3 Film Characterization.....	69
2.3.1 Fourier Transform Infrared Spectroscopy.....	69
2.3.2 Thermal Analysis .....	70
2.3.3 SEM Analysis .....	70
2.3.4 Mechanical Properties.....	70
2.3.5 Water Absorption Testing.....	71
2.3.6 Contact Angle Measurement.....	71
2.3 Result and Discussion .....	71
2.3.1 FTIR Analysis .....	71
2.3.2 Thermal Analysis .....	74
2.3.3 Morphology.....	76
2.3.4 Mechanical Properties.....	78
2.3.5 Water Absorption Testing .....	81
2.3.6 Contact Angle Measurement.....	82
2.4 Conclusions .....	83
2.5 References .....	84
<b>Chapter 3 Properties of Cellulose–Soy Protein Blend Biofibers Regenerated from an Amine/Salt Solvent System.....</b>	<b>87</b>

3.1 Introduction .....	87
3.2 Materials.....	90
3.3 Preparation of Spinning Solutions .....	91
3.4 Fiber Formation.....	92
3.5 Characterization Techniques .....	93
3.6 Results and Discussion.....	96
3.6.1 Dynamic viscosity of the spinning solutions .....	96
3.6.2 Protein content .....	97
3.6.3 Chemical structure .....	98
3.6.4 Thermal properties .....	100
3.6.5 Morphology.....	101
3.6.6 Crystalline structure .....	103
3.6.7 Tensile properties .....	105
3.6.8 Birefringence.....	108
3.6.9 Biodegradation .....	109
3.7 Conclusions .....	110
3.8 Acknowledgement.....	110
3.9 References .....	111
<b>Chapter 4 Novel Cellulose – Collagen Blend Biofibers Prepared from an Amine/Salt Solvent System.....</b>	<b>117</b>

4.1 Introduction .....	117
4.2 Materials.....	120
4.3 Solution preparation.....	121
4.4 Fiber Formation.....	122
4.5 Characterization Techniques .....	123
4.6 Results and Discussion.....	125
4.6.1 Dynamic viscosity of the spinning solutions .....	125
4.6.2 Protein content .....	126
4.6.3 Chemical structure .....	127
4.6.4 Thermal properties .....	129
4.6.5 Morphology.....	130
4.6.6 Crystalline structure .....	132
4.6.7 Tensile properties .....	134
4.6.8 Birefringence.....	136
4.7 Conclusions .....	137
4.8 Acknowledgement.....	138
4.9 References .....	139
<b>Chapter 5 Properties of Cellulose – Keratin Blend Biofibers Regenerated from an Amine/Salt Solvent System.....</b>	<b>145</b>
5.1 Introduction .....	145

5.2 Materials.....	146
5.3 Preparation of Spinning Solutions .....	146
5.4 Fiber Formation.....	147
5.5 Characterization Techniques.....	148
5.6 Results and Discussion.....	150
5.6.1 Chemical structure .....	150
5.6.2 Thermal properties .....	151
5.6.3 Morphology.....	152
5.6.4 Crystalline structure .....	154
5.6.5 Tensile properties .....	155
5.7 Conclusions .....	157
5.8 References .....	157
<b>Chapter 6 Blend Biofilms Prepared from Gamma Irradiated Solutions.....</b>	<b>160</b>
6.1 Introduction .....	160
6.1.1 Gamma ( $\gamma$ )–Irradiation.....	162
6.2 Materials.....	163
6.3 Preparation of Film Forming Solution.....	164
6.4 Gamma Irradiation .....	165
6.5 Film Casting.....	165

6.6 Characterization Techniques .....	166
6.7 Results and Discussion.....	167
6.7.1 Chemical structure .....	167
6.7.2 Thermal properties .....	168
6.7.3 Tensile properties .....	169
6.7.4 Transparency .....	171
6.7.5 Water absorption .....	171
6.8 Conclusions .....	172
6.9 References .....	173

## LIST OF TABLES

<b>Table 1.1.</b> Solubility of silk fibroin in NMMO with varying water content. Adapted with permission from [86]. Copyright 2016, Springer.....	32
<b>Table 1.2.</b> Tensile properties of collagen (C)/hydroxyethyl cellulose (HEC)/albumin (A) fibers. Adapted with permission from [143]. Copyright 2016, Springer.....	47
<b>Table 1.3.</b> List of cellulose/protein biofibers reported in the literature.....	49
<b>Table 2.1.</b> TGA data for the films of SPI, CH, and 50/50 blend from acetic and formic acids .....	76
<b>Table 2.2.</b> Weight percent increase after 24 hours in water.....	81
<b>Table 2.3.</b> Results of contact angle measurements.....	82
<b>Table 3.1.</b> Spinning conditions applied for all fibers .....	93
<b>Table 3.2.</b> Protein content ( $W_{pro}$ ) of CE, CESP fibers, and raw SPI.....	98
<b>Table 3.3.</b> The percent crystallinity of CE, CESP fibers, and raw SPI.....	105
<b>Table 3.4.</b> Tensile properties of CE and CESP fibers .....	106
<b>Table 3.5.</b> Refractive indices (RI) and birefringence of the CE and CESP fibers. ....	108
<b>Table 4.1.</b> Fiber spinning conditions [38] .....	123
<b>Table 4.2.</b> Protein content of CE [38], CECOL fibers, and raw collagen.....	127
<b>Table 4.3.</b> Tensile properties of CE [38] and CECOL fibers.....	135
<b>Table 4.4.</b> Refractive indices (RI) and birefringence of the CE [38] and CECOL fibers ....	137
<b>Table 5.1.</b> Spinning conditions applied for all fibers .....	148
<b>Table 5.2.</b> Tensile properties of CE [12] and CEKER fibers.....	156
<b>Table 6.1.</b> The tensile properties of all films.....	169

## LIST OF FIGURES

<b>Figure 1.1.</b> Chemical structure of cellulose: a linear polymer composed of beta (1–4) linked D–glucose (anhydroglucose) units – adapted and redrawn from [12]; originally published under open access license. Available from: <a href="http://www.intechopen.com/books/cellulose-fundamental-aspects/direct-dissolution-of-cellulose-background-means-and-applications">http://www.intechopen.com/books/cellulose-fundamental-aspects/direct-dissolution-of-cellulose-background-means-and-applications</a> {DOI:10.5772/52144} and ( <a href="https://www.fibersource.com/f-tutor/cellulose.htm">https://www.fibersource.com/f-tutor/cellulose.htm</a> as accessed on February 21, 2016).....	3
<b>Figure 1.2.</b> The intra– and intermolecular hydrogen bonds in cellulose. Redrawn with permission from [14]. Copyright 2016, ACS.....	4
<b>Figure 1.3.</b> X-ray diffraction patterns of different cellulose polymorphs. Adapted with permission from [19,20]. Copyright 2016, ACS and Hanser Publications.....	6
<b>Figure 1.4.</b> Chemical structure of $\alpha$ -amino acids .....	8
<b>Figure 1.5.</b> Secondary ( $\alpha$ -helix and $\beta$ -sheet) structures of proteins .....	10
<b>Figure 1.6.</b> Alkali and carbon disulfide treated cellulose to yield cellulose xanthate. Modified and redrawn with permission from [34]. Copyright 2016, ACS.....	13
<b>Figure 1.7.</b> Schematic illustration of mixing method of viscose and protein solution 1. gear pump, 2. protein solution, 3. inline mixer. (From Yamada, M. and Ohshima, K., U.S. Patent 20090166919, July 2, 2009.).....	16
<b>Figure 1.8.</b> SEM images of the cellulose/protein (53% silk fibroin) fiber (55 $\mu\text{m}$ in diameter). Adapted with permission from [55]. Copyright 2016, Elsevier.....	18
<b>Figure 1.9.</b> Dye uptake of viscose /wool powder blended fiber with different powder contents. Adapted with permission [56]. Copyright 2016, IBWCh.....	19

**Figure 1.10.** SEM images of the cross sections of (a) viscose fiber and (b) cyclotriphosphazene/keratin/ viscose fiber, (c) residues of a and (d) b after burning behavior test. Adapted with permission from [57]. Copyright 2016, Springer ..... 20

**Figure 1.11.** TEM images of (A), (B) WPI fiber and (C), (D) cellulose/WPI blend fibers. Adapted with permission from [68]. Copyright 2016, Elsevier..... 23

**Figure 1.12.** A likely interaction of cellulose with the LiCl/DMAc solvent system. Redrawn with permission from [73]. Copyright 2016, Elsevier ..... 25

**Figure 1.13.** Effect of dissolution temperature on silk fibroin dissolved in lithium halide/organic amide solvent systems: ○, in LiCl/DMAc; ●, in LiBr/DMAc; △, in LiCl/DMF; ▲, in LiBr/DMF; □, in LiCl/NMP; ■, in LiBr/NMP. Dissolved at [LiX] = 1.86 mol/l in 1 h. Adapted with permission from [76]. Copyright 2016, The Japanese Society of Sericultural Science ..... 27

**Figure 1.14.** SEM images of the CE/SF blend fiber ( $C_p = 7$  wt% and  $D_r = 2$ ). Adapted with permission from [78]. Copyright 2016, John Wiley and Sons ..... 28

**Figure 1.15.** WAXD analysis of (a) CE and (b) CE/SF blend fibers ( $C_p = 7$  wt% and  $D_r = 2$ ). Adapted with permission from [78]. Copyright 2016, John Wiley and Sons..... 29

**Figure 1.16.** Polarized optical microscopy images (200X) of silk fibroin dissolving in NMMO·1.0H<sub>2</sub>O at different temperatures. Adapted with permission from [84]. Copyright 2016, Elsevier ..... 31

**Figure 1.17.** Variation of Young's modulus (○) and stress at break (□) by increasing CE content for CE/SF blend fibers at  $D_r = 3$ . Adapted with permission from [95]. Copyright 2016, Elsevier ..... 34

**Figure 1.18.** The dynamic viscosity of the spinning dope versus its composition; the temperatures of viscosity measurements are included in the parentheses adjacent to the viscosity values; the  $C_p$  of dopes were 6.5 wt% (100:0), 6.63 wt% (98:2), 6.83 wt% (95:5), 7.15 wt% (90:10), and 7.48 wt% (85:15). Adapted with permission from [109]. Copyright 2016, IBWCh ..... 37

**Figure 1.19.** The tenacity and the elongation of CE/SF fibers by increasing silk fibroin content. Adapted with permission from [109]. Copyright 2016, IBWCh ..... 38

**Figure 1.20.** Biodegradation of cellulose and cellulose/keratin composite fibers by composting. Adapted with permission from [110]. Copyright 2016, IBWCh..... 39

**Figure 1.21.** FTIR spectra of raw SPI, cellulose fiber and CE/SPI fibers. “Reproduced courtesy of Journal of Engineered Fibers and Fabrics, P.O. Box 1288, Cary, North Carolina 27512-1288, USA. Tel: (919) 459-3700 Fax: (919) 459-3701 Internet: www.jeffjournal.org.” [112] ..... 41

**Figure 1.22.** Suggested dissolution process of cellulose in ILs. Redrawn with permission from [117]. Copyright 2016, Elsevier..... 43

**Figure 1.23.** LSCM micrograph of cellulose and CE/SF fibers along the fiber axes (top raw at  $D_r = 3.3$ , bottom raw at  $D_r = 4.3$ ). Adapted with permission from [140]. Copyright 2016, Springer..... 45

**Figure 2.1.** FTIR spectra of the films from acetic acid ..... 72

**Figure 2.2.** FTIR spectra of the films from formic acid..... 72

**Figure 2.3.** TGA thermograms for the films from (a) acetic acid and (b) formic acid ..... 75

**Figure 2.4.** 5000X images of the films of CH (left), 50/50 blend (middle), and SPI (right) from acetic acid..... 77

<b>Figure 2.5.</b> 5000X images of the films of CH (left), 50/50 blend (middle), and SPI (right) from formic acid .....	77
<b>Figure 2.6.</b> Stress-strain curves of the films prepared from acetic acid (a) and formic acid (b) .....	78
<b>Figure 2.7.</b> Tensile modulus (a), failure stress (b) and failure strain (c) of all films as a function of SPI .....	80
<b>Figure 3.1.</b> A schematic illustration of dry-jet wet spinning system utilized to fabricate cellulose/SPI fibers .....	92
<b>Figure 3.2.</b> Dynamic viscosities of the spinning solutions with varying SPI concentrations at 75°C .....	97
<b>Figure 3.3.</b> FTIR spectra of CE, CESP fibers and raw SPI.....	99
<b>Figure 3.4.</b> TGA thermograms of CE, CESP fibers and raw SPI .....	100
<b>Figure 3.5.</b> FESEM images of the fractured cross-sections of CE and CESP fibers .....	102
<b>Figure 3.6.</b> WAXD results of CE, CESP fibers and raw SPI.....	104
<b>Figure 3.7.</b> Effect of the SPI ratio on the tenacity and the elongation of the fibers.....	107
<b>Figure 3.8.</b> Stress – strain curves of the fibers .....	107
<b>Figure 3.9.</b> Peak load and elongation at peak load of the control and 30 days composted CE and CESP fibers .....	109
<b>Figure 4.1.</b> An illustration of dry-jet wet spinning system [38].....	122
<b>Figure 4.2.</b> Dynamic viscosity of the dope solutions measured at 75°C .....	126
<b>Figure 4.3.</b> FTIR spectra of CE [38], CECOL fibers and raw collagen.....	128
<b>Figure 4.4.</b> TGA thermographs of CE [38], CECOL fibers and raw collagen .....	129

<b>Figure 4.5.</b> FESEM micrographs of CE [38] and CECOL fibers' cross-sections at 5000X (left) and 10000X magnifications (right).....	132
<b>Figure 4.6.</b> WAXD plot of CE [38], CECOL fibers and raw collagen.....	134
<b>Figure 4.7.</b> Dependence of initial modulus and tenacity of CE [38] and CECOL fibers on the collagen content .....	136
<b>Figure 5.1.</b> An illustration of dry-jet wet spinning system .....	147
<b>Figure 5.2.</b> FTIR spectra of CE [12], CEKER fibers and raw keratin.....	150
<b>Figure 5.3.</b> TGA (a) and DTG (b) thermographs of CE [12], CEKER fibers and raw keratin .....	152
<b>Figure 5.4.</b> FESEM images of the fractured cross-sections of CE [12] and CEKER fibers	154
<b>Figure 5.5.</b> WAXD results of CE [12], CEKER fibers and raw keratin .....	155
<b>Figure 5.6.</b> Effect of the keratin ratio on the initial modulus and the tenacity of CE [12] and CEKER fibers .....	156
<b>Figure 6.1.</b> Illustrated crosslinking of protein network to form network structure via dialdehyde mediated interchain crosslinking (redrawn and modified) [1] .....	161
<b>Figure 6.2.</b> FTIR spectra of all blend films.....	168
<b>Figure 6.3.</b> TGA thermograms of the films from irradiated control solutions.....	169
<b>Figure 6.4.</b> Effect of $\gamma$ -radiation dose on tensile strength and elongation of the blend film with 40% SPI .....	170
<b>Figure 6.5.</b> Effect of $\gamma$ -irradiation on the light transmission of the blend film.....	171
<b>Figure 6.6.</b> Influence of $\gamma$ -irradiation on the water absorption capacity of the blend film..	172

# Chapter 1 Formation of Cellulose and Protein Blend Biofibers

Reprint of Book Chapter Accepted for Publication in Springer (2016)

by Ramiz Boy, Ganesh Narayanan, Richard Kotek

Fiber and Polymer Science program, North Carolina State University, Raleigh, NC-27606

**Abstract:** Cellulose and proteins are potential polymers for developing biodegradable materials for high value-added applications. A combination with these natural polymers could be useful to enhance the properties of final materials and to extend their application areas. In particular, blend biofibers that are degradable and sustainable can be engineered from a mixture of cellulose and proteins, such as soy protein, silk fibroin, collagen, etc. In a binary polymeric blend, the compatibility of cellulose and proteins is influenced by the characteristics of each polymer in the employed solvent system as well as processing conditions. Therefore, utilizing solvents that can dissolve cellulose and proteins, and coagulants that are non-solvents for both polymers is of importance. In this book chapter, the formation and characteristics of blend biofibers from these polymers will be discussed.

## 1.1 Introduction

Materials developed from synthetic polymers are widely utilized in the form of films, membranes, coatings and fibers for a myriad of applications. Synthetic materials have a broad array of attractive properties because they can be more easily processed into a particular form and as a result can have good performance for specific applications. On the other hand, the utilization of materials from renewable resources, i.e. cellulose and proteins, is not broadly adopted. These polymers' main drawbacks are a relatively limited range of performance properties which are only appropriate for some applications and narrower processing windows

than for synthetic materials. In particular, the combination and modification of these natural polymers could be useful to enhance the characteristics of the final materials and to extend their application areas [1].

Regenerated cellulose fibers have suitable mechanical properties for textiles but regenerated protein fibers lack such properties for that target. This is due in large part to the insufficient information available on how amino acid sequences influence mechanical properties [2].

Cellulose and proteins are potential polymers for developing biodegradable materials for high added-value applications, and blending is a straightforward and efficient method to further improve the performance properties of each polymer in its final applications [3].

### **1.1.1 Cellulose**

Cellulose is abundantly available in nature as a sustainable organic raw macromolecule; however, it has not yet achieved its true potential in many areas of application. A main challenge is that cellulose must be in a different structure from that found in nature before it can be utilized for numerous final applications. Since cellulose does not melt, the polymer must be dissolved by some means that can lead to its desired final form. An early technique widely adopted by industry focused on chemical modification of cellulose to produce nitrocellulose and cellulose acetate. Based on this premise, a derivative viscose process forming called cellulose xanthogenate was also developed to make cellulose fibers (viscose rayon) and films (cellophane). All chemically modified cellulose materials have been utilized in a wide array of applications from textiles to special technical products. However, this technique includes several stages and creates pollution. Therefore, alternate methods that can facilitate and expedite the dissolution of cellulose have been put forward [4-7].

As a linear homopolysaccharide, cellulose is composed of  $\beta$ -D-anhydroglucopyranose (often called anhydroglucose or simply glucose) units joined together through  $\beta$ -1,4-glycosidic bonds in the  ${}^4C_1$  chair conformation. Therefore, it is a 1,4- $\beta$ -D-glucan forming disaccharide cellobiose moieties which constitutes a repeating element of cellulose. Moreover, the thermodynamically favorable  ${}^4C_1$  chair conformation of pyranose rings signifies that hydroxymethyl ( $-\text{CH}_2\text{OH}$ ) and hydroxyl ( $-\text{OH}$ ) groups besides the glycosidic bonds are central as regards to the average planes of the rings as shown in Figure 1.1. Two end groups of cellulose are in a different equilibrium state from one another; one has a normal  $\text{C}_4-\text{OH}$  group (the non-reducing end), while the other having  $\text{C}_1-\text{OH}$  group is in equilibrium with an aldehyde structure (the reducing end) [4,8-11].

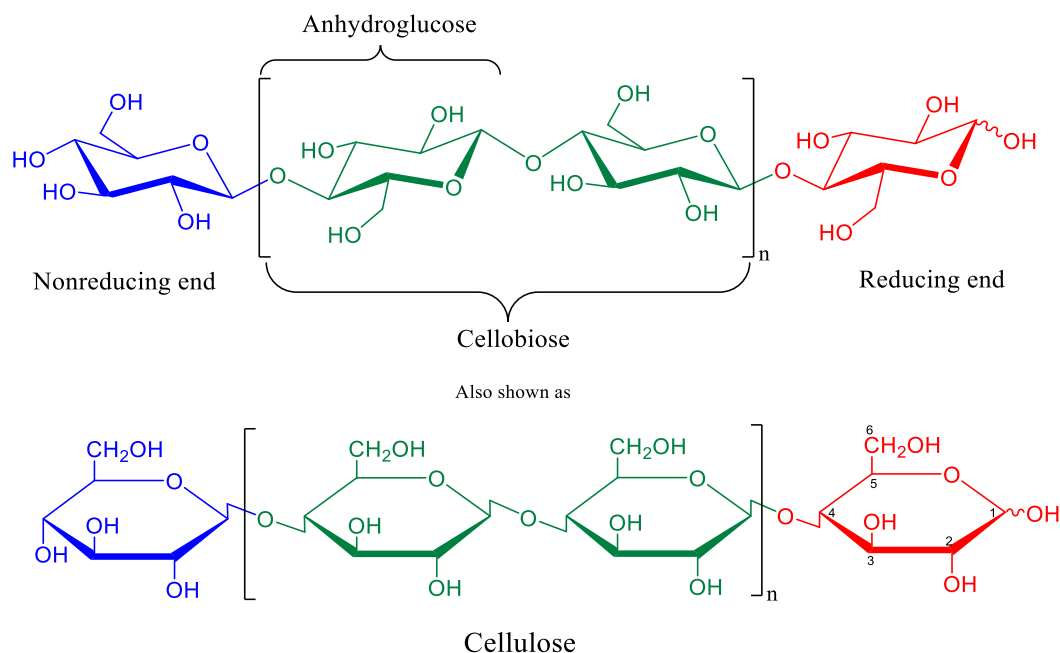


**Figure 1.1.** Chemical structure of cellulose: a linear polymer composed of beta (1–4) linked D–glucose (anhydroglucose) units – adapted and redrawn from [12]; originally published under open access license. Available from: <http://www.intechopen.com/books/cellulose-fundamental-aspects/direct-dissolution-of-cellulose-background-means-and-applications> {DOI:10.5772/52144} and (<https://www.fibersource.com/f-tutor/cellulose.htm> as accessed on February 21, 2016)

This molecular structure delivers characteristic properties, such as significant hydrophilicity and resulting surface energy, chirality, biodegradability, relative thermal stability, and the chemical versatility related to the reactive hydroxyl groups. While other polysaccharides, e.g. starch, chitosan, and alginate have similar properties, cellulose is characterized by strong inter-chain forces. A relatively large network of intra- and intermolecular hydrogen bonds (Figure 1.2), along with dipole-dipole and van der Waal' interactions, contribute to a partial crystalline structure and morphology of native cellulose with a moderate to low degree of accessibility. As a result, it becomes degraded before it begins to melt [4,11,13].

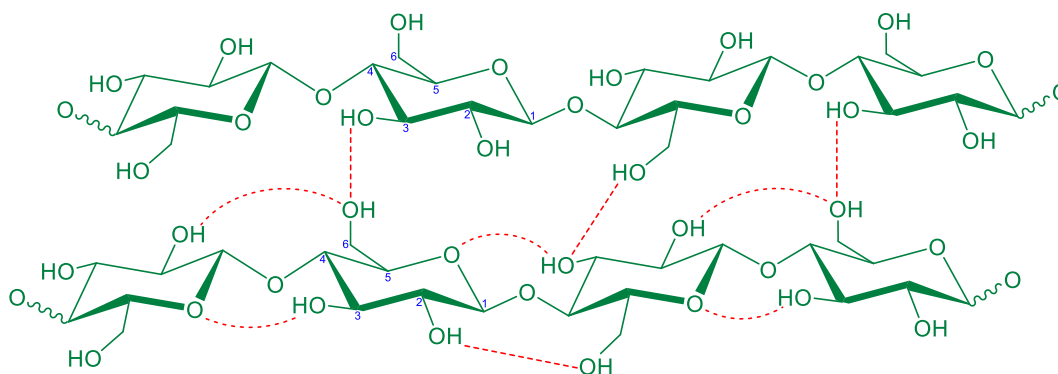


**Figure 1.2.** The intra- and intermolecular hydrogen bonds in cellulose. Redrawn with permission from [14]. Copyright 2016, ACS

The number of component anhydroglucoses determines the degree of polymerization (DP) of cellulose, which changes widely with the source, and the treatment of the raw material. For instance, wood pulp has a DP of 300–1700, flax 36000, cotton and other plant fibers 800–10000, regenerated cellulose fibers 500–1000 [4,15,16].

Native cellulose is perpetually synthesized in a form of fibrils that are long threadlike bundles of cellulose chains. These fibrils are constituted from smaller units. Nearly 36 cellulose chains aggregate to form elementary fibrils (protofibrils). These initial bundles are stacked into

nanofibrils that are 2–20 nm in cross-sectional dimension. The nanofibrils, stabilized by hydrogen bonds and van der Waal forces, are then packed into a final form, cellulose fibers. This fibrillar morphology of cellulose provides load-bearing function and structural integrity to plant cell walls. In addition, crystalline and amorphous domains of cellulose can differ in percentage at the large scale of its fiber assembly, but it is apt to prefer the oriented regions towards the nanofibril level. This improves tensile strength and lowers chemical reactivity [11,16,17].

The cellulose chains in crystalline domains are compact and oriented due to high density of –OH groups forming hydrogen bonds along and between the polymer chains. In combination with other secondary bonds (mainly van der Waals forces), they are packed into different levels of lateral order varying from ideal dimensional packing to an arbitrary arrangement. This depends on the origin, the isolation and purification method and the treatment of cellulose that generate multiple forms of its polymorphism. There are four major types of reported cellulose polymorphs; cellulose I, II, III, and IV that can easily be identified by X–ray diffraction as graphed in Figure 1.3 [16,18,19].

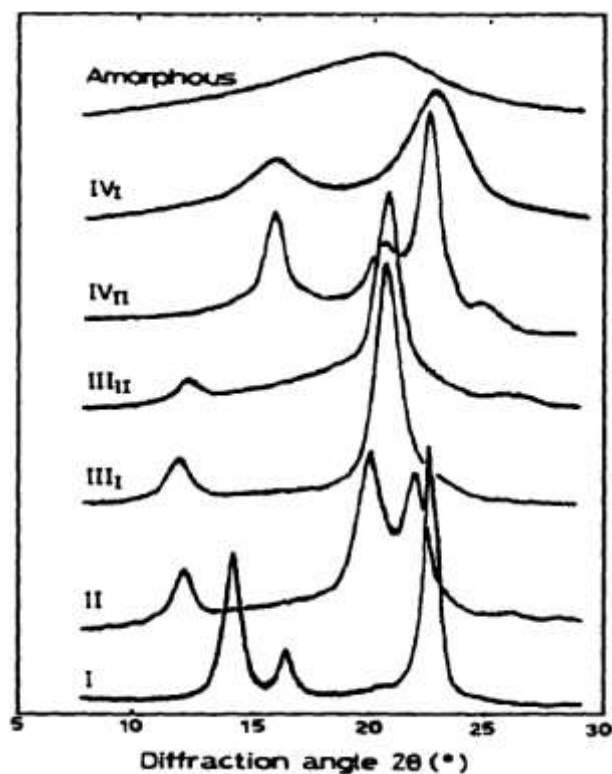


**Figure 1.3.** X-ray diffraction patterns of different cellulose polymorphs. Adapted with permission from [19,20]. Copyright 2016, ACS and Hanser Publications

The crystal structure of native cellulose (wood, bacterial and algal celluloses, cotton, ramie, etc.) is recognized as cellulose I. It displays parallel chain alignment, related to the both reducing and non-reducing ends of cellulose polymer. Although cellulose I is the most abundant form, it is thermodynamically less stable than the others are. Those polymorphic forms are obtained through chemical means or heat treatment of cellulose I. For instance, cellulose II, containing antiparallel chains, is formed by strong alkali treatment (also known as mercerization) or by precipitation of dissolved cellulose (also called regeneration). As discussed earlier, viscose rayon and cellophane are commonly known regenerated forms of cellulose. Both cellulose I and II can be converted to cellulose III<sub>I</sub> and III<sub>II</sub> respectively by processing in liquid ammonia or organic amines (e.g. ethylenediamine), and then removing their corresponding anhydrous residues. In addition, cellulose III is thermodynamically the

most stable form. Finally, cellulose IV<sub>I</sub> and IV<sub>II</sub> are produced by heating respective cellulose III<sub>I</sub> and III<sub>II</sub> in glycerol. These forms could be interconverted; however, partial degradation occurs for reversion to cellulose I. [15,18,21-23].

### **1.1.2 Proteins**

Proteins together with polysaccharides and nucleic acids are key macromolecules for living organisms. They enable biological and organic systems to live and propagate. Simply extracted from nature, proteins have been investigated for a long time in aspect of their inherent potential of constituting three-dimensional structures that provide biological functions. Fibroin from silk and spider web, keratin from hair and wool, and all types of enzymes that stimulate bio-reactions in animal bodies are entirely proteins [24,25].

As natural polymers, proteins have been intuitively utilized in edible packaging and materials, such as soy protein sheets and collagen envelopes. Before synthetic polymers were discovered, plastics from proteins were of interest in terms of finally substituting for cellulose. Molded plastic of casein (milk protein) crosslinked by formaldehyde was developed before the beginning of 20<sup>th</sup> century to produce articles, for instance, buttons [26,27]. Several applications in textile fibers, coatings, resins were made possible by utilizing zein (maize protein), which was patented after 1920. About the same time, formaldehyde was also broadly employed for the same purpose in a mixture of soy protein and blood meal to produce parts, namely, distributor caps for cars [28]. Furthermore, gelatin was an accessible polymeric material to cast films for photography, drug shells and foodstuff. Nowadays, there is gaining interest in producing bio-based plastics and materials from proteins as well as other natural polymers. Besides the mentioned ones, there are numerous other proteins, such as gluten from wheat or

maize, cottonseed flour, whey proteins, myofibrillar proteins, etc., that could be utilized in various applications [29].

Proteins are much more complex than polysaccharides and are fallen into the class of polyamides with amino acids as their building blocks. Thousands of amino acids can be synthesized *in vitro* but only 20 amino acids commonly occur in nature and called  $\alpha$ -amino acids. The 20  $\alpha$ -amino acids that vary in dimension, form, charge, hydrogen-bonding sites, and chemical reactivity are the basic monomer units of proteins. The structure of every  $\alpha$ -amino acid possesses a basic amine group ( $-\text{NH}_2$ ), a carboxyl group ( $-\text{COOH}$ ), and a typical side chain, R. The polarity of R groups can classify these  $\alpha$ -amino acids into four different groups as shown in Figure 1.4: nonpolar, polar but neutral, basic, and acidic. The nonpolar side chains are water repellant (hydrophobic), while the others are hydrophilic. The properties of R groups highly affect the nature and behavior of a protein. For instance, many hydrophobic amino acids form the core of protein's globular structure including many other hydrophilic ones at the exterior. Furthermore, half of the 20  $\alpha$ -amino acids are essential for humans in that they are not produced by their metabolic system but a part of their diet [30-32].

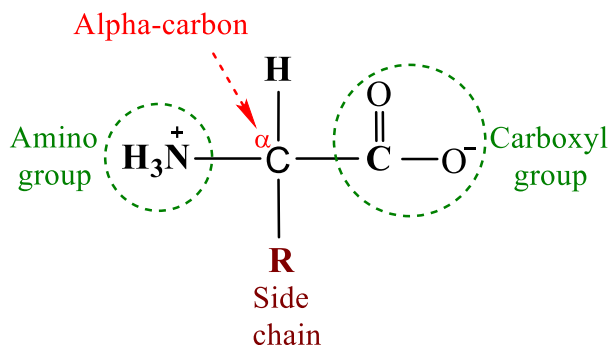


**Figure 1.4.** Chemical structure of  $\alpha$ -amino acids

Compared to polysaccharides, proteins are monodisperse and made of  $\alpha$ -amino acids that are naturally polymerized to constitute an infinite number of sequential arrangements

ensuing exceptional molecular diversity. As a condensation polymer, the monomer units (amino acid residues) of proteins are linked by amide bonds ( $-\text{CO}-\text{NH}-$ ) which are also called peptide bonds. Two amino acids form a dipeptide, three a tripeptide, and so on. In general, chains with up to 50  $\alpha$ -amino acids are often called polypeptides and larger ones are referred to proteins. In addition to peptide bonds, disulfide bridges ( $-\text{S}-\text{S}-$  bonds formed between two cysteine units) are also possible in proteins [25,30].

A common type of classification of proteins is based on their three dimensional (3D) shapes which are fibrous (scleroproteins) and globular (spheroproteins). Fibrous proteins have elongated thread-like polymers chains that are held strongly together by hydrogen bonds rendering them water-insoluble. As a result, they have structural functions in animal tissues. Collagen (tendons and connective tissue), myosin (muscles tissue), keratin (skin, hair, feathers, horn), and fibroin (silk) are all examples of fibrous proteins. On the other hand, globular proteins have compact spheroidal structures and are fairly soluble in water. This provides them to be able to move freely in cells. Enzymes and hormones are typical globular proteins of living organisms [25,30].

Figure 1.4 shows the deprotonated carboxyl group (negative charge) and the protonated amino group (positive charge) of an amino acid existing as a dipolar ion, or zwitterion, in an aqueous solution as well as in solid state. Amino acids are therefore ionic compounds incorporating internal salts. This also induces comparable physical properties to a salt, such as water solubility and high melting point. Moreover, amino acids are amphoteric molecules: They can react as acids but also as bases in an aqueous solution with varying pHs. An intermediate pH at which molecules have equal positive and negative net charges is a characteristic of amino acids and is called isoelectric point,  $pI$  [25,32].

The amino acid sequence of a polypeptide chain is referred to primary structure that constitutes three-dimensional structure of a protein. This spatial geometry of proteins invariably occurs due to inter- and intramolecular bonds, such as hydrogen bonds, electrostatic and dipole interactions, etc. While regular folding of the chain determines the secondary structure (Figure 1.5) of a protein, its overall 3D shape is referred to the tertiary structure. There even a higher degree structure, quaternary, exists due to several polypeptide chains interacting and aggregating into a single protein [25,32].

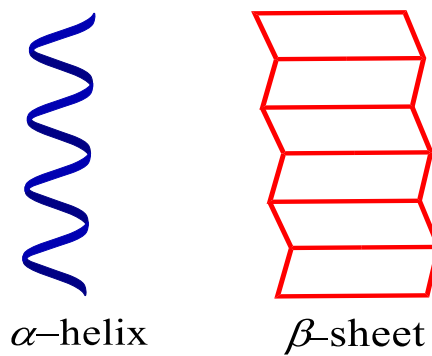


**Figure 1.5.** Secondary ( $\alpha$ -helix and  $\beta$ -sheet) structures of proteins

Along the structural hierarchy, the secondary structures are of importance since the chains of most proteins show particularly defined confirmations.  $\alpha$ -Helix and  $\beta$ -pleated sheet confirmations are the most prevalent ones.  $\alpha$ -Helices are formed through creating ample space for large R groups stabilized by hydrogen bonding between N-H and C=O within an amino acid residue. The  $\alpha$ -helix is a prevalent secondary structure and is involved with virtually all globular proteins (Figure 1.5). On the other hand,  $\beta$ -pleated sheets are constructed by amino acids with relatively small R groups arranged in a more extended chain conformation than  $\alpha$ -helices. These sheets are composed of more than one chain, lying next to each other, forming inter- and intramolecular hydrogen bonding. Furthermore,  $\beta$ -sheet or  $\alpha$ -helix is rarely found as single structure of a protein. These two structures together just make up a limited percentage

of confirmation in many proteins, particularly in globular ones. The remaining percentage consists of random coil. As secondary structures, these three types of confirmation form in different segments of the polymer chains of globular proteins [25,30,32].

Keratin is the well-known protein of hair, fingernails, horns and wool. It is a fibrous protein occurring mainly in  $\alpha$ -helix form. Particularly in wool, this structure contributes to high extensibility and flexibility. Fibroin, another notable fibrous protein, is extracted from silk. It forms a predominantly  $\beta$ -pleated sheet structure which account for high strength and toughness in spider and silkworm silk. Their mentioned properties are much superior to any synthetic fibers [32].

Most proteins do not maintain perfectly uniform confirmations. Some segments of polypeptide chains could interact through side chains (hydrogen bonding), disulfide bridges, salt bridges, hydrophobic interactions, metal ion coordination. Therefore, the overall three dimensional form of proteins is specified as the tertiary structure. By either or both of chemical and physical treatment, the secondary and tertiary structure can be disturbed to modify the proteins. This method is referred to denaturation of protein. It consequently affects the solubility, water absorbency, intrinsic viscosity, and biological activity of proteins [30-32].

Proteins along with polysaccharides, for instance, cellulose, form the tissue of animals and plants, respectively. The extraction from these sources results in different structures of the natural polymers to be exploited in a myriad of applications. As naturally occurring polymers, they are renewable, biocompatible, biodegradable and immensely common on Earth. Due to their numerous biological functions and significant properties, a mixture of the both classes of polymers could deliver superior properties compared to their individual components in biomedical applications. In addition, blends have already been investigated as conceivable

novel materials in fields of research, such as textiles, medicine, food, cosmetics and electronics [3,33].

From the perspective of the background and significance including the promising development and utilization of cellulose and proteins, research on developing materials from their combinations shows great potential. In this literature review, the most relevant solvents that dissolve both cellulose and proteins to form fibers, and the solution blending of the two polymers will be elaborated.

## 1.2 Viscose Process

Viscose (or rayon) process is one of the oldest industrial methods of dissolving wood pulp [10]. It includes a derivatizing solvent system, producing a cellulose derivative that can dissolve in water or dilute caustic soda. This process begins with alkali treatment [ $\text{Cell-OH} + \text{NaOH} \rightarrow \text{Cell-O}^- \text{Na}^+ + \text{H}_2\text{O}$ ] in order to purify and mercerize the pulp. Then, obtained alkaline cellulose is aged to achieve a certain degree of oxidative degradation to control DP of cellulose. The next major step is the reaction of the cellulose with carbon disulfide ( $\text{CS}_2$ ) resulting in cellulose xanthate [ $\text{Cell-O}^- \text{Na}^+ + \text{CS}_2 \rightarrow \text{Cell-OCS}_2^- \text{Na}^+$ ] (Figure 1.6). This step renders the process complicated since adding  $\text{CS}_2$  induces several reactions at once, yielding by-products, such as  $\text{H}_2\text{S}$  and  $\text{Na}_2\text{CS}_3$ . The latter one discolors the cellulose xanthate and gives its typical orange color [10,22,23].

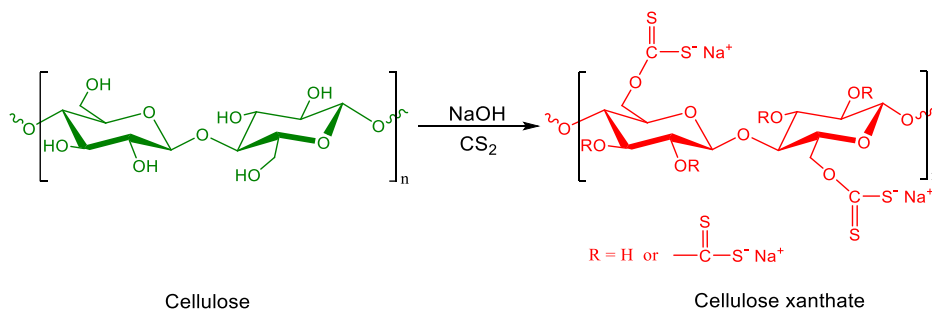


**Figure 1.6.** Alkali and carbon disulfide treated cellulose to yield cellulose xanthate. Modified and redrawn with permission from [34]. Copyright 2016, ACS

The xanthate is later dissolved in dilute NaOH to form viscose that is a very viscous solution. Subsequently, viscose is left for ripening during which xanthate groups are redistributed and dexanthation takes place, followed by filtration and deaeration. Finally, viscose is spun (or cast) into a coagulation bath, consisting of mainly acid and salt  $[2\text{Cell-OCS}_2^- \text{Na}^+ + \text{H}_2\text{SO}_4 \rightarrow 2\text{Cell-OCS}_2^- \text{H}^+ + \text{Na}_2\text{SO}_4]$  in order to produce rayon fibers (or films)  $[\text{Cell-OCS}_2^- \text{H}^+ \rightarrow \text{Cell-OH} + \text{CS}_2]$ . This final step is invariably combined with washing and drying to stabilize the final form [10,35].

Through viscose processing, the DP of the pulp, as received is around 750–850, drops to about 270–350 due to oxidative depolymerization. In addition, the polymorph of cellulose is transformed from I to II. As an interesting phenomenon, the ballooning effect was first noted on the fibers swollen with alkali and carbon disulfide [34,36].

An attempt, as early as 1910, to bring cellulose and proteins together was made by a French scientist H. L. J. Chavassieu [37]. He used viscose process to produce so-called “proteo-cellulosic products”. Proteins from any origin were first treated with alkali, then the resulted alkaline mixture was treated with  $\text{CS}_2$  resulting in a protein derivative, so-called “proteid xanthate”. The obtained derivative was mixed with cellulose xanthate. Following the same steps in viscose process, different forms of materials were produced from

cellulose/protein mixture. Similarly, a British patent briefly claimed preparing blend solution by adding caustic soda of a protein, such as keratin, fibrin, etc. into cellulose xanthate. More alkali was added to dilute the blend solution before the ripening [38]. While earlier patents relied on alkali mixture of proteins and viscose, Esselmann et al. [39] directly added relatively high molecular weight albuminous substances to viscose solution before or during the deaeration step. Therefore, the decomposition of protein was avoided to provide so-called “animalization” of cellulose fibers in order to enhance their colorization with acid dyes. To reduce the decomposition of proteins, their dissolution in sodium sulfide ( $\text{Na}_2\text{S}$ ) was realized to be efficient to produce blend fibers possessing enhanced mechanical properties [40]. Furthermore, another patent was filed by American Enka Corp. providing details about a method of spinning homogeneous cellulose/protein blend fibers via the viscose process. Mainly, globular proteins, including casein, soy protein, zein, were used. Initially, proteins were decomposed in aqueous solution of  $\text{NaOH}$  and  $\text{Na}_2\text{SO}_3$  and reacted with formaldehyde to saturate their free amino groups. Later, the obtained protein solution was mixed with viscose solution to obtain fibers with wool-like characteristics. This means provided homogeneous viscose solution containing 20-25% casein and paved the way for stronger fibers [41]. The ultimate goal of these early patents was to replace viscose/wool yarn blend with the blend fibers to overcome the dyeability of both components.

Nicoll [42] of Du Pont patented regenerated cellulose/casein and cellulose/soy protein fibers that can maintain a substantial crimp upon stretching that is similar to wool. The crimps on the fibers could be mechanically removed and restored. Despite non-specified protein loading, relatively high tenacity crimped fibers were reported within a range 2.25–3 g/den for dry and 1.25–2 g/den for wet tenacity. Comparable to Du Pont’s, Kanegafuchi Spinning Co.

also patented blend fibers with protein derivatives so that rotting and decomposing of protein can be avoided after mixing with viscose. Proteins from milk, corn, and soybean, were derivatized by (a) using a nitrile compound with an attached functional group, e.g. epoxy radicals, halogen atoms, or unsaturated ethylene radical, (b) chemically treating (a), (c) graft-polymerizing with an ethylenic unsaturated monomer. The resulting protein derivatives were utilized to form uniform and stable mixtures with cellulose [43].

Mahomed [44] from Courtaulds Ltd. incorporated 10–40% urea based on 10–40% casein added into the viscose solution at the final stages prior to the extrusion. The resulting fibers aged in formaldehyde, alkali cyanates, and zirconyl salts to prevent protein leaching. This process supposedly helped to produce higher tenacity blend fibers than viscose fiber. However, the results related to the claimed method were not reported. Similarly, Itaya [45] of Fuji Spinning Corp. employed a grafting agent, epichlorohydrin, in order to form viscose fiber grafted with milk casein. 15 wt% casein solution, prepared from 1% (v/v) NaOH, was reacted with the grafting agent (1–3 wt% of the weight of casein), and then mixed with cellulose xanthate. Casein formed from 13 to 17 wt% of the dope solution of fiber spinning. Compared to viscose rayon, the resulting fiber had some advantages, such as the dyeability with wool dyestuff, better light fastness, higher resistance to burning, heat-retaining property, and resistance against wool-attacking insects, molds and mildews.

Yamazaki [46,47] from Daiwabo Rayon filed two (Japanese) patents on making antibacterial viscose rayon and the rayon with modified touch feeling. The author directly incorporated cow's milk (either fresh milk or processed milk powder) into viscose solution. The blend fibers were commercialized under the trade name MILEY [48] by the company. The

fibers were emphasized as antibacterial since it combines the two biodegradable polymers and contains no formaldehyde as opposed to the most commercial regenerated protein fibers [49].

Yamada et al. [50] who were also affiliated with Daiwabo Rayon filed a (Japanese) patent describing the blends of cellulose with alkali soluble proteins including keratin, soy protein, and gelatin. The selected protein was first mixed with a water-soluble cross-linking agent, such as formaldehyde, glutaraldehyde, and N-methylol compound, in alkali solution. Then, the crosslinked protein was added to viscose solution (Figure 1.7) that was blended with polyethyleneimine (0.5 to 5.0 wt% of cellulose). The resulting blend fibers were claimed as cellulose/protein conjugate fibers with modified properties compared to sole viscose rayon. Similar patents on the blend fibers containing keratin were also filed to utilize recovered wool, feathers, hair, etc. as well as to provide higher dye affinity for viscose rayon towards acid dyes [51,52].

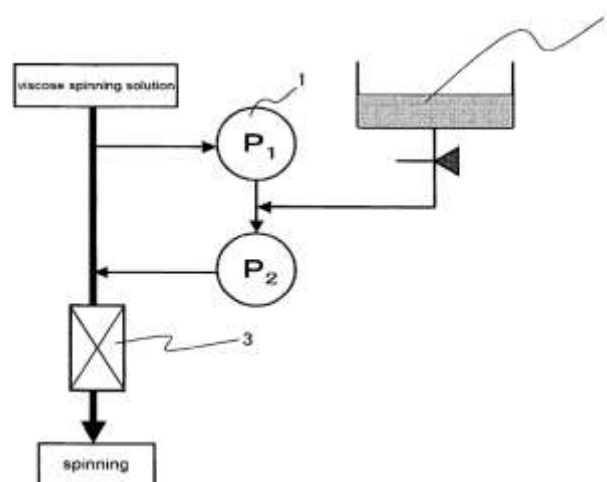


**Figure 1.7.** Schematic illustration of mixing method of viscose and protein solution 1. gear pump, 2. protein solution, 3. inline mixer. (From Yamada, M. and Ohshima, K., U.S. Patent 20090166919, July 2, 2009.)

A recent patent by Yamada and Ohshima [53] on manufacturing cellulose/gelatin composite viscose rayon explains sufficient details about the mechanical properties of the

blend fiber. Applying the same preparation method in their previous patent [50], the authors were able to produce the cellulose/gelatin blend fiber with 16.6% protein content. Gelatin solutions varied in the molecular weight of the polymer were prepared to produce four different blend fibers with the same percentage of protein in addition to the viscose rayon. The blend fibers had tenacity between 1.94 and 2.19 g/den and elongation between 10.5 and 14.2% that were slightly lower than those of the rayon, the tenacity and elongation of which were 2.32 g/den and 18.5%, respectively. The surface of the blend fibers, however, was much smoother and it did not show grooved morphology compared to viscose fiber.

A fabric made of hollow viscose fibers sprayed with casein was used to absorb moisture in order to keep one's body warm. The protein was added to provide smoothness and soft texture to the fabric [54].

Hirano et al. [55] briefly included mechanical and morphological properties of cellulose/silk fibroin blend fibers in their report. The linear density of the blend fibers tended to increase with more silk fibroin content. The fiber denier of viscose rayon and the blend fiber (53% protein content) was measured 4.1 and 19.7, respectively. This, however, was on the contrary for the tenacity of fibers. The blend fibers with less than 10% fibroin content showed relatively good mechanical properties. Above 10%, the values drastically reduced. From 2 to 10%, the blend fibers had the tenacity of 1.08–1.20 g/den and the elongation of 29.7–35.0% that were slightly lower than those of the control fiber (100% cellulose or viscose rayon).

Scanning Electron Microscopy (SEM) images of the cellulose/silk fibroin (47/53 w/w) blend fiber (Figure 1.8) revealed tiny vertical striped patterns on the surface that were similar to those on silk fiber surface. The authors concluded that only weak molecular interactions except some physical entanglements occurred between cellulose and silk fibroin. It was also

noted that cellulose behaved as a skeleton and silk fibroin acted as a filling material [55]. However, there was no other evidence to support their conclusion. For instance, it was not clear how the entanglements occurred and how the role of the polymers was determined. In addition, Fourier Transform Infrared Spectroscopy (FTIR) results that were briefly mentioned did not have any indication of any sort of interaction.

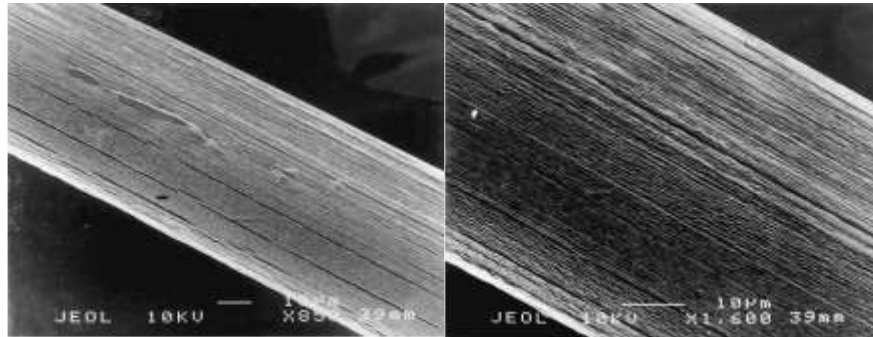


**Figure 1.8.** SEM images of the cellulose/protein (53% silk fibroin) fiber (55  $\mu\text{m}$  in diameter). Adapted with permission from [55]. Copyright 2016, Elsevier

A recent study regarding the formation of viscose/wool powder fibers showed that acid dye affinity of the blend fibers rises with increasing protein content. It can be observed from Figure 1.9 that the dye uptake of the fibers with 15 to 20% protein loading exceeds 50% in about 5 min. In comparison with the viscose fiber, the percentage of dye uptake doubled for the fiber with 20% protein. Although acid dyeability of the cellulosic fibers improved, 15% of the both dry and wet tenacity was sacrificed. For instance, the dry tenacity of viscose fibers decreased from 2.70 g/d to 2.29 g/d for the fiber with 15% wool powder [56].

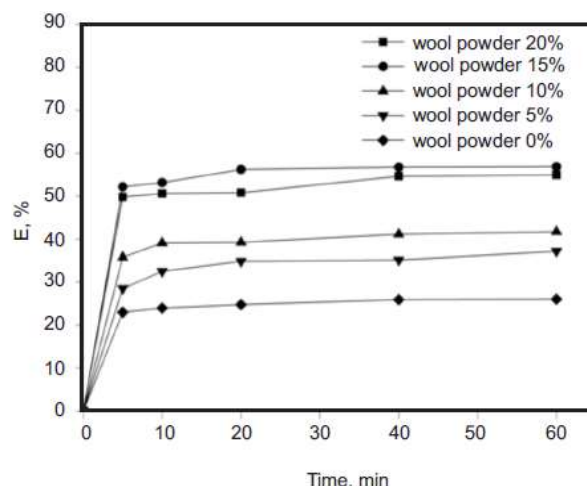


**Figure 1.9.** Dye uptake of viscose /wool powder blended fiber with different powder contents. Adapted with permission [56]. Copyright 2016, IBWCh

Zhou et al. [57] developed a flame retardant viscose rayon by adding a derivative of keratin. The protein was extracted from wool that was treated with 12% NaOH solution at 70°C. Then, it was reacted with chlorine atoms of a phosphazene derivative called hexachlorocyclo-triphosphazene to form cyclotriphosphazenerkeratin (CCTPK). This protein derivative provided the flame retardancy to the viscose fiber. As a result, the limiting oxygen index (LOI) of the fiber increased from 16.5% to 28.6% by 10% CCTPK loading. After 30 washing cycle, the LOI value decreased to 27.5%. Furthermore, the burning behavior test revealed that while the viscose fiber was decomposed to ashes, flame retardant viscose fiber retained its fiber structure (Figure 1.10). Similar to the effect of wool powder, CCTPK also lessened the tensile properties of viscose fiber.

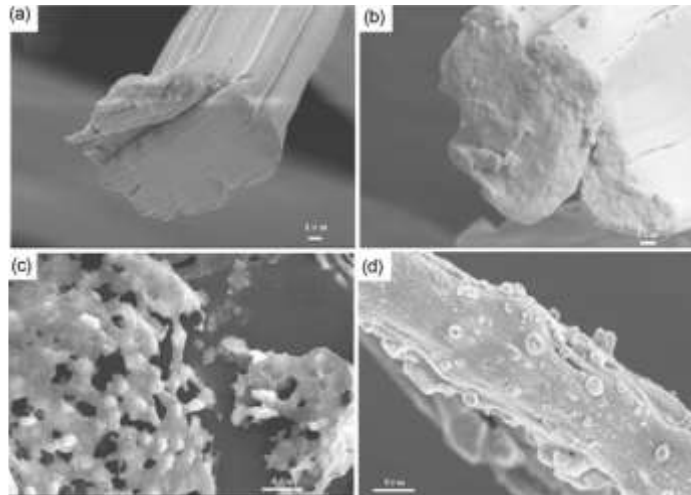


**Figure 1.10.** SEM images of the cross sections of (a) viscose fiber and (b) cyclotriphosphazene/keratin/ viscose fiber, (c) residues of a and (d) b after burning behavior test. Adapted with permission from [57]. Copyright 2016, Springer

Practically any protein, either in solution or in solid state, can be blended with viscose solution [50]. Therefore, there have been quite a few blend fibers produced through viscose process. Most of these fibers were found in patent applications and the information about their properties is either very limited or not available. The patents mostly focused on the preparation of blend solutions for extrusion.

In general, introducing proteins into viscose solution weakened the tensile properties of resulting viscose rayon fibers. This is most likely due to a decrease in the viscosity of the solution indicating compatibility issues for the two polymers processed by this system. On the one hand, these combination and modification of viscose rayon with proteins was a good method to increase the functionality of final material. On the other hand, this method consisted of blending alkaline solution of cellulose xanthate and alkaline solutions of the mentioned proteins, which were either decomposed or crosslinked, or grafted onto cellulose xanthate. This approach added more steps to the process of obtaining blend fibers. The viscose process is already multi-stepped, complex, and notorious for releasing  $CS_2$  and  $H_2S$  along with other

chemicals, which are hazardous, and menace to environment. Their recovery and recycling are difficult and thus raises the cost [23]. Due to these challenges, many alternative solvent systems have been proposed to dissolve cellulose and some are used as co-solvents for proteins as well.

### 1.3 Cuprammonium Process

Cuprammonium hydroxide (tetraamminecopper(II) hydroxide), also known as cuoxam and cuam, was the first solvent discovered by Schweizer [58] to dissolve natural fibers, such as cotton, linen and silk. It was later recognized as Schweizer reagent. In 1901, E. Thiele made a stride with a stretch spinning along a spinning funnel. It was then commercially used by the Bemberg Rayon Industry to manufacture cuprammonium fiber (or rayon). In this process, copper hydroxide solution is freshly prepared from copper sulfate and sodium hydroxide and transferred into aqueous ammonia to form cuprammonium hydroxide. For effective dissolution, the concentration of copper must be more than 25 g/l and that of ammonia should be in the range of 124–250 g/l [23,59].

It is commonly acknowledged that cuprammonium ( $\text{Cu}[\text{NH}_3]_4^{+2}$ ) ions form a complexation with  $[\text{OH}]^-$  groups of cellulose. It is highly decomposable upon exposure to light. Therefore, freshly made solution should be prepared. This solution is later degassed to avoid oxygen, and then filtered before the extrusion. The formed extrudate is then spun into an alkaline coagulation bath designed as funnel-type where the coagulant cycles down, contracts and solidifies the jet. The rising jet velocity through the funnel induces stretching up to 400%. The process is finally completed by washing the fibers with 5%  $\text{H}_2\text{SO}_4$ . In addition, cuprammonium fiber is the most closely resembling rayon to silk. These fibers could be hollow to make dialysis membranes, called as cuprophane by Akzo Nobel [7,23].

In 1934, a patent on preparing copper-ammonium-fibroin solutions was awarded to Börner et al. [60]. The possibilities of regenerating silk from cuprammonium hydroxide into fiber form were discussed by Wakeham et al. [61]. Hori and his coworkers [62] from Japan were able to produce the filaments of silk fibroin dissolved in the same solvent and precipitated in an acid bath. They also explored the commercial aspects of producing fabrics out of these filaments. Similarly, Wormell and Happey [63] from Courtaulds managed to regenerate the fibers from  $\alpha$ -keratin of wool by using the same solvent [64].

Jayme and Broschinski [65] experimented a set of metal complex solvent systems with copper and nickel (Ni) as central atoms to dissolve proteins, e.g. casein, gelatin, collagen, zein, and silk fibroin. Their report was a progress of what Schweizer [58] discovered. A substantial amount of metal complex bound the proteins during dissolution with the solid metal hydroxide contributing to the process. The solution of proteins with only high concentrations could yield intact material coagulated in organic solvents. Using in sulfuric acid for coagulation, the blend of cellulose and protein at 1:1 ratio gave superior properties compared to only protein material. Overall, they developed complex solvent systems to regenerate alkali insoluble proteins and, more importantly, the blends with cellulose.

Two Japanese patents based on cellulose/silk [66] and cellulose/keratin [67] blends were claimed to utilize cuprammonium process to produce fibers. However, the detailed descriptions on their production and properties cannot be sufficiently interpreted.

Recently, Tomczyńska-Mleko et al. [68] produced cellulose/whey protein isolate fibers through cuprammonium process. First, 1 g cellulose was dissolved in 30 g of Schweizer's reagent for half an hour and blended with 15 g of 8.5 wt% whey protein isolate (WPI) dispersion (preheated at 80°C). After complete dissolution, the obtained solution contained

about 56% whey protein isolate. The solution was then pumped into a 33% sulfuric acid using a syringe/needle spinning system to form the blend fiber. During coagulation, the acid caused gelation of whey protein into cellulose network. The fiber was then rinsed with distilled water and 5% aqueous ammonia solution and subsequently washed with the water. Applying the same procedure, control fibers from each component was also produced. For instance, the cellulose fiber showed microspores structure and contained significant traces of the solvent indicating incomplete coagulation of all of the reported fibers. According to the authors, 0.156% (53.8 mM)  $\text{Cu}^{2+}$  left in the blend fiber can be tolerated for daily human consumption. Since some diseases can be treated with copper, it was mentioned that the fibers could be used for medical applications, such as drug release. Furthermore, the transmission electron microscopy (TEM) images revealed phase separated morphology of the blend fiber (Figure 1.11). In comparison with WPI fiber, protein aggregation was observed in the blend fibers that indicates their composite morphology. Consequently, the infrared spectroscopy of blend fiber did not show distinct peaks relating to the intermolecular interaction between the polymers.

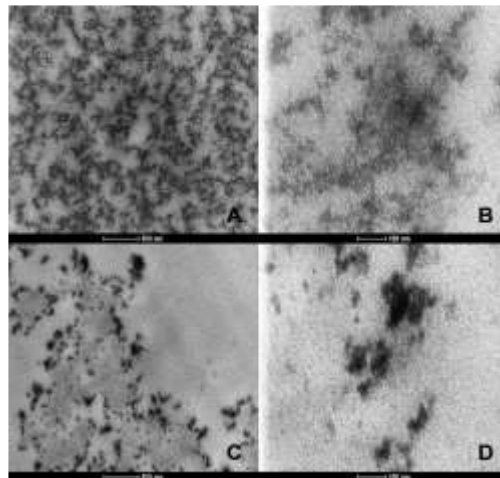


**Figure 1.11.** TEM images of (A), (B) WPI fiber and (C), (D) cellulose/WPI blend fibers. Adapted with permission from [68]. Copyright 2016, Elsevier

Tomczyńska-Mleko et al. [69] also reported cellulose/egg white protein blend fiber using the same process as they did for cellulose/WPI fiber. In the final solution, the concentration of cellulose was 6.25% and that of egg white isolate (EWI) was 1.875%. The resulting blend fiber showed comparable results to the cellulose/WPI blend fiber. In addition, the authors intended to utilize the blend fibers for biomedical applications. Consequently, they disregarded the tensile properties of fibers in their initial reports. The properties were mentioned to be tailored for textile materials that are resistant to microbial degradation.

The main drawback of cuprammonium process is the recovery of copper, ammonia, and the coagulant that are expensive and not fully achievable [23]. Despite the disadvantage, the remained copper in cellulose/protein fibers was useful for biomedical applications.

#### **1.4 Lithium Chloride and *N,N*-Dimethylacetamide**

McCormick et al. [70] developed the mixtures of lithium chloride (LiCl) in *N,N*-dimethylacetamide (DMAc) with which homogenous solutions of cellulose can be prepared. These mixtures had been previously employed to dissolve proteins, polyamides and chitin. As an aprotic solvent, LiCl/DMAc system does not cause any chain degradation or reaction with cellulose. Being a nonderivatizing solvent, it can directly dissolve cellulose in a rapid, facile and reproducible manner. It is also utilized to determine MW distribution of cellulose and other soluble polymers [71].

Dissolution of cellulose by this solvent requires a pretreatment (also referred to activation) step for chain relaxation of the polymer and for the solvent to diffuse into crystalline segments to cause swelling. This contributes to chain unfolding and ease of processing for most polymers. The higher the DP and crystallinity are, the longer the time is required to acquire useful polymer solution. This activation can be achieved by either refluxing cellulose

in hot DMAc (close to its boiling point) or a solvent exchange method that is carried out with water later replaced by DMAc [71]. The latter is usually preferred because low temperatures do not cause oxidative degradation of cellulose. However, the former takes significantly less time and the related thermal oxidation could be minimized by a constant flow of dry nitrogen [70].

Although the concentration of LiCl in DMAc varies from 8 to 13 wt% in the literature, 8.46 wt% is the highest solubility attained experimentally at 25°C. In addition, both of the two molecules are so hygroscopic that their mixture can absorb water very easily. Consequently, this could hamper the solvent to form complex with cellulose and to cause aggregation. On the other hand, cellulose solution from LiCl/DMAc is very stable and the polymer does not degrade over a long period of time at ambient temperature [71].

The dissolution is assumed to involve a macrocation  $[\text{Li}(\text{DMAc})_x]^+$  in the form of an ion–dipole complex (Figure 1.12). A complexation occurs through a  $\text{Li}^+$  cation, residing next to the oxygen of DMAc' carbonyl group, and a  $\text{Cl}^-$  anion interrupting the hydrogen bonds of cellulose [72].

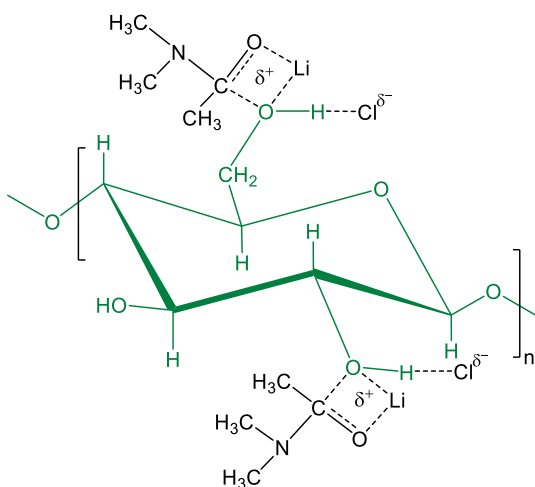


**Figure 1.12.** A likely interaction of cellulose with the LiCl/DMAc solvent system. Redrawn with permission from [73]. Copyright 2016, Elsevier

Pretreatment with DMAc is a facile activation for the dissolution of cellulose. Typically, a given amount of dry cellulose is soaked into a known weight of DMAc. The activation continues at 165°C by refluxing the mixture for 20–30 min under nitrogen atmosphere. Then, it is chilled to 100°C and a given amount of LiCl is incorporated into the mixture while stirring. At 80°C, stirring resumes for 10–40 min to ensure that the dissolution is complete. A maximum concentration of 15 wt% cellulose with the DP of 1130 can be achieved. Above 15 wt%, suspended particles, which are undissolved and swollen fragments of cellulose, are found in the viscous solution [23,74].

Besides LiCl/DMAc, some other lithium halide/organic amide solvent systems including lithium bromide (LiBr) and N,N-dimethylformamide (DMF) or N-methyl-2-pyrrolidone (NMP) that dissolve cellulose were also reported [75]. This research was also conducted for silk fibroin expecting a comparable dissolution mechanism to cellulose due to its intermolecular hydrogen bonding. By analogy with the dissolution of cellulose in LiCl/DMAc, a calculated amount of degummed silk fibers was pretreated with DMAc at 90°C under nitrogen for 2 h. Then, the silk fibroin/DMAc mixture is cooled down the dissolution temperature, e.g. 50°C, and a given amount of LiCl was added. After an hour of stirring, the content was filtered to remove undissolved matter. Finally, the fibroin was regenerated in ethanol. This process is also repeated with other combinations of lithium halide and organic amide. As seen in Figure 1.13, concentrations above 20 wt%, which is relatively high, were obtained in LiCl/DMAc solvent at 90°C. However, temperatures over 70°C caused degradation that decreased the viscosity. Highly viscous solutions of silk fibroin with LiCl/DMAc and LiCl/DMF were not altered even after one year of storage. Dense but transparent films were cast from these solutions by coagulating in alcohol (ethanol or methanol) bath [76].

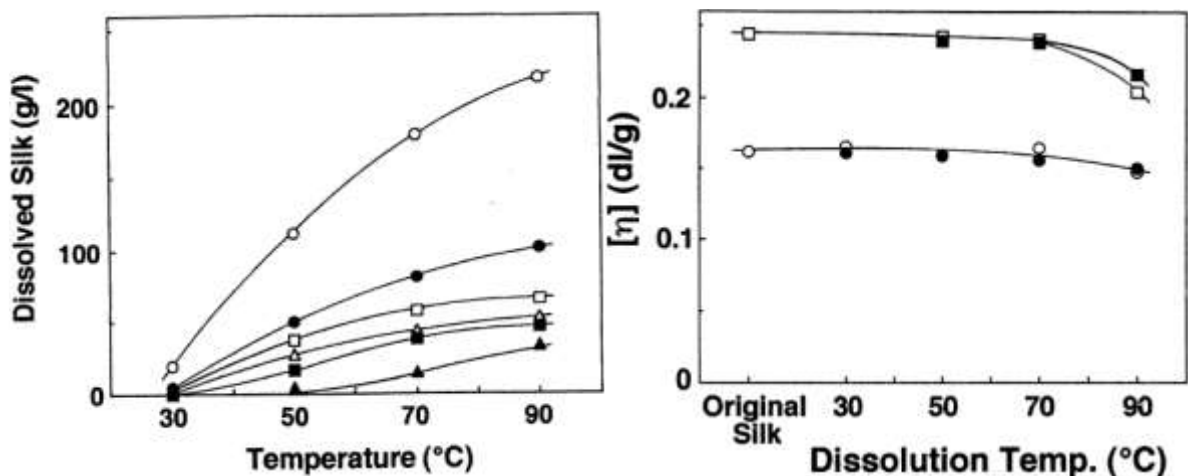


**Figure 1.13.** Effect of dissolution temperature on silk fibroin dissolved in lithium halide/organic amide solvent systems: ○, in LiCl/DMAc; ●, in LiBr/DMAc; △, in LiCl/DMF; ▲, in LiBr/DMF; □, in LiCl/NMP; ■, in LiBr/NMP. Dissolved at  $[LiX] = 1.86$  mol/l in 1 h. Adapted with permission from [76]. Copyright 2016, The Japanese Society of Sericultural Science

The solubility of silk fibroin in LiCl/DMAc solvent system occurs through the solvent ions interacting with functional groups of the fibroin macromolecules. Comparable to the cellulose dissolution in this system, it is presumed that the hydrogen bonds in the fibroin are disrupted due to the nucleophilic attack by the anion [70]. The solvent ions rupture the hydrogen bonds between the polymer chains by interacting with polar and charged groups of pendant chains of fibroin [77]. This structural change of fibroin could contribute to formation of novel hydrogen bonding with cellulose in the same solvent system.

Marsano et al. [78] studied wet and dry-jet wet spinning of the blend solution of cellulose/silk fibroin (CE/SF) in LiCl/DMAc solvent system. The blending ratio of cellulose to silk fibroin was 70/30 (w/w) and the total polymer concentration ( $C_p$ ) was 5–9 wt%. Using a 100  $\mu\text{m}$  spinneret orifice, the blend solution was pumped into a coagulation bath (25°C) at an extrusion speed of 7.9 m/min. Monofilaments were spun at draw down ratios ( $D_r$ ) from 1 to 3 and collected on a set of spools then washed in the selected coagulant for 3–4 days to remove

all LiCl salt residue. Water and ethanol were the two coagulants compared in terms of their effect in the resulting blend fiber.

Water had a solubilizing effect for silk fibroin in the spinning dope thus decreased the protein content of the blend fiber. Ethanol, on the other hand, performed better for the blend fibers with almost no loss of protein. As seen on SEM images in Figure 1.14, the blend fiber coagulated in ethanol possessed a smooth surface, a round-like cross section and no phase separation. Furthermore,  $C_p = 9$  wt% increased the viscosity of the blend solution enough to extrude through an air gap before the coagulation bath turning the method into dry-jet wet spinning. Therefore, the resulting blend fibers had a perfectly round cross section exhibiting no phase separation, no micro-voids, and no micro-fractures at macroscopic scale [78].

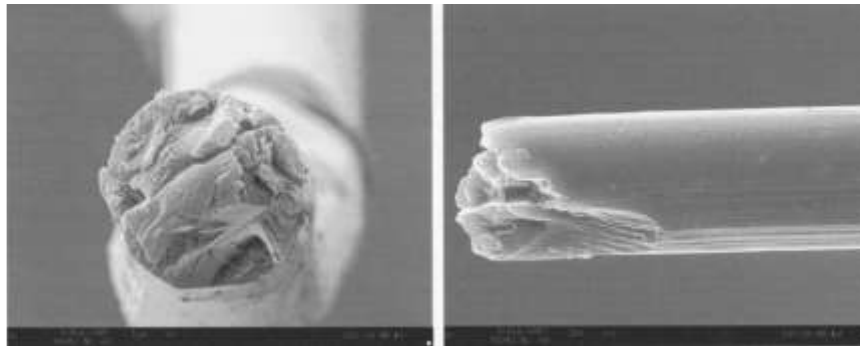


**Figure 1.14.** SEM images of the CE/SF blend fiber ( $C_p = 7$  wt% and  $D_r = 2$ ). Adapted with permission from [78]. Copyright 2016, John Wiley and Sons

X-ray analysis (Figure 1.15) of the blend fibers in comparison with the cellulose fiber showed an amorphous structure and suggested a homogeneous distribution of the protein domains into the cellulose matrix [78].

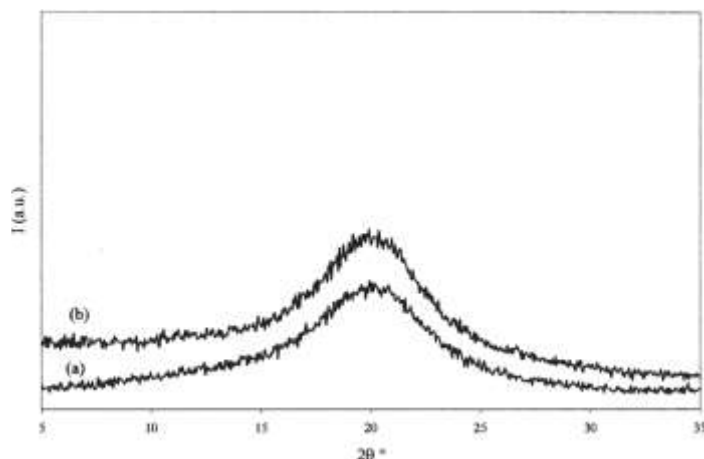


**Figure 1.15.** WAXD analysis of (a) CE and (b) CE/SF blend fibers ( $C_p = 7$  wt% and  $D_r = 2$ ). Adapted with permission from [78]. Copyright 2016, John Wiley and Sons

The diameters of the blend fibers with  $C_p = 9$  wt% were between 21.6 and 32.7  $\mu\text{m}$ . Increasing the  $D_r$  from 1 to 2 resulted in smaller diameters and adding an air gap ( $h = 20$  mm) at  $D_r = 1$  ended in even further decrease. Even though the elastic modulus of the fibers ( $\sim 13$  GPa) remained the same, the tenacity and the elongation of the blend fibers significantly improved due to the air gap. This suggested more orientation and less defects in the final fiber structure. It must be also highlighted that the wet-spun blend fibers had nearly the same modulus ( $\sim 16$  GPa) as the cellulose fibers with lower concentration in similar spinning conditions. The tenacity (179 MPa) and the elongation (3.4%) were, however, lower than that of the cellulose fiber (243 MPa and 13.5%, respectively) [78].

LiCl/DMAc system performed well in blending cellulose and silk fibroin to produce their blend fibers. Compared to viscose process, the miscibility and the compatibility of the two polymers were clearly improved since the system used to dissolve both of the polymer. No other protein reported to blend with cellulose in this solvent system. Additionally, the pre-activation step and high temperature requirement are the overall disadvantages for this system compared to other direct solvents.

## 1.5 N-Methylmorpholine N-Oxide and Water

The success of N-Methylmorpholine N-Oxide (NMMO) is based on the strong N–O dipoles forming hydrogen bonds with –OH groups of cellulose [79]. It can simply be yielded by oxidizing N-methylmorpholine (synthesized from ethylene oxide and ammonia) with hydrogen peroxide. Its melting point is 170°C that is dropped to 74°C for NMMO monohydrate (13.3 wt% H<sub>2</sub>O) to increase its dissolving power. Aqueous solutions of NMMO can dissolve cellulose with no derivatization, complexation or special activation involved [80]. NMMO–water system simply swells cellulose by diffusing into its fiber matrix. Then, fragmentation into rod like segments occurs through breaking intermolecular hydrogen bonding followed by formation of new ones between NMMO and cellulose chains [10].

Johnson's work [81] on NMMO was about not only the dissolution of cellulose, but also the solubility of other natural and synthetic polymers that are characterized by intermolecular hydrogen bonding. Such natural polymers including wool, silk, hair, feathers,  $\beta$ -amylose, casein, zein, gelatin, gum arabic, lignin and such synthetic polymers including nylon were all mentioned in his patent. He later filled another one that covers the blending of cellulose in NMMO with other polymers by using a diluent, e.g. dimethyl sulfoxide (DMSO), N-methylpyrrolidone or sulfolane, to decrease the viscosity. These polymers include gelatin, starch, gum arabic, some vinyl polymers and polyanhydroglucoses [82].

NMMO–water system was found to solubilize solely proteins (either fibrous or globular) that could be processed into different final forms, such as fibers, films, membranes, coatings and particles. For instance, 6–30 wt% collagen, a major fibrous protein, was dissolved in NMMO monohydrate in order to use as edible food casing [83]. Silk fibroin, a well-known fibrous protein, was particularly studied by different groups of researchers to obtain

concentrations from 6 to 36 wt% in aqueous NMMO. A process that is very similar to the dissolution of cellulose at relatively lower temperatures was successfully applied. It was also suggested that the same forces as in the dissolution mechanism of cellulose drive the dissolution of silk fibroin in NMMO-water system [84-87]. Figure 1.16 illustrates the swelling and dissolution of degummed silk fibers (silk fibroin) in NMMO monohydrate. The fibers were swollen at 100°C and almost completely dissolved at 120°C with barely visible birefringent silk left. However, a transparent solution of silk fibroin was not achievable and the degradation of silk fibroin was also experimentally observed above 100°C [84].

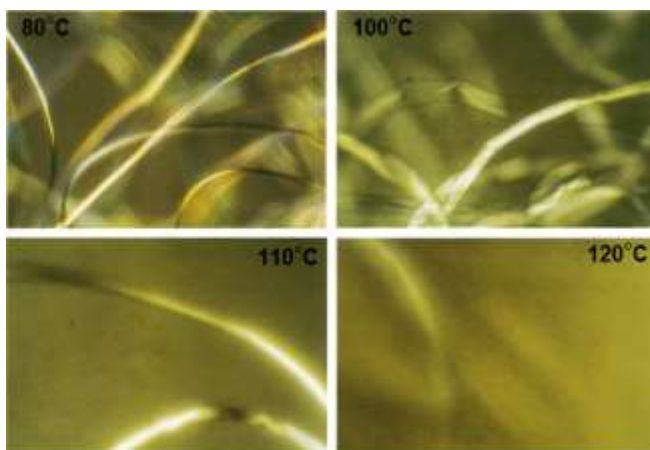


**Figure 1.16.** Polarized optical microscopy images (200X) of silk fibroin dissolving in NMMO·1.0H<sub>2</sub>O at different temperatures. Adapted with permission from [84]. Copyright 2016, Elsevier

Sashina et al. [86] reported the data in Table 1.1 showing the solubility of silk fibroin in aqueous NMMO with less than 10 wt% water, which is equal to the molar compositions of NMMO·0.8H<sub>2</sub>O. The authors obtained clear yellowish solutions of silk fibroin with 5 and higher wt% polymer concentrations. Although a detailed study of the dissolution of silk fibroin in the mixtures of NMMO with organic solvents was also included, the degradation of the polymer at any extent was not investigated.

**Table 1.1.** Solubility of silk fibroin in NMMO with varying water content. Adapted with permission from [86]. Copyright 2016, Springer

<b>Water content in NMMO (wt%)</b>	<b>Molar composition of the solvent</b>	<b>T<sub>d</sub> (°C)</b>	<b>Fibroin concentration in the solvent (wt%)</b>
13.3	NMMO·1.0H <sub>2</sub> O		Insoluble
11.5	NMMO·0.85H <sub>2</sub> O		Insoluble
10.6	NMMO·0.77H <sub>2</sub> O	120	≥ 6
8.4	NMMO·0.6H <sub>2</sub> O	> 120	≥ 6
4.4	NMMO·0.3H <sub>2</sub> O	> 120	≥ 6

In contrast to regular silk fibroin obtained by degumming silk fiber, regenerated silk fibroin can easily form homogeneous solutions with NMMO monohydrate. The silk fibroin, regenerated from aqueous LiBr solution in at least one-day processing, was amorphous and thus soluble in NMMO·1.0H<sub>2</sub>O at high temperatures. The polymer concentrations between 10 and 25 wt% was attained and spun into fibers coagulated in an alcohol bath [87,88]. Even though the resultant fibers were comparable to the others dissolved in salt containing solvents, the dissolution and processing of silk fibroin became multi-stepped and time consuming.

Solubility of globular proteins in NMMO was pointed out in the patent of Buerger et al. [89] to produce various shaped articles. Casein, zein and ardein (peanut protein) were optionally used globular proteins that were crosslinked either before by Lewis acids or after by acetylation, aldehyde treatment, etc. Furthermore, proteins along with synthetic polymers, oils, fats, waxes, dyes, etc. that could contribute functionality to Lyocell fibers by coating were patented by Schuster et al. [90] at Lenzing AG.

Firgo et al. [91] at Lenzing AG added gelatin into NMMO-water-cellulose solution in order to decrease and to control the fibrillation properties. Stall and Turbak [92] at Alfacel S.A.

also used gelatin to slow down and to control the rapid precipitation of cellulose from NMMO solution. Weigel et al. [93] studied NMMO solubility of various proteins that are soluble in different media: Water-soluble proteins (gelatin), acidic media-soluble ones (collagen), ethanol-soluble ones (zein), and alkali soluble ones (soy protein) did not form true solutions but colloidal ones. Nevertheless, the proteins blended with cellulose were able to form homogenous solutions that could be spun. These solutions were used to produce tubular films for food packaging. Similarly, Gord et al. [94] cast chewable films containing cellulose, a protein (preferably natural globular proteins), and a filler from NMMO monohydrate. In addition, there have been a few reports on cellulose/silk fibroin blends coagulated from an alcohol–water mixture in the form of fibers with improved mechanical and thermal properties compared to the sole cellulose compound [85,95]. The compatibility studies by thermal analysis showed strong interactions between the two polymers in their blend from NMMO-water system [96].

A further study by Marsano et al. [95] focused on the same blend fibers that were spun from the blend solutions prepared from another co-solvent, NMMO-water. As mentioned earlier, regenerated silk fibroin by using LiBr could be easily regenerated again by using NMMO-water system. Therefore, the authors reported fibers from 100% silk fibroin and 100% cellulose as well as the blend solutions at 3 compositions: 75/25, 50/50, and 25/75 CE/SF.  $C_p$  was 17 wt% and ethanol was used as the coagulant. The extrusion speed was 4 m/min and the diameter of spinneret was again 100  $\mu\text{m}$  but the height of air gap was 100 mm that was five time longer than the previous setup. The resulting fibers with applied  $D_r$  of 1, 3 and 6 were collected on a spool then were kept in ethanol for 3 days to remove residual NMMO.

Compared to the blend fibers from LiCl/DMAc system, the ones from NMMO-water formed a two-phase morphology. The authors explained the two-phase system from the results of FTIR, DSC and WAXD analyses in addition to the SEM images of the blend films. The phase separation observed in the film cross sections was hypothesized for the blend fibers of all composition. It was essentially concluded that the polymers were not miscible in NMMO-water system [95].

Although the polymers were immiscible, their blend solutions were spinnable. Their blend fibers were obtained with different  $D_r$  on a dry-jet wet spinning line. The results for the Young's modulus and tenacity of all fibers with applied  $D_r = 3$  were graphed in Figure 1.17 to show the trend in increasing amount of cellulose. Regardless of the miscibility issue, there is a close linear behavior of the mechanical properties between the two polymers. The blend fiber with 25% fibroin content possessed moderately higher tenacity (stress at break) and slightly higher modulus than the cellulose fiber. These results suggest a particular interaction between the two polymer domains indicating a proper compatibility [95].

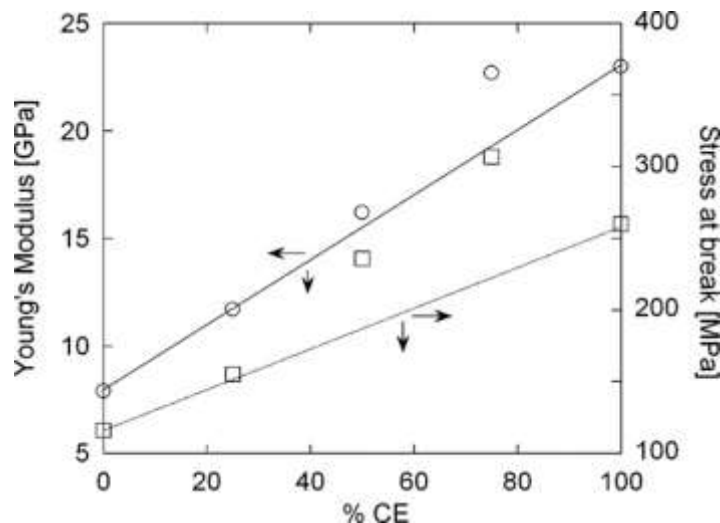


**Figure 1.17.** Variation of Young's modulus (○) and stress at break (□) by increasing CE content for CE/SF blend fibers at  $D_r = 3$ . Adapted with permission from [95]. Copyright 2016, Elsevier

Heinemann and Taeger [85] from Thuringisches Inst. Textile Inc. patented similar CE/SF blend fibers in Germany much earlier than the study of Marsano et al. [95]. The English translation of the patent is accessible and describes sufficient details about the preparation of the blend solutions but not the properties of the obtained blend fibers.

Although they are different in the composition of blend solutions and the spinning conditions, the CE/SF blend fibers processed by NMMO/water system showed overall better mechanical properties than those produced from LiCl/DMAc system. On the other hand, cellulose and silk fibroin were not completely miscible in NMMO/water and their compatibility in this system is comparable to LiCl/DMAc.

While NMMO is an excellent direct solvent for cellulose, it appeared that blending with proteins contributed to the fibrillation problem of Lyocell fibers. This approach also facilitated some modifications and enhancements in the blend materials. However, the disadvantages of NMMO, such as demand for high temperature, the high cost, byproducts, and the degradation of the polymers, are the driving force for investigating other solvents for both cellulose and proteins.

## **1.6 Aqueous Alkali and Aqueous Alkali/Urea**

Mercerization that causes the change in crystal structure from cellulose I to cellulose II by reforming the hydrogen bonding is an important process that could also be tailored to further modify and to dissolve cellulose. The polymer is only partially solvable in 10% aqueous NaOH and the amount of solubility can vary depending on the molecular weight and the type of crystal structure [97]. Using additives, such as urea [98] and/or thiourea [99,100] improved the dissolving power of NaOH-water system. The dissolution mechanism of cellulose in aqueous NaOH/urea system was investigated by analytical techniques, e.g., NMR ( $^{13}\text{C}$ ,  $^{15}\text{N}$ , and  $^1\text{H}$ ),

FTIR, X-Ray and neutron scattering [101-103]. The analytical results indicated that the hydrates of NaOH can establish hydrogen bonding with cellulose chain at low temperatures. At the same time, aqueous NaOH/cellulose complex was surrounded by urea molecules shielding it from other cellulose chains in order to prevent polymer aggregation [12].

Freeze thawing is the commonly applied method to dissolve cellulose in aqueous solution of 7 wt% NaOH/ 12 wt% urea system. Cellulose (4 wt%) is mixed with the solvent that is already cooled down to  $-12^{\circ}\text{C}$  at which its dissolution occurs within 2 minutes [102]. Subsequently, the resultant polymer solution is precipitated to regenerate cellulose in coagulants, such as diluted acids (acetic acid or  $\text{H}_2\text{SO}_4$ ), ethanol, *t*-butanol, acetone,  $\text{Na}_2\text{SO}_4$ ,  $(\text{NH}_4)_2\text{SO}_4$ , and water [104,105]. This solution, however, is relatively unstable and sensitive to polymer concentration, temperature, and storage time [34,106,107]. Moreover, potassium hydroxide (KOH) and lithium hydroxide (LiOH) can substitute for NaOH in cellulose dissolution. Addition of urea enhances these systems' dissolving power and makes NaOH/urea much superior than KOH/urea but inferior than LiOH/urea. Overall, aqueous solutions of NaOH and LiOH with the additive induce faster dissolution of cellulose compared to that of KOH [12,108].

A group of researchers from Institute of Biopolymers and Chemical Fibers (IBWCh), Łódź, Poland, studied cellulose-based blends with different proteins that are all soluble in aqueous alkaline solutions. For instance, 6.5 wt% bio-modified cellulose ( $\text{DP}_v=670$ ) obtained from enzymatically treated cellulose pulp was dissolved in 10 wt% NaOH and blended with regenerated silk fibroin. To enable the dissolution of silk fibroin in aqueous alkali, the polymer was processed for more than 6 days: It was first degummed from silk cocoons, and then dissolved in saturated LiBr solution. It must be recalled that a very similar process was also

applied for the dissolution of silk fibroin in NMMO-water system. Later, 10 wt% regenerated silk fibroin is solubilized in 5 wt% NaOH and the blend solutions were prepared at the compositions of cellulose to the fibroin: 98:2, 95:5, 90:10 and 85:15. The increasing fibroin content induced gradual decrease in the dynamic viscosity: 9.950 cP for the cellulose solution dropped down to 8.200 cP with addition of 15% silk-fibroin in the blend solution (Figure 1.18). The solutions were used to form blend fibers by wet spinning process lined up with a coagulation bath containing sulfuric acid ( $100 \text{ g/dm}^3$ ) and ammonium sulfate ( $450 \text{ g/dm}^3$ ) [109]. It is important to note that the choice of cellulose type and the use of regenerated silk fibroin enabled the polymers to blend in aqueous NaOH. This made the blending process multi-stepped and time-consuming. In addition, the percentage of silk fibroin higher than 15% could not be examined due most likely to the anticipated viscosity decrease.

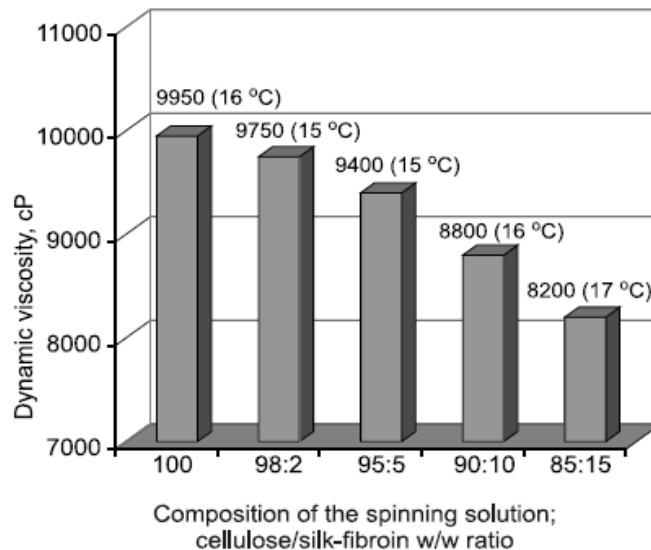


**Figure 1.18.** The dynamic viscosity of the spinning dope versus its composition; the temperatures of viscosity measurements are included in the parentheses adjacent to the viscosity values; the  $C_p$  of dopes were 6.5 wt% (100:0), 6.63 wt% (98:2), 6.83 wt% (95:5), 7.15 wt% (90:10), and 7.48 wt% (85:15). Adapted with permission from [109]. Copyright 2016, IBWCh

The blend solutions were extruded at 15 m/min and the resulting fibers were drawn in air at  $D_r = 30\%$ . The fibers were further washed by water and ethanol to remove the residues of coagulants. The blend fibers were formed with about 10% loss of silk fibroin from the corresponding solutions. This was referred to the peptide fractions due to a partial degradation during the extraction of the fibroin. The SEM images of the blend fibers showed no phase separation and distorted cylindrical cross-sections, which is typical for wet-spun cellulose fibers. However, the authors suggested that the shape of cross-section was a result of the weak coagulation properties of cellulose in ammonium sulfate that was good for silk fibroin. Even though the  $C_p$  of the solutions was increased by addition of more silk fibroin, the viscosity decreased gradually as shown in Figure 1.18. As one can expect, the tenacity of the resulting fibers was also affected correspondingly (Figure 1.19). Despite decreasing tenacity, the elongation of the fibers was improved by an increasing silk fibroin content. In other words, blending silk fibroin with cellulose made the cellulose fibers more flexible [109].

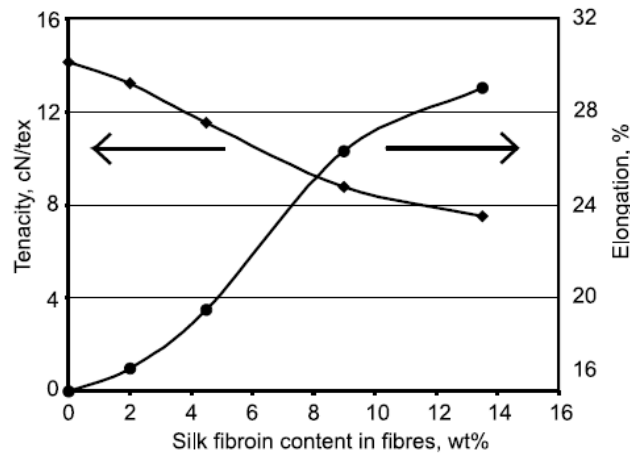


**Figure 1.19.** The tenacity and the elongation of CE/SF fibers by increasing silk fibroin content. Adapted with permission from [109]. Copyright 2016, IBWCh

It can be concluded that the CE/SF blend fibers produced with the aqueous alkali system showed good miscibility and compatibility. Compared to the CE/SF blend fibers by

LiCl/DMA and NMMO-water systems, the ones by this system had more elongation by addition of more silk fibroin. Moreover, the blend fibers with 2–9% silk-fibroin content were characterized by tensile properties suitable for their further processing towards wound dressing materials [109].

Cellulose/keratin biocomposite fibers were also studied in the same research institute as the CE/SF blend fibers from aqueous alkali. Keratin extracted from chicken feathers was first suspended in alkaline solution and then mixed with the bio-modified cellulose solutions at different proportions. Following similar processing conditions to their previous report, cellulose/keratin fibers with up to 48% protein content were formed. As expected, adding the protein suspension resulted in two-phase morphology observed on the cross-section of fibers. Furthermore, these fibers were characterized by their enhanced sorption properties, higher hygroscopy, and a smaller wetting angle than the cellulose fibers. The tensile properties of cellulose fibers lessened by addition of keratin, and yet, applicable fibers were attained as composite fibrous materials from biodegradable polymers. As seen in Figure 1.20, the total biodegradation of fibers was achieved in 3 weeks [110].



**Figure 1.20.** Biodegradation of cellulose and cellulose/keratin composite fibers by composting. Adapted with permission from [110]. Copyright 2016, IBWCh

The researchers at the IBWCh also utilized an alkali soluble cellulose ( $DP_w = 346$ ) pulp (hydrothermally treated at 100–200°C) that was dissolved in 10.2% NaOH with added zinc oxide (for antibacterial purposes) between 2 and 12°C. It was later blended with the alkaline solutions of proteins derived from rape and sunflower seeds. The blend solutions containing 5.15–5.82 wt% cellulose, 0.47–1.26 wt% protein, and 7.16–7.74 wt% aqueous NaOH were used to produce fibers. They were successfully wet-spun using coagulation bath with sulfuric acid and sodium sulfate. Due mainly to the varying  $C_p$ , the tensile properties of blend fibers did not show any trend by the increasing protein content. While the tenacity of blend fibers was inferior to the cellulose fiber, their elongation was slightly higher. The blend fibers had also somewhat higher water retention values and slightly higher LOI than the cellulose fiber. In addition, the zinc content (217.8 mg/kg) in cellulose/sunflower protein fiber showed bacteriostatic activity against *Staphylococcus aureus* bacteria. On the other hand, proteins were largely agglomerated in the blend fibers and thus extensive defects along the fibers' axes occurred [111].

Zhang et al. [112] prepared a solvent from a combination of urea (6.5 wt%), thiourea (8 wt%) and aqueous NaOH (8 wt%) to dissolve 5 wt% cellulose that was blended with soy protein isolate (dissolved in 6 wt% NaOH). On a laboratory-scale wet spinning line, the extrudate was pumped with 0.1 MPa pressure into the coagulating bath containing 10 wt%  $H_2SO_4$  – 12.5 wt%  $Na_2SO_4$  aqueous solution.  $D_r$  of 90%, subsequent washing, and 120% post-drawing were applied along the spinning system. The resulting fibers were dried by a heating roller at 65–80°C and collected on a spool. Although from 10 to 40% protein content was examined in the blend solution, due to high viscosity decrease, only the blend fiber with 10% protein content was successfully spun.

The X-ray analysis showed almost no difference between the cellulose and the blend fibers. Both had the structure of cellulose II. Furthermore, the FTIR spectra in Figure 1.21 indicated the formation of interactions between the two polymers in their blends. The peaks at  $1650\text{ cm}^{-1}$  and  $1545\text{ cm}^{-1}$  were specific to the blend fiber. This suggested the hydrogen bonding between the amide and carbonyl groups of protein and hydroxyl groups of cellulose [112].

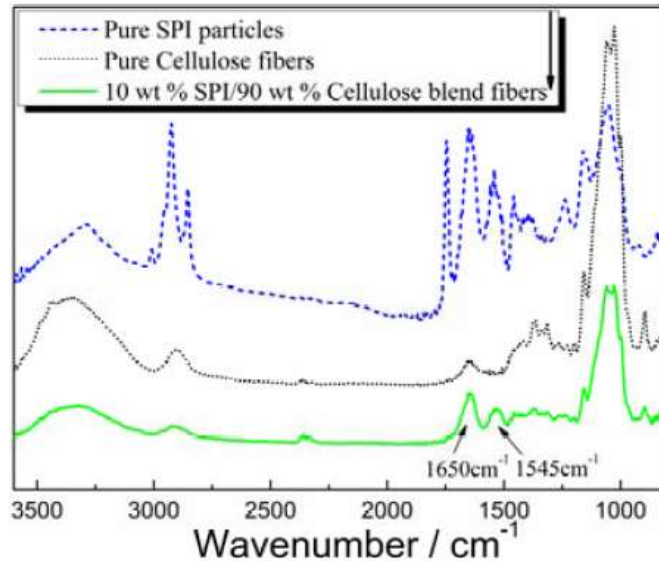


**Figure 1.21.** FTIR spectra of raw SPI, cellulose fiber and CE/SPI fibers. “Reproduced courtesy of Journal of Engineered Fibers and Fabrics, P.O. Box 1288, Cary, North Carolina 27512-1288, USA. Tel: (919) 459-3700 Fax: (919) 459-3701 Internet: [www.jeffjournal.org](http://www.jeffjournal.org).” [112]

The fiber had a round-like cross section and some irregularities were observed along its axis. However, SPI was fragmented into particles on the surface of the fiber indicating a partial phase separation. The authors also reported some micro-voids based on the cross-sections that cannot be clearly seen on the SEM images. In addition, the tenacity and the elongation of the blend fiber were 2.1 g/den and 12.3%, respectively. The corresponding values for the cellulose fiber were 2.05 g/den and 12%. Considering the reported standard deviations of tensile properties, the blend fiber did not differ from the cellulose fiber. However, according to the authors the tensile properties slightly increased by addition of 10% SPI [112].

Compared to the previous solvent systems, alkali/urea system is inexpensive and more ecofriendly [113]. It allows rapid dissolution of cellulose and its blending with alkali soluble proteins. However, the stability and sensitivity of aqueous alkali/urea solvent system towards polymer concentration, temperature and storage are already major concerns for the solubility of cellulose. The cellulose used in some blend solution was either modified or regenerated to facilitate the dissolution in alkaline solvent. In addition, proteins were separately solubilized with usually a different concentration from the same solvent of cellulose, and then were blended with cellulose. Excessive centrifugation and stirring were necessary. The regeneration of blend solution required modification of the coagulation bath. Due to mentioned drawbacks, a simple way of blending the polymers and their regeneration are pending requirements for the co-solvents.

## 1.7 Ionic Liquids

Ionic liquids (ILs) represent a broad group of molten organic salts that are in liquid state below 150°C or most preferably below 100°C [114]. In 1934, Graenacher [115] prepared a solution of cellulose with *N*-alkylpyridinium salts by heating in a liquid base media containing nitrogen, such as pyridine. The novelty of this study was ignored for a long time since the practical value of ILs as a class of solvents was not recognized until the early 2000s. Swatloski et al. [116] reported the dissolution of cellulose up to 25 wt% requiring no pretreatment or activation in 1-butyl-3-methylimidazolium chloride ([C<sub>4</sub>MIm]Cl or [BMIm]Cl) and other hydrophilic ILs. Its regeneration was simply achieved by addition or extrusion into water.

Swatloski et al. [116] discussed the effect of the alkyl substituent (R) of the cation and the anion on cellulose dissolution. Their research showed that ILs are nonderivatizing solvents

for cellulose. ILs containing anions that have strong hydrogen bonding capacity had the highest dissolving power, particularly elevated by microwave heating. However, ILs incorporating non-coordinating anions, such as  $\text{BF}_4^-$  and  $\text{PF}_6^-$ , could not solubilize cellulose. ILs with chloride anions effectively dissolved cellulose, most likely through disrupting and reforming the hydrogen bond network (Figure 1.22). Furthermore, increasing chain length of R reversely affected the solubility of the polymer.

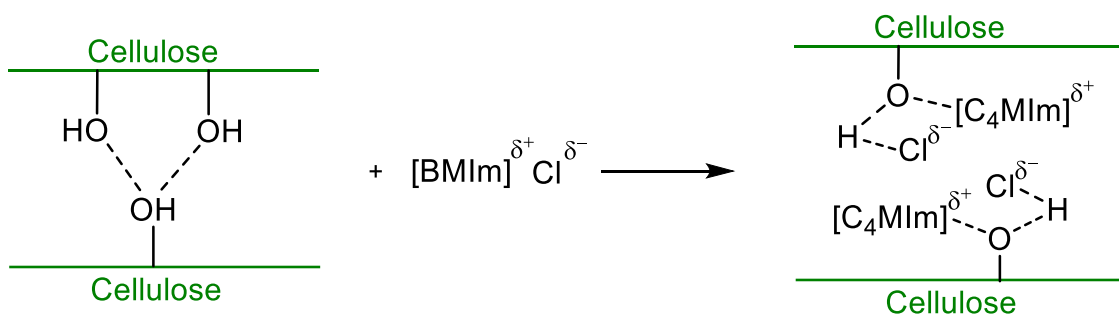


**Figure 1.22.** Suggested dissolution process of cellulose in ILs. Redrawn with permission from [117]. Copyright 2016, Elsevier

Since their report, research on the applications of ILs in natural polymers has made an important progress and thus several other ILs have been developed to dissolve cellulose [118-121] and proteins [122]. Silk fibroin [123-127], keratin [128-130], collagen [124,131,132], zein [133-136], gluten [134], soy protein [137], and gelatin [138] were proven to dissolve in ILs. Most of these ILs have appeared to effectively dissolve and process the biopolymers without causing degradation and emitting gas. They can also be economically recovered and recycled. Interestingly, one type of IL, for instance, 1-butyl-3-methylimidazolium chloride, could dissolve rather different biopolymers [139].

A team of researchers from the US army laboratories worked on the solubility of silk fibroin using  $[\text{BMIm}]\text{Cl}$ ,  $[\text{DMBIm}]\text{Cl}$ , and  $[\text{EMIm}]\text{Cl}$ . They first focused on the dissolving power of  $[\text{BMIm}]\text{Cl}$ : Silk fibroin was dissolved in the solvent at  $100^\circ\text{C}$ , and cooled down to

30°C to analyze crystallinity using wide angle X-ray scattering (WAXS). It was confirmed that [BMIm]Cl disrupted the  $\beta$ -sheet crystalline structure in silk fibroin: Several peaks related to antiparallel  $\beta$ -sheet structure in silk fiber did not appear for so called “amorphous silk/BMIm”. This result in combination with optical microscopy observation (which was not reported) of silk fibroin in the solvent agreed in the dissolution of the polymer [123].

This research was expanded to the solubility of several biopolymers including cellulose, chitin, silk, collagen and elastin. The focus though was mainly on the dissolution of silk fibroin in the selected ionic liquids. Based on their ability to disrupt the hydrogen bonds, imidazolium chlorides were useful solvents for the biopolymers. The cation’s potential for rupturing the bonds enhanced the dissolution of proteins, which did not occur for polysaccharides. Therefore, the dissolving power of [EMIm]Cl was similar to that of [BMIm]Cl in the solubility of cellulose [124].

Recently, Yao et al. [140] studied blend fibers from cellulose and silk fibroin both dissolved in [BMIm]Cl. With a  $C_p$  of 8 wt%, spinning dopes were prepared at CE/SF 100/0, 80/20 and 60/40 by kneading at 90°C. The spinning dopes were extruded at 85°C into ethanol bath (10°C) passing 5 cm air gap at room temperature. The obtained fibers were stretched at  $D_r = 1-5$ . Before drying, the fibers were further washed in ethanol. Although 100% silk fibroin solution was experimented, its viscosity was not high enough to be used for spinning. Similar to other reported CE/SF solutions, the viscosity decreased by addition of silk fibroin.

The CE/SF fibers possessed lower crystallinity than the cellulose fiber both regenerated by using [BMIm]Cl solvent. Consequently, the blend fibers had lower modulus, tensile strength and elongation compared to the cellulose fiber. The author referred the changes in the tensile properties to fibrillar structure of the protein continuously dispersed in cellulose

network. Because amino acids of proteins have intrinsic fluorescence, their phase morphology in the blend fibers (Figure 1.23) was successfully analyzed by laser scanning confocal microscope (LSCM). This technique enabled the researchers to observe the dimension and the distribution of protein phase of the blend fibers. For instance, the radial size of silk fibroin phase was measured 0.5–1.0  $\mu\text{m}$ . In addition, more protein content and higher draw ratio increased the size of the protein phase and hydrogen bonding was observed between the two phases [140].

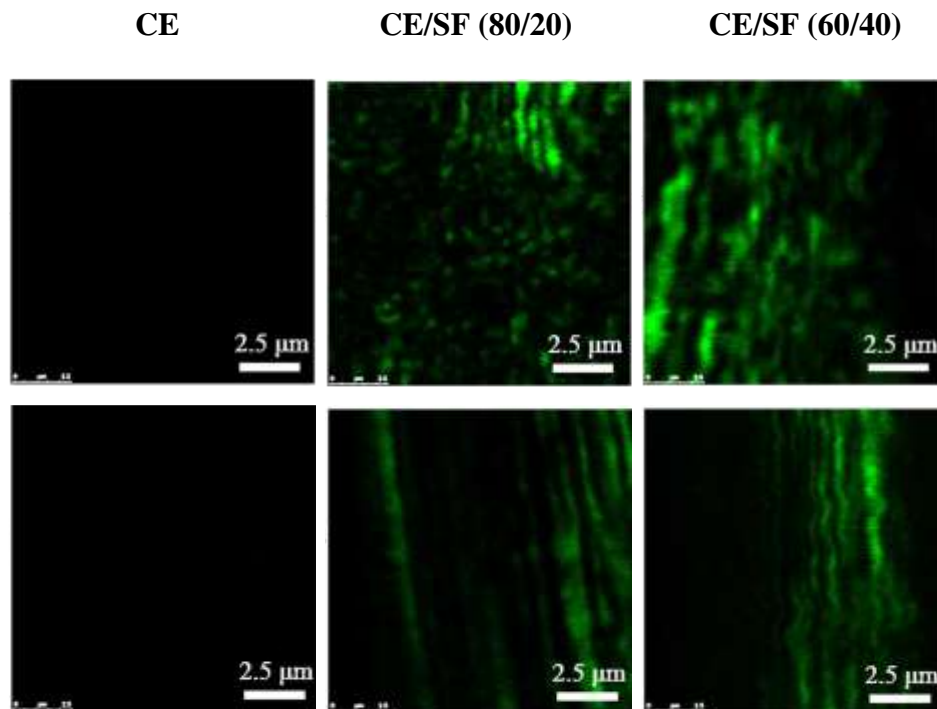


**Figure 1.23.** LSCM micrograph of cellulose and CE/SF fibers along the fiber axes (top row at  $D_r = 3.3$ , bottom row at  $D_r = 4.3$ ). Adapted with permission from [140]. Copyright 2016, Springer

Ionic liquids are direct solvents for both cellulose and proteins. They are very recently introduced and their cost is too high to develop an economic process and application.

## 1.8 Cellulose Derivatives/Protein Blend Fibers

Edible nanofibers were produced from blends of cellulose derivative and egg albumen by electrospinning. Cellulose acetate (20 wt%) and egg albumen (12 wt%) were dissolved in 85% acetic acid and 50% formic acid solution, respectively. The polymer solutions were mixed at three compositions: 9, 23, and 34% protein solution with respect to the cellulose acetate solution. Due to insufficient entanglement and high surface tension of the globular protein in formic acid solution, nanofibers of egg albumen could not be obtained. Incorporation of cellulose acetate and a surfactant (Tween40<sup>®</sup>) enabled the protein to be spun into nanofibers. SEM images revealed that increased protein resulted in nanofibers with smoother surface. Moreover, FTIR confirmed the interaction of both components in the resulting nanofibers. These nanofibers presumably could be used in food packaging and drug delivery applications [141].

In a similar study to edible nanofibers of cellulose acetate and egg albumen (white), the same group of researchers fabricated bicomponent nanofibers: Their core layer was composed of polyethylene glycol (PEG), amoxicillin (model drug) and soybean oil. Their shell layer consisted of blends of cellulose acetate, gelatin and Tween40<sup>®</sup>. The resulting fibers had an average diameter of  $913 \pm 180$  nm. The composition of shell layer was increased from 10 to 30% protein decreased the viscosity of its solution and consequently lessened the thickness of the layer. Overall, the fibers were useful for controlled release of the encapsulated drug along the digestive tract [142].

Amsaveni et al. [143] studied the formation of blend fibers from collagen of animal skin, a cellulose derivative, hydroxyethyl cellulose (HEC), and bovine serum albumin. The fibers were produced on benchtop equipment including a syringe pump and a 0.5 mm needle

attached to a syringe. At a flow rate of 0.5 ml/min, the blend solutions of polymers all dissolved in aqueous acetic acid at different proportions were pumped into a Petri dish containing ethanol and acetone (1:1) solution. The obtained fibers were then transferred into ethyl acetate bath where they were subjected to mild stretching. After drying, the fibers were crosslinked with glutaraldehyde vapor. The blend fibers as shown in Table 1.2 had relatively high linear mass density (fiber denier). The addition of HEC into the protein fibers increased the fiber denier, the tenacity as well as the elongation of the blend fibers. The swelling of blend fibers was also enhanced by more HEC content. In addition, increasing albumen content reduced the surface roughness. Having low tenacity (below 1 g/den), the fibers could find use as bioresorbable materials in wound management and related biomedical applications.

**Table 1.2.** Tensile properties of collagen (C)/hydroxyethyl cellulose (HEC)/albumin (A) fibers. Adapted with permission from [143]. Copyright 2016, Springer

<b>Fiber</b>	<b>Fiber denier</b>	<b>Tenacity (g/den)</b>	<b>Elongation (%)</b>
Collagen	12.5±1.1	0.65±0.05	12.6±1.1
2:1 C:A	16.0±1.3	0.69±0.06	11.4±0.8
1:1 C:A	19.0±1.7	0.72±0.05	13.4±1.2
2:1 C:HEC	16.6±1.5	0.84±0.08	17.2±1.2
1:1 C:HEC	22.5±2.1	0.87±0.09	18.5±1.3
2:1:1 C:HEC:A	20.8±1.8	0.73±0.06	13.0±0.9
2:1:2 C:HEC:A	17.3±1.4	0.69±0.05	13.7±1.2
2:2:1 C:HEC:A	21.2±1.9	0.83±0.07	16.2±1.4
1:1:1 C:HEC:A	24.5±2.2	0.84±0.08	18.1±1.6

Although it is less efficient than using cellulose itself, depending on the derivation of cellulose, a co-solvent could be employed to prepare solution blends of cellulose derivative

and proteins. Consequently, blending the two polymers could become even more complicated than using cellulose without derivatization. However, utilizing cellulose derivative contributed to the formation of nanofibers from proteins, which is a challenge due to their complex polymer structure. Overall, blend fibers from cellulose derivative/proteins can be produced that are especially aimed for biomedical applications.

**Table 1.3.** List of cellulose/protein biofibers reported in the literature

Co-solvent	Protein	$W_{pro}$ (wt%)	Spinning method	Application	Reference
Viscose process	Casein	50	Wet	Fabrics with enhanced properties, such as acid dyeability, permanently crimped, heat-retaining, antimicrobial	[38-50]
	Soy protein				
	Zein				
	Gelatin	20		Acid dyeable and deodorized fabrics	[54]
	Silk fibroin	53		High performance biofiber	[56]
	Keratin	20		Acid dyeable, flame retardant	[51-53, 57-58]
Cuprammonium process	Whey protein	56	Wet	Active ingredients release	[69]
	Egg albumen	23		Biomedicine	[70]
LiCl/DMAc	Silk fibroin	30	Dry-jet wet	High performance biofiber	[79]
NMMO/H <sub>2</sub> O		75			[96]
Aqueous alkali and alkali/urea	Silk fibroin	15	Dry-jet wet	Wound dressing	[110]
	Keratin	48	Wet	Biomedical and hygienic	[111]
	Rape and sunflower protein	19		Antibacterial	[112]
	Soy protein	10		Biomedicine	[113]
Ionic liquid	Silk fibroin	40	Dry-jet wet	High performance biofiber	[141]
Cellulose derivatives	Egg albumen	34	Electro-spinning	Drug release	[142]
	Gelatin	30			[143]
	Collagen	67	Wet	Biomedicine	[144]

Note:  $W_{pro}$  is the maximum protein content in the blend solution formed with cellulose.

## 1.9 Concluding Remarks

Various blends of cellulose and proteins listed in Table 1.3 was studied using different solvents and processing methods. Except viscose process and cellulose derivatives, all solvent systems used similar blending methods. Depending on the system, the both polymers could be dissolved separately prior to mixing their solutions at varying compositions. Some systems required pretreatment or chemical modification of the polymers. Some dissolved them at different conditions or used the same conditions to facilitate their processing. For instance, Yao et al. [140] used an ionic liquid (BMImCl) was used for dissolution of cellulose and silk fibroin together to prepare blended polymer solutions. In particular, proteins showed similar dissolution mechanism to cellulose in direct solvents.

Producing strong regenerated protein fibers has been a challenge. Therefore, blending proteins with cellulose is found to overcome this issue. The blend fibers with a relatively low protein content possessed comparable tensile strength to the cellulose fibers. However, higher protein content decreased their strength due to the viscosity drop in their blend solutions. In general, the blend fibers showed intermolecular interactions and two-phase morphology. Furthermore, blending cellulose with proteins added some functionalities, such as acid dyeability, flame retardancy, antibacterial activity, shorter biodegradation, edibility.

## 1.10 References

1. Kelly RJ, Ali MA, Roddick-Lanzilotta AD, Worth G, Hassan MM, McLaughlin JR, McKinnon AJ (2008) Composite materials containing keratin. US Patent 7,767,756, 3 Jan 2008
2. Vincent JFV, Shewry PR, Tatham AS, Bailey AJ (2003) Mechanical applications of elastomeric proteins -A biomimetic approach. In: Shewry PR, Tatham AS, Bailey AJ (eds)

Elastomeric proteins: structures, biomechanical properties, and biological roles. Cambridge University Press, New York, pp 352-365

3. Zhou Z, Zheng H, Wei M, Huang J, Chen Y (2008) Structure and mechanical properties of cellulose derivatives/soy protein isolate blends. *J Appl Polym Sci* 107 (5):3267-3274

4. Klemm D, Heublein B, Fink HP, Bohn A (2005) Cellulose: fascinating biopolymer and sustainable raw material. *Angew Chem Int Ed Engl* 44 (22):3358-3393

5. Turbak AF, Hammer RB, Davies RE, Portnoy NA (1977) A critical review of cellulose solvent systems. In: Turbak AF (ed) *Solvent spun rayon, modified cellulose fibers and derivatives*, vol 58. ACS Symposium Series. American Chemical Society, Washington, D.C., pp 12-24

6. Hudson SM, Cuculo JA (1980) The solubility of unmodified cellulose: A critique of the literature. *J Macromol Sci Rev Macromol Chem Phys* C18 (1):1-82

7. Kotek R (2002) Regenerated cellulose fibers. In: Lewin M (ed) *Handbook of fibre chemistry*, vol 16. 3 edn. CRC Press, Boca Raton, FL, pp 667-771

8. Nevell TP, Zeronian SH (1985) Cellulose chemistry fundamentals. In: Nevell TP, Zeronian SH (eds) *Cellulose chemistry and its applications*. Halsted Press, New York, pp 15-29

9. Wang Y, Zhang L, Yu L (2009) Blends and composites based on cellulose and natural polymers. In: Yu L (ed) *Biodegradable polymer blends and composites from renewable resources*. John Wiley & Sons, Inc, Hoboken, NJ, pp 129-161

10. Wertz J-L, Bédué O, Mercier JP (2010) *Cellulose science and technology*. EPFL Press, Lausanne, Switzerland

11. Belgacem MN, Gandini A (2011) Production, chemistry and properties of cellulose-based materials. In: Plackett D (ed) Biopolymers-new materials for sustainable films and coatings. John Wiley & Sons, Inc, West Sussex, UK, pp 151-178
12. Olsson C, Wesman G (2013) Direct dissolution of cellulose: background, means and applications. Cellulose - Fundamental aspects. InTech, Online
13. Rowland SP, Bertoniere NR (1985) Chemical methods of studying supramolecular structure. In: Nevell TP, Zeronian SH (eds) Cellulose chemistry and its applications. Ellis Horwood Limited, West Sussex, England, pp 112-137
14. Pinkert A, Marsh KN, Pang S, Staiger MP (2009) Ionic liquids and their interaction with cellulose. Chem Rev 109 (12):6712-6728
15. Gilbert RD, Kadla JF (1998) Polysaccharides - Cellulose. In: Kaplan DL (ed) Biopolymers from renewable resources. Springer, New York, pp 47-95
16. Winkworth-Smith C, Foster TJ (2013) General overview of biopolymers: structure, properties, and applications. In: Thomas S, Durand D, Chassenieux C, Jyotishkumar P (eds) Handbook of biopolymer-based materials: from blends and composites to gels and complex networks. Wiley-VCH, Weinheim, Germany, pp 7-36
17. Hon DNS (1994) Cellulose: a random walk along its historical path. Cellulose 1 (1):1-25
18. Sangwatanaroj U (1995) The mechanism of dissolution of cellulose in the ammonia/ammonium thiocyanate solvent. Dissertation/Thesis, North Carolina State University, Raleigh NC
19. Isogai A (1994) Allomorphs of cellulose and other polysaccharides. In: Gilbert RD (ed) Cellulosic polymers, blends and composites. Hanser, Munich, Germany, pp 1-24

20. Isogai A, Usuda M, Kato T, Uryu T, Atalla RH (1989) Solid-state CP/MAS carbon-13 NMR study of cellulose polymorphs. *Macromolecules* 22 (7):3168-3172
21. Ciolacu D, Popa VI (2010) Cellulose allomorphs: Structure, accessibility and reactivity. *Polymer Science and Technology*. Nova Science Publishers, New York
22. French AD, Bertoniere NR, Brown RM, Chanzy H, Gray D, Hattori K, Glasser W (2002) Cellulose. In: Mark HF, Kroschwitz JI (eds) *Encyclopedia of Polymer Science and Technology*, vol 5. 3 edn. John Wiley & Sons, Inc, Hoboken, NJ, p 473. doi:10.1002/0471440264.pst042
23. Aminuddin N (1998) Ammonia/ammonium thiocyanate - cellulose system: dissolution, viscoelastic behavior and fiber formation. Dissertation, North Carolina State University, Raleigh NC
24. Butler MM, McGrath KP (1998) Protein-based materials. In: Kaplan DL (ed) *Biopolymers from renewable resources*. Springer, New York, pp 177-194
25. McMurry J (2007) *Organic Chemistry*. 7 edn. Cengage Learning, Belmont, CA
26. Saechtling H (1995) *Saechtling international plastics handbook: For the technologist, engineer, and user*. 3 edn. Hanser, Munich, Germany
27. Kruszewska I (1997) Clean production action report of greenpeace international toxic campaign. Greenpeace, Amsterdam, The Netherlands
28. Jane J, Lim S, Paetau I, Spence K, Wang S Biodegradable plastics made from agricultural biopolymers. In: Fishman M, Friedman R, Huang S (eds) *Symposium on Polymers from Agricultural Coproducts*, at the 206th National Meeting of the American-Chemical-Society, Chicago, IL, 1994. ACS Symposium Series. American Chemical Society, pp 92-100

29. Guilbert S, Cuq B (2005) Material formed from proteins. In: Bastioli C (ed) Handbook of biodegradable polymers. Rapra Technology Limited, Shropshire, UK, p 339
30. Stevens MP (1999) Polymer chemistry: An introduction. 3 edn. Oxford University Press, New York
31. Vaz CM, Cunha AM (2007) Soy-based materials for drug release applications. In: Fakirov S, Bhattacharyya D (eds) Handbook of engineering biopolymers: Homopolymers, blends and composites. Hanser, Munich, Germany, p 465
32. Bettelheim FA, Brown WH, Campbell MK, Farrell SO, Torres OJ (2012) Introduction to general organic and biochemistry. 10 edn. Brooks/Cole Cengage Learning, Belmont, CA
33. Sionkowska A, Lewandowska K, Planecka A, Szarszewska P, Krasinska K, Kaczmarek B, Kozłowska J (2014) Biopolymer blends as potential biomaterials and cosmetic materials. Key Eng Mater 583:95-100
34. Libert TF Cellulose solvents-remarkable history, bright future. In: Libert TF, Heinze TJ, Edgar KJ (eds) 235th American-Chemical-Society National Meeting, New Orleans, LA, 2010. ACS Symposium Series. American Chemical Society, pp 3-54
35. Woodings C (2002) Cellulose fibers, regenerated. In: Mark HF, Kroschwitz JI (eds) Encyclopedia of Polymer Science and Technology, vol 5. 3 edn. John Wiley & Sons, Inc, Hoboken. NJ, p 532
36. Wilkes AG, Woodings C (2001) The viscose process. In: Regenerated cellulose fibres. Woodhead Publishing Limited, Cambridge, England, pp 37-61
37. Chavassieu HLJ (1910) Process of obtaining proteo-cellulosic products. US Patent 950,435, 22 Feb 1910

38. Attwater R, Heinemann A (1926) Improved Artificial Textile Fibre and the Process of the Manufacturing of same. GB Patent 255,623, 29 Jul 1926
39. Esselmann P, Kosslinger K, Bitterfeld WK (1936) Manufacture of artificial silk. US Patent 2,059,632, 3 Nov 1936
40. D'Ambrosio A, Corbellini A (1939) Improvements in or Relating to the Manufacture of Artificial Spinnable Material from Mixed Solutions of Protein and Viscose. GB Patent 511,700, 23 Aug 1939
41. Koch T (1944) Manufacture of rayon. US Patent 2,345,345, 28 Mar 1944
42. Nicoll WD (1950) Process for producing artificial filaments. US Patent 2,515,889, 18 Jul 1950
43. Kanegafuchi Spinning CL (1966) Method for producing composite protein-cellulose fibres. GB Patent 1,025,798, 14 Apr 1966
44. Mahomed RS (1966) Improvements in and relating to viscose rayon filaments. GB Patent 1,029,838, 18 May 1966
45. Itaya M (1969) Study on the viscose fiber grafted with milk casein. Sen'i Gakkaishi 26 (6):286-296
46. Yamazaki F (2001) Antibacterial viscose rayon and its production. JP Patent 2001-003223, 09 Jan 2001
47. Yamazaki F (2001) Viscose rayon having modified feeling. JP Patent 2001-003224, 09 Jan 2001
48. Daiwabo Rayon Co. Ltd. (2016) MILEY "Milk-protein containing viscose rayon". <http://www.daiwabo.co.jp/en/products.html?crd=4>. Accessed 17 Jan 2016

49. Lennox-Kerr P (2000) Milk protein improves rayon. *Advances in Textiles Technology*, vol October. International Newsletters Ltd, UK
50. Yamada M, Ohshima K, Arimochi M, Nakajima K (2004) Spinning dope for cellulose/protein compound fiber and cellulose/protein compound fiber. JP Patent 2004-149953, 24 May 2004
51. Ikeda M, Mukoyama H (1997) Regenerated Cellulosic Fiber Excellent in Dyeability and Its Production. JP Patent 09-241920,
52. Saleh MS (2014) Fibrous protein processing method. US Patent 20140326165, 6 Nov 2014
53. Yamada M, Ohshima K (2009) Method of manufacturing cellulose-gelatin composite viscose rayon filament. US Patent 20090166919, 2 Jul 2009
54. Chua JM (2009) Uniqlo's HeatTech Clothing Created Heat From Your Sweat. <http://www.ecouterre.com/uniqlos-heattech-clothing-creates-heat-from-yoursweat/>. Accessed 17 Jan 2016
55. Hirano S, Nakahira T, Zhang M, Nakagawa M, Yoshikawa M, Midorikawa T (2002) Wet-spun blend biofibers of cellulose–silk fibroin and cellulose–chitin–silk fibroin. *Carbohydr Polym* 47 (2):121-124
56. Li W, Ke G, Li G, Xu W (2015) Study on the structure and properties of viscose/wool powder blended fibre. *Fibres Text East Eur* 23 (1 (109)):26-29
57. Zhou Z, Weiren B, Youbo D, Jinming D (2015) Preparation and characterization of cyclotriphosphazene/keratin/viscose fibers. *Fiber Polym* 16 (3):560-564
58. Schweizer E (1857) Das kupferoxyd-ammoniak, ein auflösungsmittel für die pflanzenfaser. *J Prakt Chem* 72 (1):109-111

59. Browning BL, Sell LO, Abel W (1954) Cellulose solvents for viscosity measurement - The effect of copper and base concentrations in cuprammonium and cupriethylenediamine solutions. TAPPI 37 (7):273-283
60. Börner K, Rossner E, Mahn H, Irion W (1934) Copper-ammonia-fibroin solutions. US Patent 1,955,221,
61. Wakeham H, Toner RK, Jolley HR, Taylor HS (1951) The technical possibilities for a regenerated silk. Text Res J 21 (2):110-115
62. Howitt FO (1955) Silk fibroin as a fibrous protein. Text Res J 25:242-246
63. Happey F, Wormell RL (1949) Regenerated keratin fibres from wool. J Text Inst Trans 40 (12):T855-T869
64. Wormell RL, Happey F (1949) Regenerated keratin fibres. Nature 163 (4131):18
65. Jayme G, Broschinski L (1976) Copper and nickel complex solutions as dissolving media for proteins and cellulose. Cell Chem Technol 10 (6):655-672
66. Akira H, Eisaku I, Rensuke K, Kenji K (2001) Molecularly composite polymeric material of fibroin/cellulose and process for producing the same. WO Patent 2001036531, 25 May 2001
67. Abe K, Murate H, Teramoto A, Nagasse Y (2002) Method for producing keratin-cellulose complex regenerated product and method for recycling keratin- containing fiber product. JP Patent 2002167401,
68. Tomczyńska-Mleko M, Terpiłowski K, Mleko S (2015) Physicochemical properties of cellulose/whey protein fibers as a potential material for active ingredients release. Food Hydrocolloids 49:232-239
69. Tomczyńska-Mleko M, Terpiłowski K, Mleko S (2015) New product development: Cellulose/egg white protein blend fibers. Carbohydr Poly 126:168-174

70. Dawsey TR, McCormick CL (1990) The lithium chloride/dimethylacetamide solvent for cellulose: a literature review. *J Macromol Sci Rev Macromol Chem Phys* 30 (3-4):405-440
71. Dupont A-L (2003) Cellulose in lithium chloride/N,N-dimethylacetamide, optimisation of a dissolution method using paper substrates and stability of the solutions. *Polymer* 44 (15):4117-4126
72. Striegel AM (2003) Advances in the understanding of the dissolution mechanism of cellulose in DMAc/LiCl. *J Chil Chem Soc* 48 (1):73-77
73. Tosh B, Saikia CN, Dass NN (2000) Homogeneous esterification of cellulose in the lithium chloride–N,N-dimethylacetamide solvent system: effect of temperature and catalyst. *Carbohydr Res* 327 (3):345-352
74. McCormick CL, Callais PA, Hutchinson Jr BH (1985) Solution studies of cellulose in lithium chloride and N, N-dimethylacetamide. *Macromolecules* 18 (12):2394-2401
75. Furuhashi K-i, Koganei K, Chang H-S, Aoki N, Sakamoto M (1992) Dissolution of cellulose in lithium bromide-organic solvent systems and homogeneous bromination of cellulose with N-bromosuccinimide-triphenylphosphine in lithium bromide-N, N-dimethylacetamide. *Carbohydr Res* 230 (1):165-177
76. Furuhashi K, Okada A, Chen Y, Xu YY, Sakamoto M (1994) Dissolution of silk fibroin in lithium halide/organic amide solvent systems. *J Seric Sci Jpn* 63 (4):315-322
77. Sashina ES, Bochek AM, Novoselov NP, Kirichenko DA (2006) Structure and solubility of natural silk fibroin. *Russ J Appl Chem* 79 (6):869-876
78. Marsano E, Canetti M, Conio G, Corsini P, Freddi G (2007) Fibers based on cellulose–silk fibroin blend. *J Appl Polym Sci* 104 (4):2187-2196

79. Franks NE, Varga JK (1979) Process for making precipitated cellulose. US Patent 4,145,532, 20 Mar 1979
80. Fink HP, Weigel P, Purz HJ, Ganster J (2001) Structure formation of regenerated cellulose materials from NMMO-solutions. *Prog Polym Sci* 26 (9):1473-1524
81. Johnson DL (1969) Compounds dissolved in cyclic amine oxides. US Patent 3,447,939, 3 Jun 1969
82. Johnson DL (1970) Method of preparing polymers from a mixture of cyclic amine oxides and polymers. US Patent 3,508,941, 28 Apr 1970
83. Gord H, Hammer KD, Melle J (2006) Collagen-based shaped body. WO Patent 2006131285, 14 Dec 2006
84. Freddi G, Pessina G, Tsukada M (1999) Swelling and dissolution of silk fibroin (*bombyx mori*) in N-methyl morpholine N-oxide. *Int J Biol Macromol* 24 (2):251-263
85. Heinemann K, Taeger E (2000) Production of solutions of fibrillar proteins, especially silk, comprises dissolving the protein in N-methylmorpholine N-oxide. DE Patent 19,841,649, 27 Apr 2000
86. Sashina ES, Novoselov NP, Heinemann K (2003) Dissolution of silk fibroin in N-methylmorpholine-N-oxide and its mixtures with organic solvents. *Russ J Appl Chem* 76 (1):128-131
87. Xu Y, Zhang Y, Shao H, Hu X (2005) Solubility and rheological behavior of silk fibroin (*bombyx mori*) in N-methyl morpholine N-oxide. *Int J Biol Macromol* 35 (3):155-161
88. Marsano E, Corsini P, Arosio C, Boschi A, Mormino M, Freddi G (2005) Wet spinning of *bombyx mori* silk fibroin dissolved in N-methyl morpholine N-oxide and properties of regenerated fibres. *Int J Biol Macromol* 37 (4):179-188

89. Buerger H, Taeger E, Eilers M, Berghof K (2004) Protein shaped body and method for the production thereof according to the NMMO method. US Patent 20040046277, 11 Mar 2004
90. Schuster KC, Rous MA, Hainbucher KM, Richardt D, Redlinger S, Firgo H, Kroner G (2012) Functionalized molded cellulose body and method for producing the same. US Patent 20120318169, 20 Dec 2012
91. Firgo H, Seidl S, Bartsch P, Koll B, Mulleder E (1998) Cellulose fibre. US Patent 5,795,522, 18 Aug 1998
92. Stall AD, Turbak AF (1999) Slowing and controlling the rapid precipitation of cellulose from tertiary amine oxide solutions by adding a water soluble polymer having a high molecular weight. US Patent 5,951,933, 14 Sep 1999
93. Weigel P, Fink HP, Doss M, Beckers S, Hendrikx R (2003) Tubular films formed from cellulose/protein blends. US Patent 20030062648, 3 Apr 2003
94. Gord H, Hammer KD, Neeff R, Berghof K, Eilers M, Taeger E, Buerger H (2004) Chewable film containing cellulose. US Patent 20040166209, 26 Aug 2004
95. Marsano E, Corsini P, Canetti M, Freddi G (2008) Regenerated cellulose-silk fibroin blends fibers. *Int J Biol Macromol* 43 (2):106-114
96. Sashina ES, Janowska G, Zaborski M, Vnuchkin AV (2007) Compatibility of fibroin/chitosan and fibroin/cellulose blends studied by thermal analysis. *J Therm Anal Calorim* 89 (3):887-891
97. Kamida K, Okajima K, Matsui T, Kowsaka K (1984) Study on the solubility of cellulose in aqueous alkali solution by deuteration IR and <sup>13</sup>C NMR. *Polym J* 16 (12):857-866

98. Zhang L, Ruan D, Zhou J (2001) Structure and properties of regenerated cellulose films prepared from cotton linters in NaOH/urea aqueous solution. *Ind Eng Chem Res* 40 (25):5923-5928
99. Zhang L, Ruan D, Gao S (2002) Dissolution and regeneration of cellulose in NaOH/thiourea aqueous solution. *J Polym Sci B Polym Phys* 40 (14):1521-1529
100. Jin H, Zha C, Gu L (2007) Direct dissolution of cellulose in NaOH/thiourea/urea aqueous solution. *Carbohydr Res* 342 (6):851-858
101. Egal M, Budtova T, Navard P (2008) The dissolution of microcrystalline cellulose in sodium hydroxide-urea aqueous solutions. *Cellulose* 15 (3):361-370
102. Cai J, Zhang L, Liu S, Liu Y, Xu X, Chen X, Chu B, Guo X, Xu J, Cheng H (2008) Dynamic self-assembly induced rapid dissolution of cellulose at low temperatures. *Macromolecules* 41 (23):9345-9351
103. Qi H, Yang Q, Zhang L, Liebert T, Heinze T (2011) The dissolution of cellulose in NaOH-based aqueous system by two-step process. *Cellulose* 18 (2):237-245
104. Mao Y, Zhou J, Cai J, Zhang L (2006) Effects of coagulants on porous structure of membranes prepared from cellulose in NaOH/urea aqueous solution. *J Membr Sci* 279 (1):246-255
105. Yang Q, Fukuzumi H, Saito T, Isogai A, Zhang L (2011) Transparent cellulose films with high gas barrier properties fabricated from aqueous alkali/urea solutions. *Biomacromolecules* 12 (7):2766-2771
106. Cai J, Zhang L (2006) Unique gelation behavior of cellulose in NaOH/urea aqueous solution. *Biomacromolecules* 7 (1):183-189

107. Qi H, Chang C, Zhang L (2008) Effects of temperature and molecular weight on dissolution of cellulose in NaOH/urea aqueous solution. *Cellulose* 15 (6):779-787
108. Cai J, Zhang L (2005) Rapid dissolution of cellulose in LiOH/urea and NaOH/urea aqueous solutions. *Macromol Biosci* 5 (6):539-548
109. Strobin G, Wawro D, Stęplewski W, Ciechańska D, Józwicka J, Sobczak S, Haga A (2006) Formation of cellulose/silk-fibroin blended fibres. *Fibres Text East Eur* 14 (4 (58)):32-35
110. Wrzesniewska-Tosik K, Wawro D, Ratajska M, Steplewski W (2007) Novel biocomposites with feather keratin. *Fibres Text East Eur* 15 (5-6):157-162
111. Wawro D, Stęplewski W (2010) Producing of Continuous Cellulose Fibres Modified with Plant Proteins. *Fibres Text East Eur* 18 (6):83
112. Zhang SA, Li FX, Yu JY (2011) Novel Cellulose/SPI Blend bio-fibers Prepared via Direct Dissolving Approach. *J Eng Fibers Fabr* 6 (1):31-37
113. Cai J, Zhang L, Zhou J, Li H, Chen H, Jin H (2004) Novel fibers prepared from cellulose in NaOH/urea aqueous solution. *Macromol Rapid Commun* 25 (17):1558-1562
114. Holbrey J, Swatloski R, Chen J, Daly D, Rogers R (2005) Polymer dissolution and blend formation in ionic liquids. US Patent 20050288484, 29 Dec 2005
115. Graenacher C (1934) Cellulose solution. US Patent 1,943,176,
116. Swatloski RP, Spear SK, Holbrey JD, Rogers RD (2002) Dissolution of cellulose with ionic liquids. *J Am Chem Soc* 124 (18):4974-4975
117. Feng L, Chen Z-I (2008) Research progress on dissolution and functional modification of cellulose in ionic liquids. *J Mol Liq* 142 (1):1-5

118. Heinze T, Schwikal K, Barthel S (2005) Ionic liquids as reaction medium in cellulose functionalization. *Macromol Biosci* 5 (6):520-525
119. Zhang H, Wu J, Zhang J, He J (2005) 1-Allyl-3-methylimidazolium chloride room temperature ionic liquid: a new and powerful nonderivatizing solvent for cellulose. *Macromolecules* 38 (20):8272-8277
120. Fukaya Y, Sugimoto A, Ohno H (2006) Superior solubility of polysaccharides in low viscosity, polar, and halogen-free 1, 3-dialkylimidazolium formates. *Biomacromolecules* 7 (12):3295-3297
121. Fukaya Y, Hayashi K, Wada M, Ohno H (2008) Cellulose dissolution with polar ionic liquids under mild conditions: required factors for anions. *Green Chem* 10 (1):44-46
122. Fujita K, MacFarlane DR, Forsyth M (2005) Protein solubilising and stabilising ionic liquids. *Chem Commun* (38):4804-4806
123. Phillips DM, Drummy LF, Conrady DG, Fox DM, Naik RR, Stone MO, Trulove PC, De Long HC, Mantz RA (2004) Dissolution and regeneration of bombyx mori silk fibroin using ionic liquids. *J Am Chem Soc* 126 (44):14350-14351
124. Mantz RA, Fox DM, Green JM, Fylstra PA, De Long HC, Trulove PC (2007) Dissolution of biopolymers using ionic liquids. *Z Naturforsch A* 62 (5-6):275-280
125. Goujon N, Wang X, Rajkova R, Byrne N (2012) Regenerated silk fibroin using protic ionic liquids solvents: towards an all-ionic-liquid process for producing silk with tunable properties. *Chem Commun* 48 (9):1278-1280
126. Wang Q, Yang Y, Chen X, Shao Z (2012) Investigation of rheological properties and conformation of silk fibroin in the solution of AMImCl. *Biomacromolecules* 13 (6):1875-1881

127. Goujon N, Rajkhowa R, Wang X, Byrne N (2013) Effect of solvent on ionic liquid dissolved regenerated *Antheraea assamensis* silk fibroin. *J Appl Polym Sci* 128 (6):4411-4416
128. Xie H, Li S, Zhang S (2005) Ionic liquids as novel solvents for the dissolution and blending of wool keratin fibers. *Green Chem* 7 (8):606-608
129. Idris A, Vijayaraghavan R, Rana UA, Fredericks D, Patti AF, MacFarlane DR (2013) Dissolution of feather keratin in ionic liquids. *Green Chem* 15 (2):525-534
130. Idris A, Vijayaraghavan R, Rana UA, Patti AF, MacFarlane DR (2014) Dissolution and regeneration of wool keratin in ionic liquids. *Green Chem* 16 (5):2857-2864
131. Meng Z, Zheng X, Tang K, Liu J, Ma Z, Zhao Q (2012) Dissolution and regeneration of collagen fibers using ionic liquid. *Int J Biol Macromol* 51 (4):440-448
132. Hu Y, Liu L, Dan W, Dan N, Gu Z (2013) Evaluation of 1-ethyl-3-methylimidazolium acetate based ionic liquid systems as a suitable solvent for collagen. *J Appl Polym Sci* 130 (4):2245-2256
133. Biswas A, Shogren RL, Stevenson DG, Willett JL, Bhowmik PK (2006) Ionic liquids as solvents for biopolymers: Acylation of starch and zein protein. *Carbohydr Polym* 66 (4):546-550
134. Brauer S, Kosan B, Meister F, Bauer RU (2009) Method for producing molded bodies from proteins. US Patent 20090051068, 26 Feb 2009
135. Choi H-M, Kwon I (2010) Dissolution of zein using protic ionic liquids: N-(2-hydroxyethyl) ammonium formate and N-(2-hydroxyethyl) ammonium acetate. *Ind Eng Chem Res* 50 (4):2452-2454
136. Tomlinson SR, Kehr CW, Lopez MS, Schlup JR, Anthony JL (2014) Solubility of the corn protein zein in imidazolium-based ionic liquids. *Ind Eng Chem Res* 53 (6):2293-2298

137. Wu R-L, Wang X-L, Wang Y-Z, Bian X-C, Li F (2009) Cellulose/soy protein isolate blend films prepared via room-temperature ionic liquid. *Ind Eng Chem Res* 48 (15):7132-7136
138. Zhang L, Qiao C, Ding Y, Cheng J, Li T (2012) Rheological behavior of gelatin/1-allyl-3-methylimidazolium chloride solutions. *J Macromol Sci B* 51 (4):747-755
139. Wang H, Gurau G, Rogers RD (2014) Dissolution of biomass using ionic liquids. In: Zhang S, Wang J, Lu X, Zhou Q (eds) *Structures and interactions of ionic liquids*. Springer-Verlag Berlin Heidelberg, pp 79-105
140. Yao Y, Zhang E, Xia X, Yu J, Wu K, Zhang Y, Wang H (2015) Morphology and properties of cellulose/silk fibroin blend fiber prepared with 1-butyl-3-methylimidazolium chloride as solvent. *Cellulose* 22 (1):625-635
141. Wongsasulak S, Patapeejumruswong M, Weiss J, Supaphol P, Yoovidhya T (2010) Electrospinning of food-grade nanofibers from cellulose acetate and egg albumen blends. *J Food Eng* 98 (3):370-376
142. Kiatyongchai T, Wongsasulak S, Yoovidhya T (2014) Coaxial Electrospinning and Release Characteristics of Cellulose Acetate-Gelatin Blend Encapsulating a Model Drug. *J Appl Polym Sci* 131 (8)
143. Amsaveni M, Anumary A, Ashokkumar M, Chandrasekaran B, Thanikaivelan P (2013) Green synthesis and characterization of hybrid collagen–cellulose–albumin biofibers from skin waste. *Appl Biochem Biotechnol* 171 (6):1500-1512

## **Chapter 2 Properties of Chitosan/Soy Protein Blended Films with Added Plasticizing Agent as a Function of Solvent Type at Acidic pH**

Reprint of manuscript published in International Journal of Polymeric Materials and Polymeric Biomaterials 65:1, 11-17, DOI:10.1080/00914037.2015.1038821

by Ramiz Boy, Chandler Maness, and Richard Kotek

College of Textiles, North Carolina State University, Raleigh, NC 27695, USA

**Abstract:** Pure and blends from chitosan (CH) and soy protein isolate (SPI) were produced in varying compositions (CH/SPI 75/25, 50/50, 25/75 w/w) in order to determine the changes in properties based on the solvent type (acetic and formic acids). Glycerol was used as a plasticizer for the films to ensure appropriate tensile properties required for the testing. Soy protein was denatured by applying heat and by reducing pH. The interaction between the two biopolymers was confirmed by FTIR and TGA, indicating their miscibility and compatibility. Furthermore, increasing the amount of soy protein in the blend films decreased the tensile strength as well as the absorptive properties, but improved the ability of the film to withstand thermal degradation. Regarding the solvents, it was determined that blend films cast using acetic acid gave higher hydrophobicity, better internal blend miscibility, and better tensile properties than blend films cast from formic acid.

### **2.1 Introduction**

Films produced from biopolymers have drawn a considerable amount of attention in recent years, as their biocompatibility and low cost make them attractive for a wide array of uses. Specifically, their application in the biomedical domain has been widely targeted. For instance, wound dressing is a commonly researched topic, one that has recently gained steam

in terms of the utilization of biomaterials. The overall goal is to imitate the mechanical properties of a given damaged tissue all the while providing protection, breathability, and comfort for the wound. Polysaccharides such as chitin and chitosan have shown promise in this regard, as they are known to have good antimicrobial properties, permeability to oxygen, and good adhesive ability [1,2]. This brings large value to chitosan as a proponent not only in the biomedical industry, but also in food and cosmetic industry, as it is the second most abundant natural polymer in existence. Furthermore, studies have shown that varying the molecular weight and degree of deacetylation of chitosan films can change their tensile strength and elongation as well as moisture absorption [3]. The ability to tailor the properties of this widely found biopolymer makes it very attractive for a variety of applications.

On the other hand, soy protein isolate does not lend itself well to similar applications. Although it is cheap, biodegradable, and readily available, the films produced from soy protein isolate tend to be brittle and hygroscopic [4,5]. These characteristics, without antibiotic agents, would prove detrimental to the cause of biomedical application. Some attempts have been made to moderate these properties via the addition of glycerol [6]. It was determined that the plasticizing effect of glycerol locally deforms the protein matrix and result in unpredictable fluctuations of tensile properties. In previous studies, measures to counter this nature included blending soy protein isolate with other proteins [7-9] as well as blending with polysaccharides [5,10,11].

Blends of chitosan and soy protein have been investigated for applications, such as drug delivery systems [12], wound dressings and tissue regeneration [13-17], edible films and conjugates, and microencapsulation of food ingredients [18-22]. In these applications, the blends were prepared by using separate solvents for each of the polymers. Particularly, the

ones in the form of membrane or film resulted in phase separation and required crosslinking to improve compatibility, miscibility and properties.

Chitosan is soluble in most organic acids, which are also potential solvents for soy protein. In this regard, the choice of solvent has been made based on the previously well-known acids for both biopolymers to achieve homogeneous solution blends. For instance, formic acid as an organic acid was already known to dissolve soy protein [23]. In addition, acetic acid is the most commonly used solvent for chitosan and also could dissolve soy protein. To best of our knowledge, no report has been published regarding acidic solvents that can solubilize both biopolymers.

The objective of this study is to develop homogeneous blend systems consisting of chitosan and soy protein isolate with the plasticizer and evaluate the effect of solvent type on the final properties. This characterization will eventually serve to illuminate possible end uses for such blends.

## **2.2 Materials and Methods**

### **2.2.1 Materials**

The chitosan used in this research is a product of Sigma Aldrich Co. (St. Louis, MO, USA) with a molecular weight of 150 kDA and 70-80% degree of deacetylation. Soy protein isolate (PROFAM 955) containing 93.8% dry basis protein was provided by ADM Specialty Products-Oilseeds. Formic acid (puriss. p.a., ~98%) was purchased from Fluka. Glacial acetic acid and glycerol were also purchased from Sigma Aldrich Co.

### **2.2.2 Preparation of Films**

Plasticized pure and blend films of chitosan (CH) and soy protein isolate (SPI) were produced by solution casting method under acidic conditions. Two chitosan solutions (1% w/v) were prepared by slowly dispersing chitosan powder with 0.5% w/v of glycerol in aqueous solutions of 1% v/v formic acid (FA) and 1% v/v acetic acid (AA). The pH values of the solutions were adjusted to 2 by adding insignificant amount of concentrated HCl. The same procedure was applied to prepare two soy protein isolate solutions (1% w/v) by applying heat 60°C to ensure the dissolution. Prior to blending, each solution was filtered through a 325-mesh stainless-steel woven disk filter. Subsequently, the two solutions from each polymer dissolved in the same acid were mixed at the ratio of CH/SPI: 75/25, 50/50 and 25/75 w/w along with the control samples, CH and SPI. After stirring, the compositions were measured and poured into Petri dishes. This produced a total of 10 filled petri dishes, 5 compositions each for both acids. After placing under a ventilated hood for 48-72 hours at ambient temperature, the films were dried and ready to peel. This process was repeated until an adequate number of film samples from each type were obtained to complete the desired tests.

## **2.3 Film Characterization**

### **2.3.1 Fourier Transform Infrared Spectroscopy**

Fourier Transform Infrared Spectroscopy (FTIR) was performed on the Thermo Fisher Nexus 470 FTIR with Continuum Microscope and ORBIT/OMNIC ATR software to obtain infrared spectra of the films. The tip of the sensor was comprised of diamond and the spectra were recorded in absorbance mode from 4000 to 500  $\text{cm}^{-1}$ , co-adding 64 scans at 4  $\text{cm}^{-1}$  resolution. The obtained IR spectra were analyzed using OMNIC software. Peak intensity

measurement, comparison of spectra and examination of the chemical components of the films were carried out.

### **2.3.2 Thermal Analysis**

A differential scanning calorimeter (DSC) was used to analyze the denaturation temperatures of soy protein isolate dissolved by acetic and formic acids. It was conducted on a PerkinElmer Instruments Diamond DSC. Samples were heated from 25°C to 120°C at a rate of 10°C/min.

Thermo-gravimetric analysis (TGA) was utilized to study the changes of mass of the investigated polymer systems against increasing temperature. It was performed on a Perkin Elmer TGA under a dynamic nitrogen atmosphere at a heating rate of 20°C/min from 20°C to 450°C using ca. 5 mg samples of each material. Post analysis was performed using the raw data on Origin 8.5, a data analysis and graphing software.

### **2.3.3 SEM Analysis**

The cast films were first frozen and fractured in liquid nitrogen then mounted on carbon tape prior to gold/palladium sputtering. Images were taken under standard vacuum conditions with 5 kV potential difference on the FEI Phenom Scanning Electron Microscope (SEM).

### **2.3.4 Mechanical Properties**

For accurate tensile data, we opted to test 5 films from each composition. They were conditioned overnight in the testing facility. The thickness of each film to be tested was measured 10 times with the Thwing-Albert Electronic Thickness Tester. Thicknesses between 90 and 160 µm were obtained. Following this, each individual film was cut into 5 strips with

the same width (1/2 inch) and taped on both ends 5 cm apart. This produced 25 strips for each composition, resulting in a total of 250 strips to be tested.

The tensile testing was carried out using the MTS Q-test Tensile Testing Machine and performed in accordance with ASTM D882: Tensile Testing of Thin Plastic Sheeting. Testing used the 250 lb. load cell, 50 mm gauge length, and 10 mm/min initial speed.

### **2.3.5 Water Absorption Testing**

This test was performed to determine the amounts of water in each composition for both acids absorbed over a 24-hour period. All samples were weighed, submerged in deionized water for 24 hours, and then reweighed (if applicable) to obtain weight percent increase values.

### **2.3.6 Contact Angle Measurement**

The testing was examined using the FDS Dataphysics Contact Angle Measurement Apparatus. Using a 500- $\mu$ L syringe, a droplet of water was dispensed on the surface of the films and the angles of the outer edges of water droplets made with the stage were reported. These values were taken the moment a droplet contacted the surface. The resulting left and right angles were averaged to produce the contact angle. Five measurements were recorded and averaged for each film.

## **2.3 Result and Discussion**

### **2.3.1 FTIR Analysis**

FTIR spectroscopy was used to investigate the interactions between chitosan and soy protein isolate in the film network. Additionally, conclusions may be drawn concerning the effect of acidic solvent on the biopolymeric blend films.

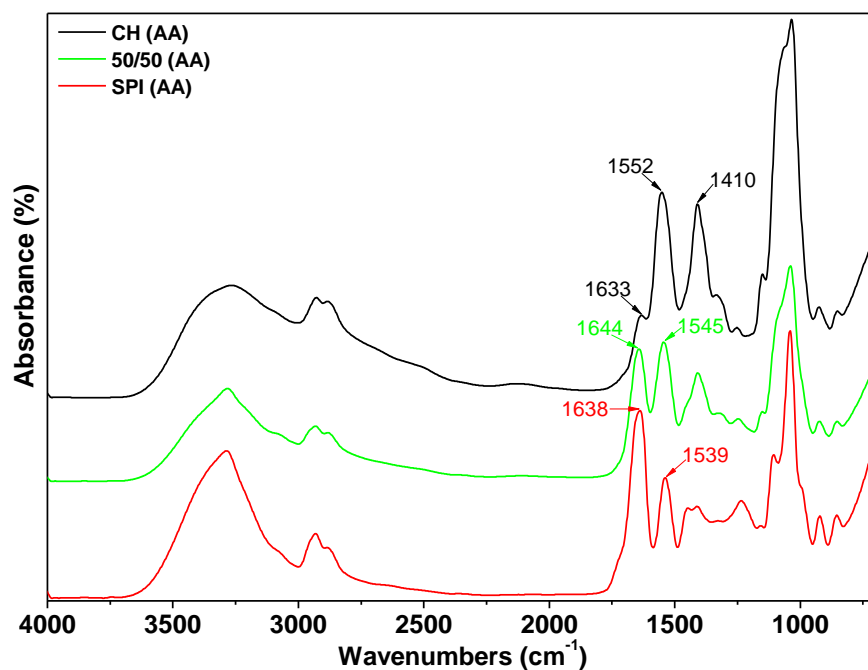


**Figure 2.1.** FTIR spectra of the films from acetic acid

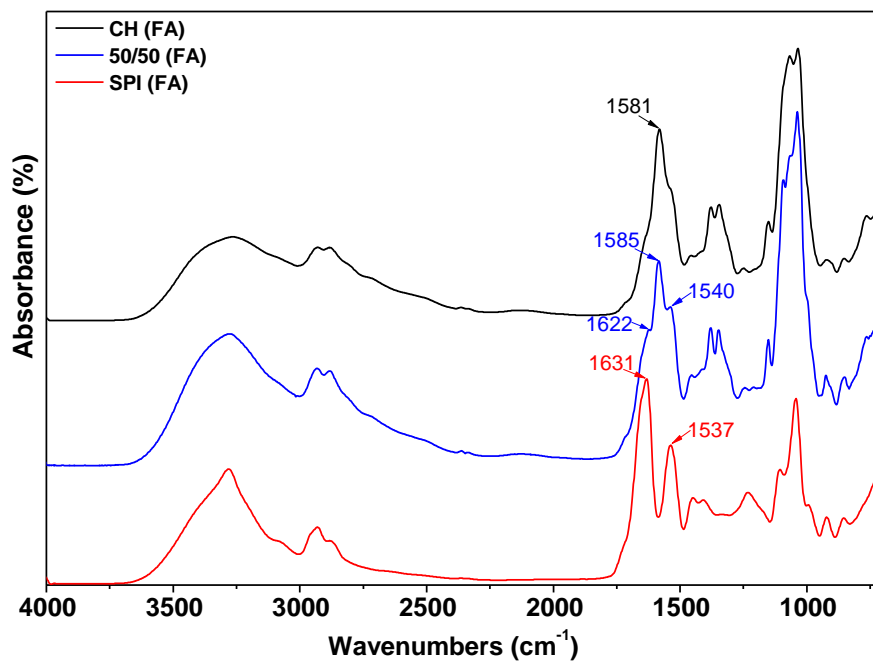


**Figure 2.2.** FTIR spectra of the films from formic acid

FTIR spectra of all six films (Figure 2.1 and 2.2) shared the same broad absorption band in the range of  $3000 - 3600 \text{ cm}^{-1}$  due to the stretching of free and bounded O-H and N-H

groups. These groups in SPI together with hydroxyl groups from the bounded water and glycerol can easily interact with carbonyl moieties through intra- and intermolecular hydrogen bonding in the peptide and carboxyl groups of the protein structure [24]. In chitosan, O-H stretching that is an indication of intermolecular hydrogen bonding occurred in the same region with N-H stretching [3,25].

The main characteristic bands of CH (AA) film appeared at  $1633\text{ cm}^{-1}$  assigned for C=O stretching (amide I) and at  $1552$  and  $1410\text{ cm}^{-1}$  for asymmetric and symmetric carboxylate anion stretching, respectively (Figure 1). This is a result of using acetic acid as the solvent forming a film of chitosonium acetate [3]. However, CH (FA) film did not show clear peaks near  $1630$  and  $1550\text{ cm}^{-1}$  suggesting the effect of solvent with low pH (Figure 2.2). A sharp peak at  $1581\text{ cm}^{-1}$  in this film appeared as N-H angular deformation [25].

The spectrum of SPI (AA) film (Figure 1) showed the absorption bands at  $1638\text{ cm}^{-1}$  and  $1539\text{ cm}^{-1}$  indicating C=O stretching (amide I) and N-H bending (amide II). The amide I band could appear at different wavenumbers for the protein and thus this leads to the analysis of secondary structure of that protein. Because no major shift was observed due to the solvent in SPI (FA) film (Figure 2), only some displacement of amide I peak ( $1631\text{ cm}^{-1}$ ) as well as amide II ( $1537\text{ cm}^{-1}$ ) was seen. Therefore, this meant no change in secondary structure of the protein compared to SPI (AA) film [5,26,27].

50/50 (AA) film had absorption bands at  $1644\text{ cm}^{-1}$  (amide I) and  $1545\text{ cm}^{-1}$  (amide II) that are mainly shifts to higher values of that of SPI (AA) film due to interaction with chitosan (Figure 2.1). The amide I band of both pure films contributes and coincides at somewhat higher wavenumbers in the blend film. In addition, the asymmetric carboxylate anion stretching of CH (AA) film at  $1552\text{ cm}^{-1}$  was either lost or superposed to the amide II band. This indicates

the participation of CH and SPI in specific interactions in their blend film from acetic acid. On the other hand, 50/50 (FA) film (Figure 2.2) had absorption bands occurring at a lower value for amide I ( $1622\text{ cm}^{-1}$ ) and at higher values for amide II ( $1540\text{ cm}^{-1}$ ) and for N-H angular deformation ( $1585\text{ cm}^{-1}$ ) in comparison with the pure films cast from formic acid. Furthermore, amide I band positioned at a lower value than that of its SPI component and of 50/50 (AA) film. These displacements of all bands suggest secondary structure bonding of the two polymers dissolved in each acid.

### 2.3.2 Thermal Analysis

The denaturation of proteins is a process of major conformational changes, causing no structural alteration in polypeptide chain order. In other words, quaternary structure of proteins is disassociated into subunits via this process [28,29]. Denaturation is therefore important for the purpose of blending soy protein isolate with chitosan. Once it is denatured, its extended chain could be relatively easily exposed to protein-protein interaction as well as protein-polysaccharide interaction. Since denaturation is an endothermic reaction, calorimetric study can provide sufficient information about this process. [30,31].

Mauri and Añón [30] reported that the heat treatment above  $60^{\circ}\text{C}$  induces denaturation for glycinin globulin, the first major protein fraction of soy. In addition to heat treatment, low acidic condition (pH 2) helps to denature  $\beta$ -conglycinin globulin, the second major protein fraction of soy [28]. These conditions were also applied for dissolution of soy protein isolate in this study and its denaturation was confirmed by DSC.

The thermal decomposition of films can provide information about the compatibility and miscibility of the polymers. Figure 2.3 shows TGA thermograms of the films of CH, SPI and 50/50 blend in each separate solvent. All six samples shared similar behavior under

increasing temperature with two main stages of weight loss after water evaporation that occurred around 100°C.

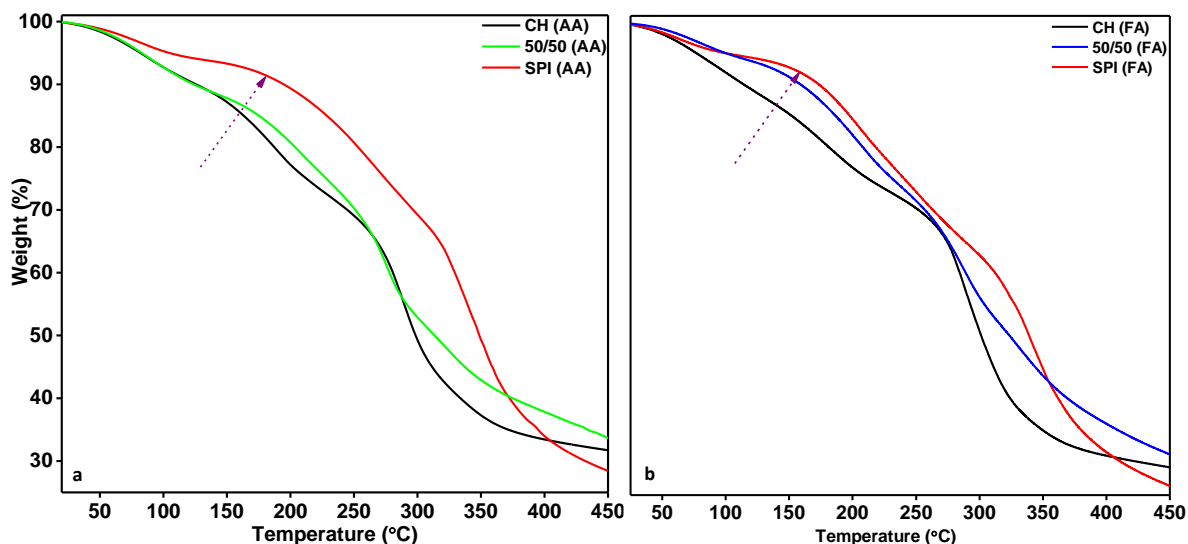


**Figure 2.3.** TGA thermograms for the films from (a) acetic acid and (b) formic acid

Because all films were plasticized, the weight loss in the first stage corresponded to the glycerol/polymer mixture above 150°C (Figure 2.3). Similar results related to the loss of glycerol in pure and blend films of chitosan and sodium caseinate as well as initial degradation of the biopolymers were also reported by Pereda et al. [32]. Interestingly, glycerol was retained stronger in SPI compared to CH films and therefore the blend films showed a trend in between the two pure films. Acetic acid film networks exhibited even higher glycerol retention suggesting improved interaction of solvent and glycerol with the polymers.

Table 2.1 shows the data for the second stage, namely main degradation stage, of the six films.  $T_{st}$  is the onset temperature,  $T_{max}$  is the maximum temperature and its corresponding percentage weight (wt.) loss along with the percentage residue (char) after 450°C are represented.

**Table 2.1.** TGA data for the films of SPI, CH, and 50/50 blend from acetic and formic acids

Solvent Type	Film Type	Main Degradation Stage			Residue after 450°C (%)
		T <sub>st</sub> (°C)	T <sub>max</sub> (°C)	Wt. loss (%)	
Acetic Acid	SPI	320	346	49	28
	CH	272	289	45	32
	50/50	258	276	39	34
Formic Acid	SPI	318	349	54	26
	CH	271	291	44	29
	50/50	265	287	39	31

Chitosan films from both solvents exhibited the degradation above 270°C and reached a maximum about 290°C. Similar results were also reported by Nieto et al., Neto et al., and Tirkistani [33-35]. In the case of SPI films, having the highest main degradation temperature in each group of the solvent type, they lost the most weight during this stage. Soares et al. [36] found similar stepwise degradation mechanism of soy protein. For 50/50 blend films, the thermal degradation began earlier compared to pure films. However, less of their weights were lost and more of the residue left after 450°C, exhibiting higher resistance to thermal decomposition. What is more, the blends had only one thermal decomposition temperature, indicating the compatibility and the miscibility between the polymers. This is most likely due to the aforementioned interactions between the polymers.

### 2.3.3 Morphology

The scanning electron microscope was used to produce a cross-sectional view of the pure films and the 50/50 blends. This provided a clear representation of how the differing acids affected the internal structures of the films. The samples were frozen in liquid nitrogen and fractured followed by sputtering with gold/palladium to ensure maximum image quality.

Magnifications of 1000X and 5000X were recorded, but only the 5000X views provided a clear picture of the internal structures (Figure 2.4 and 2.5).

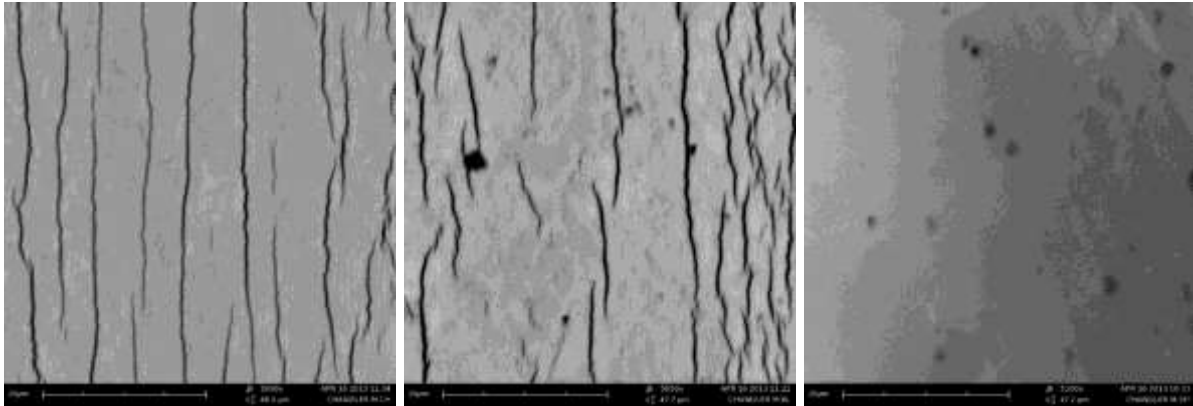


**Figure 2.4.** 5000X images of the films of CH (left), 50/50 blend (middle), and SPI (right) from acetic acid

The cross-section of all films show nonporous morphology. 50/50 (AA) blend film has rougher morphology than pure ones, but it revealed a better overall miscibility of its components compared to 50/50 (FA) blend film.

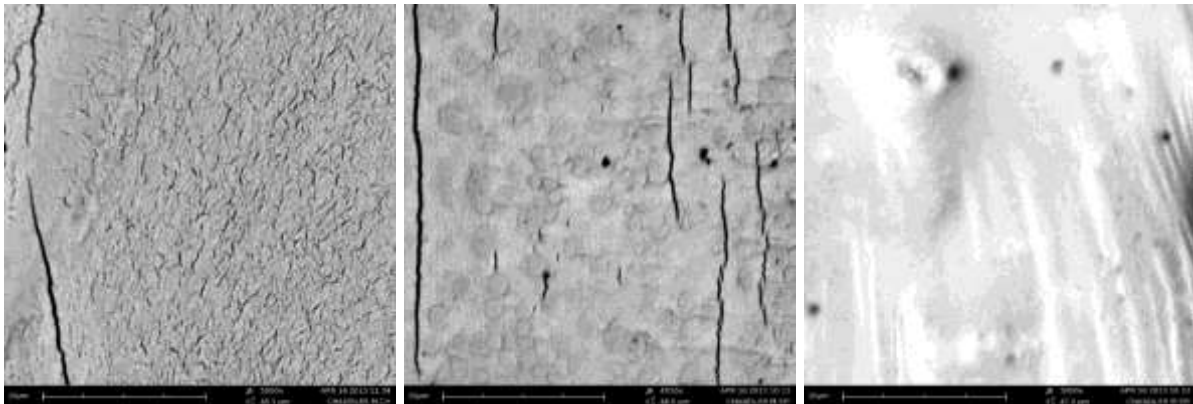


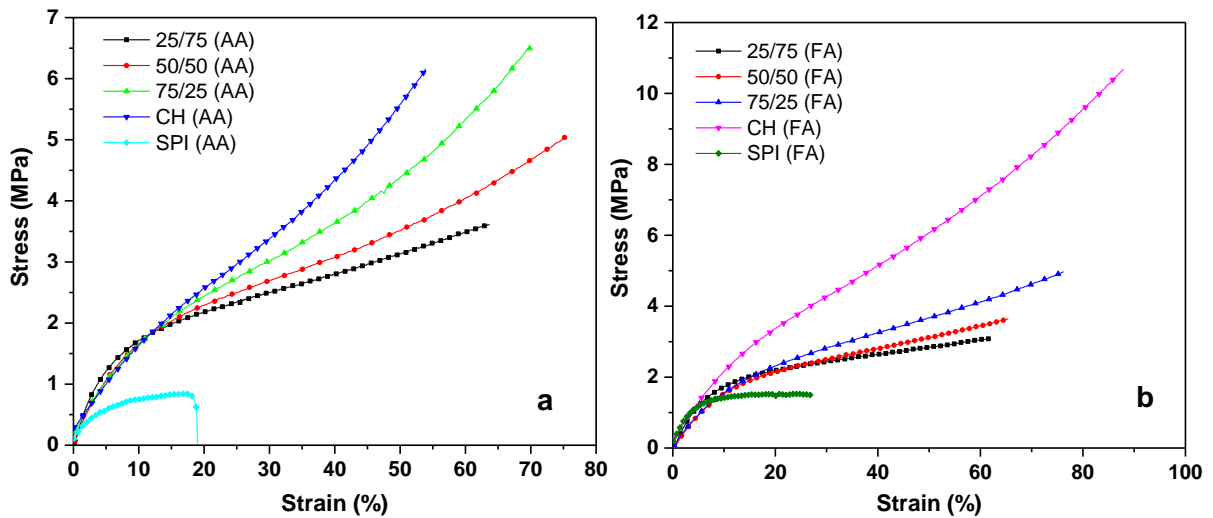
**Figure 2.5.** 5000X images of the films of CH (left), 50/50 blend (middle), and SPI (right) from formic acid

The cross-section of CH (FA) film shows a non-uniform network, a likely result of the fracture mechanism (Figure 2.5). 50/50 (FA) blend film illustrates scattered mixing of soy protein into the chitosan matrix, implying poor miscibility. A similar result of CH/SPI blend

membranes was also reported by Silva et al. [5]. They mainly referred this to the weak interaction between the polymers and used silanization treatment to improve it [15]. Furthermore, SPI (FA) shows non-porous, uniform distribution, similar to that of SPI (AA). The cracks present in CH and 50/50 blend films are a response to the liquid nitrogen freezing process. This effect was not witnessed in SPI films.

### 2.3.4 Mechanical Properties

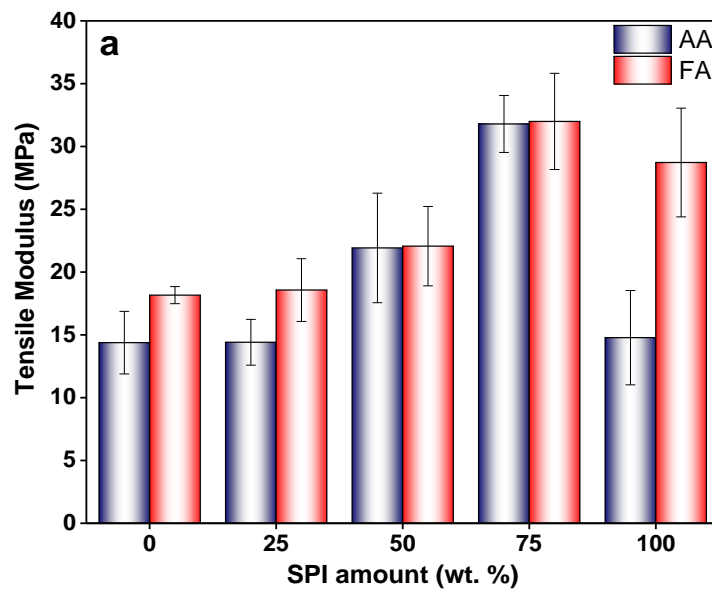
SPI films from both acids without any plasticizers were too fragile to utilize whereas adding glycerol plasticized the films and provided sufficient strength to handle. CH and SPI films were mainly employed as the control samples and the blend films of all compositions were tested for comparison purposes. The stress-strain curves of all films prepared from AA and FA are shown in Figure 2.6. Tensile modulus, failure stress and failure strain are demonstrated in Figure 2.7.



**Figure 2.6.** Stress-strain curves of the films prepared from acetic acid (a) and formic acid (b)

In general, as the concentration of SPI increased in the blend films from both acids, tensile modulus increased but failure stress and failure strain decreased in a near-linear manner.

From Figure 2.6 and 2.7a, it can be observed on the bar graph of tensile modulus, adding SPI into CH film network from either acid increased the tensile modulus compared to CH film. In addition, 25/75 films from both acids had the highest tensile modulus among all films. Although there was considerable increase in the tensile modulus, the failure stress and failure strain were inversely affected by increasing concentration of SPI, specifically for the films from formic acid.



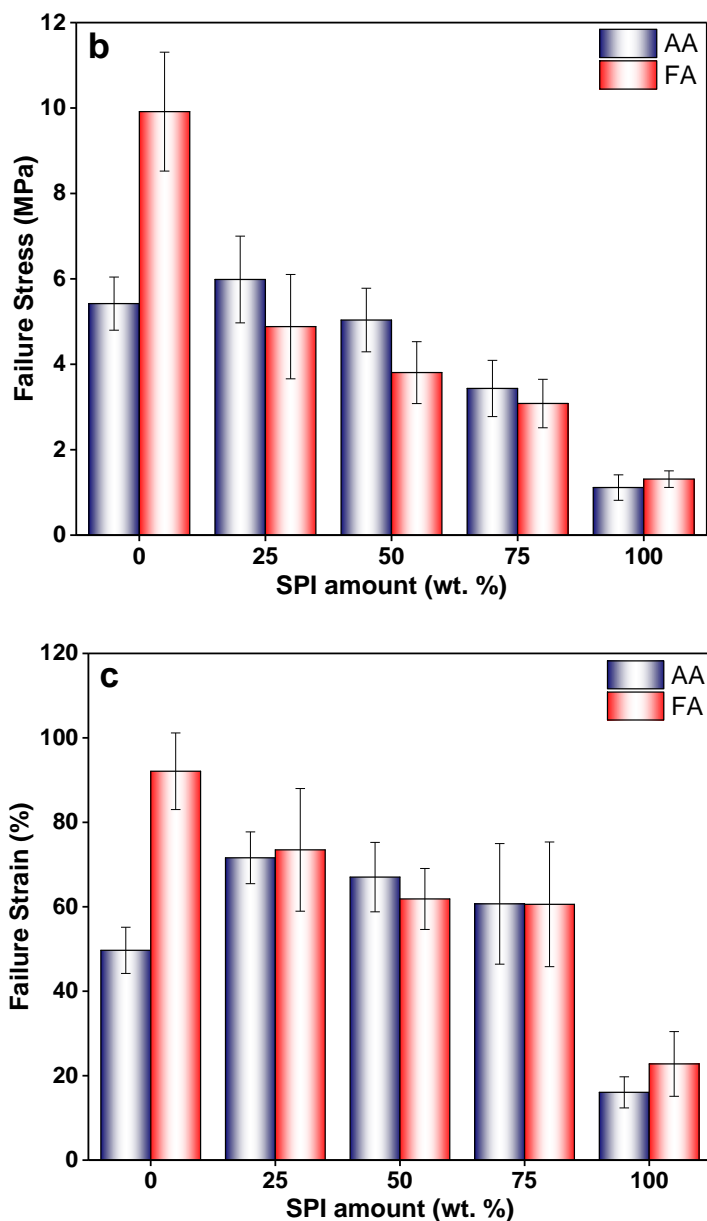


**Figure 2.7.** Tensile modulus (a), failure stress (b) and failure strain (c) of all films as a function of SPI

The decrease in failure stress and failure strain of the films from formic acid was likely related to the non-uniform distribution of SPI in CH network, generated by poor miscibility and lack of interaction between the two polymers. Nevertheless, the films from acetic acid possessed the interaction of those that elevated the failure stress and failure strain. The morphology of the 50/50 (AA) blend film (Figure 2.4) also supports this argument.

Subirade et al. [37] reported that the conformation of glycinin considerably affects the mechanical performance of soy protein films. In this study, SPI (FA) revealed doubled modulus and slightly higher failure stress and failure strain compared to SPI (AA). When blended with CH, however, the conformation of SPI was readily adaptable and capable of forming relatively strong and flexible films.

### 2.3.5 Water Absorption Testing

This test was performed to determine the amount of water each composition from both acids absorbed over a 24-hour period. This test also provided information about the solubility and physical integrity of the films. All samples were weighed initially in dry state then immersed in deionized water for 24 hours. They were finally weighed (if applicable) in wet state to obtain weight percent increase values. The results are shown in Table 2.2.

**Table 2.2.** Weight percent increase after 24 hours in water

CH/SPI	Acetic Acid			Formic Acid	
	Weight Before (g)	Weight After (g)	Weight Increase (%)	Weight Before (g)	Weight After (g)
100/0	0.859	8.36	937.22	0.783	Inconclusive
75/25	0.902	5.88	651.88	0.858	
50/50	0.847	4.49	530.12	0.82	
25/75	0.81	3.87	477.78	0.829	
0/100	0.78	Inconclusive	N/A	0.798	

As shown in the Table 2.2, all FA films as well as SPI (AA) film did not maintain composure in wet state. Upon their removal from the water, the films dissipated and aggregated into a gelatinous lump. Given their inability to be weighed, the results stand as inconclusive.

On the other hand, chitosan (AA) film, as so-called chitosonium acetate, maintained its integrity in water thus the blends from acetic acid. These results revealed that, except for SPI (AA) film, no AA films were soluble in water and they were still physically intact even after the immersion. This points out that the SPI formed a more stable structure upon blending with CH in acetic acid. This also refers to the interaction of the chains of CH and SPI through some secondary structure bonding, preventing from the dissolution in water [38].

### 2.3.6 Contact Angle Measurement

This testing method was used as it quantifies the wettability of a flat, solid surface by water via the Young equation. Since these films may contact water in their various applications, it was deemed necessary to record this data. Using a 500  $\mu$ L syringe, a droplet of water was dispersed on the surface of the films and the angle at the outer edges of the water droplet made with the stage were reported. These values were taken the moment at which the droplet contacted the surface. The resulting left and right angles were averaged to produce the contact angle. Five measurements were recorded and averaged for each film.

**Table 2.3.** Results of contact angle measurements

<b>CH/SPI</b>	<b>Acetic Acid</b>	<b>Formic Acid</b>
100/0	89.18 $\pm$ 0.23	85.50 $\pm$ 0.24
75/25	88.18 $\pm$ 0.69	80.60 $\pm$ 0.42
50/50	89.00 $\pm$ 0.35	76.56 $\pm$ 0.48
25/75	70.00 $\pm$ 0.87	48.04 $\pm$ 0.49
0/100	76.90 $\pm$ 1.01	36.44 $\pm$ 0.44

Given the films' affinities to water, the flatness of the film was often compromised before the droplet was even dispersed. Different sections of the films were cut and measured

quickly, as not to skew the data. As supported in Table 2.3, it can be concluded that AA films have greater surface tension than FA films. In conjunction with this, FA films are more hydrophilic than AA films. Furthermore, increasing the concentration of SPI decreases the surface tension of the films from both acids. The results are mostly consistent with these statements, with the exception of SPI from acetic acid. This discrepancy can be attributed to the pits and hills formed on the surface of the film in response to flattening attempts.

## **2.4 Conclusions**

This research allowed for extensive comparison of the effect of acidic solvent type of chitosan/soy protein blends. It was confirmed that the preparation method induced denaturation of soy proteins and helped to produce pure films of SPI from both acid. FTIR and TGA data indicated specific interaction of both components. In addition, blending SPI with CH resulted in higher resistance to thermal degradation. Acetic acid blends demonstrated better overall blending properties, as SEM shows better miscibility in the 50/50 blend and tensile tests give higher stress/strain values than blends produced with formic acid. The 75/25 CH/SPI blends exhibit the best tensile properties, as their strain and stress values at breakage are the highest among all films from both acids. Chitosan was responsible for water intake in CH/SPI blends, as illustrated in the water absorption test. Blends casted with formic acid are more hydrophilic and have lower surface tensions than their acetic acid counterparts have. Overall, the better internal blend miscibility produced in the acetic acid films provides the more attractive properties for application. With this knowledge, the research can be extended to other organic acids to produce the blend films.

## 2.5 References

- [1] R. Jayakumar, M. Prabakaran, P.S. Kumar, S. Nair, T. Furuike, and H. Tamura, *Biomed. Eng.*, 13 (2011).
- [2] V. Chiono, E. Pulieri, G. Vozzi, G. Ciardelli, A. Ahluwalia, and P. Giusti, *J. Mater. Sci. Mater. Med.*, 19, 889-898 (2008).
- [3] J. Nunthanid, S. Puttipipatkachorn, K. Yamamoto, and G.E. Peck, *Drug Dev. Ind. Pharm.*, 27, 143-157 (2001).
- [4] J.W. Rhim, A. Gennadios, A. Handa, C.L. Weller, and M.A. Hanna, *J. Agric. Food Chem.*, 48, 4937-4941 (2000).
- [5] S. Silva, B.J. Goodfellow, J. Benesch, J. Rocha, J. Mano, and R. Reis, *Carbohydr. Polym.*, 70, 25-31 (2007).
- [6] A. Ogale, P. Cunningham, P. Dawson, and J. Acton, *J. Food Sci.*, 65, 672-679 (2000).
- [7] C. Vaz, M. Fossen, R. Van Tuil, L. De Graaf, R. Reis, and A. Cunha, *J. Biomed. Mater. Res. A*, 65, 60-70 (2003).
- [8] P. Guerrero, P. Stefani, R. Ruseckaite, and K. De la Caba, *J. Food Eng.*, 105, 65-72 (2011).
- [9] L. Were, N. Hettiarachchy, and M. Coleman, *J. Food Sci.*, 64, 514-518 (1999).
- [10] Y. Chen and L. Zhang, *J Appl Polym Sci*, 94, 748-757 (2004).
- [11] J. Otaigbe and J. Jane, *J. Environ. Polym. Degrad.*, 5, 75-80 (1997).
- [12] R. Murakami and R. Takashima, *Food Hydrocoll.*, 17, 885-888 (2003).
- [13] S. Silva, M. Santos, O. Coutinho, J. Mano, and R. Reis, *J. Mater. Sci. Mater. Med.*, 16, 575-579 (2005).
- [14] R.M. Silva, C. Elvira, J.F. Mano, J. San Roman, and R.L. Reis, *J. Mater. Sci. Mater. Med.*, 15, 523-528 (2004).

- [15] S.S. Silva, J.M. Oliveira, J. Benesch, S.G. Caridade, J.F. Mano, and R.R. Reis, *J. Bioact. Compatible Polym.*, 28, 385-397 (2013).
- [16] T.C. Santos, B. Höring, K. Reise, A.P. Marques, S.S. Silva, J.M. Oliveira, J.F. Mano, A.G. Castro, R.L. Reis, and M. van Griensven, *Tissue Eng PT A*, 19, 860-869 (2013).
- [17] X. Wang, N. Shi, Y. Chen, C. Li, X. Du, W. Jin, Y. Chen, and P.R. Chang, *Biomed. Mater. Eng.*, 22, 143-150 (2012).
- [18] D. Jia, Y. Fang, and K. Yao, *Food Bioprod. Process.*, 87, 7-10 (2009).
- [19] M. Usui, H. Tamura, K. Nakamura, T. Ogawa, M. Muroshita, H. Azakami, S. Kanuma, and A. Kato, *Nahrung/Food*, 48, 69-72 (2004).
- [20] G. Huang, Y. Sun, J. Xiao, and J. Yang, *Food Chem.*, 135, 534-539 (2012).
- [21] J. Xiao, G. Huang, S. Wang, and Y. Sun, *J Appl Polym Sci*, 131 (2014).
- [22] Y. Yuan, Z. Wan, X. Yang, and S. Yin, *Food Res. Int.*, 55, 207-214 (2014).
- [23] S. Sinha-Ray, Y. Zhang, A. Yarin, S. Davis, and B. Pourdeyhimi, *Biomacromolecules*, 12, 2357-2363 (2011).
- [24] P. Nayak, A. Sasmal, P. Nanda, P. Nayak, J. Kim, and Y. Chang, *Polym. Plast. Technol. Eng.*, 47, 466-472 (2008).
- [25] K.M. Kim, J.H. Son, S. Kim, C.L. Weller, and M.A. Hanna, *J. Food Sci.*, 71, 119-124 (2006).
- [26] M. Beekes, P. Lasch, and D. Naumann, *Vet. Microbiol.*, 123, 305-319 (2007).
- [27] Y. Yuan, Z. Wan, S. Yin, X. Yang, J. Qi, G. Liu, and Y. Zhang, *LWT-Food Sci. Technol.*, 50, 657-664 (2013).
- [28] A. Hermansson, *J. Texture Stud.*, 9, 33-58 (1978).
- [29] J.E. Kinsella, *J. Am. Oil Chem. Soc.*, 56, 242-258 (1979).

- [30] A.N. Mauri and M.C. Añón, *J. Sci. Food Agric.*, 86, 1064-1072 (2006).
- [31] M. Puppo and M. Añón, *J. Food Sci.*, 64, 50-56 (1999).
- [32] M. Pereda, M.I. Aranguren, and N.E. Marcovich, *J Appl Polym Sci*, 107, 1080-1090 (2008).
- [33] J. Nieto, C. Peniche-Covas, and G. Padron, *Thermochim. Acta*, 176, 63-68 (1991).
- [34] C.d.T. Neto, J. Giacometti, A. Job, F. Ferreira, J. Fonseca, and M. Pereira, *Carbohydr. Polym.*, 62, 97-103 (2005).
- [35] F.A. Tirkistani, *Polym. Degrad. Stab.*, 60, 67-70 (1998).
- [36] R. Soares, F.F. Scremin, and V. Soldi, *Macromol. Symp.*, 229, 258-265 (2005).
- [37] M. Subirade, I. Kelly, J. Guéguen, and M. Pézolet, *Int. J. Biol. Macromol.*, 23, 241-249 (1998).
- [38] M.A.d. Moraes, G.M. Nogueira, R.F. Weska, and M.M. Beppu, *Polymers*, 2, 719-727 (2010).

## Chapter 3 Properties of Cellulose–Soy Protein Blend Biofibers

### Regenerated from an Amine/Salt Solvent System

Reprint of a Manuscript Submitted to Cellulose Journal After First Revision

by Ramiz Boy, Richard Kotek

Fiber & Polymer Science, College of Textiles, North Carolina State University, Raleigh, NC

**Abstract:** Blend biofibers with relatively high protein content from cellulose and soy protein isolate (SPI) were fabricated using ethylene diamine-potassium thiocyanate solvent system. Due to the decrease in solution viscosity, SPI loading was limited to 40% at most considering 100% draw down ratio applied during fiber coagulation. The results obtained from chemical and x-ray analysis support the formation of the interaction through mainly secondary bonding. Increasing protein content provided slightly higher thermal stability to the fibers. The electron microscopy images of the fibers displayed homogeneous dispersion of the protein without clear phase separation. The percent crystallinity and the tensile data revealed that the best compatibility occurred with 20% SPI ratio and the fiber had the same birefringence as the control fiber. In addition, blending cellulose with protein imparted faster biodegradation to the fibers.

### 3.1 Introduction

Cellulose is a naturally occurring, abundantly available, renewable source of raw material found in our planet. Thus, it is an invaluable biopolymer for developing sustainable products. Although significant advancements have been made in fabricating various oligosaccharide-based biomaterials in fibrous forms for various innovative applications in filtration, composites, and tissue engineering applications [1-6], cellulose with their higher

molecular weights are expected to play an even major role in emerging applications. Besides being biocompatible and biodegradable which enhances their potential in biomedical applications, cellulose possesses superior mechanical properties and characteristics that can be tailored for variety of applications [7]. For instance, blending cellulose and proteins is one way to provide more functionalities for textiles [8-11] and biomedical applications [12-14]. To compensate for the lack of surface epitopes in biomedical polymers, it is common to surface coat them with proteins [15]. One way to circumvent this problem would be to blend the proteins with polymers, and fabricate the fibers directly.

The premise of blending cellulose and proteins are nearly as old as the invention of viscose rayon: a regenerated cellulose fiber [16]. Not surprisingly, a viscose process has been patented to make a solution mixture of cellulose with alkali soluble proteins including soy protein. The resulting fibers regenerated from this mixture showed wool-like characteristics [17-19]. However, additional data on the properties of the fibers were not provided in these patents. Moreover, the incorporation of soy protein via viscose process added additional step to an already multistep procedure further complexing the procedure, which is environmentally polluting and expensive in nature [20]. Thus a novel method to incorporate protein utilizing a procedure that is less expensive and environmentally benign would be attractive for various applications. Thus is in particular attractive to utilize plant-based protein such as soy protein, which are abundantly available and renewable, with low carbon footprint.

Soy protein is attractive as they are isolated from the soybean plant, a leguminous plant and are the primary source for plant proteins. It further contains all 20  $\alpha$ -amino acids including essential amino acids that are necessary for the human diet. The amino acid arrangements of soy protein appear to imitate the functionality of animal source proteins in a designed system

[21]. Soy protein is a combination of varieties of protein subunits that have molecular weights (MW) ranging from 140 to 600 kDa with varying physical and chemical properties. When compared with most plant proteins, most of the soy protein (90%) is comprised of storage proteins with globular structure [22]. Unfortunately, the globular structure of soy protein with their molecular confirmation makes it complex to regenerate into strong fibers. To enable fiber formation, the round-like polymer chains have to be unfolded and extended, a process commonly known as denaturation. Although relatively superior fibers can be produced from denaturized soy protein, the tensile properties, such as dry and wet strength, are still inferior for engineering applications, which still needs to be improved for those applications [23].

As a biodegradable and biocompatible polymer, its combination with other natural polymers, for example, cellulose, have been explored. The results demonstrated increases in mechanical properties and bioactivity of the blend films, membranes, and sponges [14,24-30]. One study by Zhang et al. [31] reported fabrication of cellulose/soy protein blend fiber with 10% SPI ratio. Unfortunately, even at that low SPI ratio, soy protein particles were observed along the fiber indicating weak interaction between the polymers due to the globular structure of the protein. In that study, the authors utilized a combination of using aqueous NaOH/thiourea/urea solvent along with cellulose and chitin xanthate (the derivatives formed in viscose process). Likewise another study reported by Rees and Singer [32] explored the characteristics of proteins in selected non-aqueous solvents. Solubility analyses, such as ultracentrifuge, viscosity, osmotic pressure, etc. were examined for 23 proteins including soy protein. It was concluded that the majority of proteins dissolved in ethylene diamine (ED). When dissolved in these protic solvents, protein subunits were unfolded and elongated, unlike

their structures in water. In addition, thiocyanate ( $\text{SCN}^-$ ) ions have also shown to be a powerful denaturant for proteins [33-35].

To further expound on using thiocyanate ions as a denaturing agent to spin cellulose/SPI fibers, in this study, a binary solvent system of ED/potassium thiocyanate (KSCN) was utilized to form blend fibers of cellulose and soy protein. We hypothesized that by having a binary solvent mixture would facilitate the protein denaturation. This would in turn facilitate the interaction between cellulose and the unfolded subunits of soy protein. Furthermore, the ED/KSCN system is energy- and time efficient enabling rapid and direct dissolution of cellulose/protein blends to regenerate into fibers by coagulating in methanol. Thus, this superior system that is easier to fabricate resulting in structures with excellent compatibility between two interphases is attractive for various commercial applications.

### **3.2 Materials**

The amine/salt system is composed of 65 wt % ethylene diamine (ED) and 35 wt % potassium thiocyanate (KSCN), both are reagent grade and purchased from Sigma-Aldrich. KSCN was first dried overnight in a vacuum oven at 60°C to remove excess moisture. A known weight of the salt was slowly added into the corresponding weight of ED while mixing. Then, the mixture of ED and KSCN were stirred by slightly heating until the salt was completely dissolved. Finally, the prepared ED/KSCN solvent was left to cool and to equilibrate.

Cellulose was received from Buckeye Technologies Inc. as sheets of dissolving wood pulp that were acetate grade, pressed, refined and bleached. The sheets were shredded in a grinder forming cellulose crumbs. The obtained cellulose was coded as Buckeye VFC cellulose by the company and it had a DP of ca. 600. In addition, ADM Specialty Products-Oilseeds provided soy protein (PRO-FAM 955<sup>®</sup>) that was received in isolated form containing 93.8%

dry basis protein. Prior to dissolution, the cellulose and the soy protein isolate (SPI) were dried overnight in a vacuum oven at 60°C to eliminate undesired moisture. For the coagulant, ACS reagent grade methanol was purchased from BDH Industries Ltd.

### **3.3 Preparation of Spinning Solutions**

Spinning solutions with five different compositions were prepared. The total concentration ( $C_p$ ) of cellulose and SPI was 7 wt %. In other words, 7 g of the polymers and 93 g of ED/KSCN (65/35) solvent were all added into a flask that was kept in an oil bath at 90°C. The cellulose-SPI-ED/KSCN mixture was stirred for 2 – 3 h until complete dissolution. The composition of the polymers in the solution varied from 0 – 40% SPI ratio by 10% increase. The SPI ratio above 40% was not spinnable at the same draw ratio due to the reduction of the viscosity.

The dissolution of each polymer, cellulose (3 wt %) and SPI (3 wt %), in ED/KSCN solvent system was confirmed using a polarized light microscope. The polymer solutions were stirred for 120 min at 90°C. Before cooling down to room temperature, a tiny drop of each solution was quickly placed on a microscope slide and pressed carefully with a cover slide on top. Then, it was observed under cross-polarized view of Nikon H550S Eclipse 50i optical microscope. The pictures taken by the microscope's camera using NIS Elements F (version 2.20) software appeared completely dark indicating complete dissolution. A similar study was also previously performed in our research group in order to produce blend membranes [36]. A time elapse visual study demonstrated the solubility of cellulose-SPI blend solution in 30 to 120 min by 30 min intervals.

### 3.4 Fiber Formation

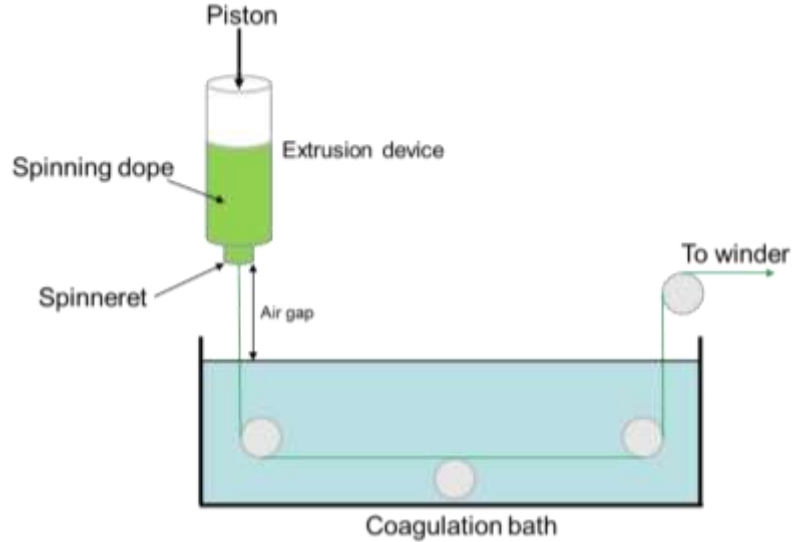


**Figure 3.1.** A schematic illustration of dry-jet wet spinning system utilized to fabricate cellulose/SPI fibers

A laboratory scale dry-jet wet spinning apparatus shown in Figure 3.1 was utilized to fabricate the blend fibers. The spinning system comprised of a Bradford piston-spinning unit, a spinneret pack, a coagulation bath, and a take-up winder. The spinning unit containing a piston applies pressure onto a stainless steel barrel covered with a heating jacket. After the spinning solution (dope) was introduced into the barrel at 75°C, a piston speed of 0.8 mm/min was applied to the spinning dope. The dope was forced through two filters and a spinneret with an orifice diameter of 127  $\mu\text{m}$  (0.005"). The spinneret had a ratio of length to diameter (L/D) of 2. The dope was then extruded into the coagulation bath at ambient temperature after passing an air gap of 10 cm. The coagulated fiber was then collected on a take-up winder at a speed of 64 m/min, with draw down ratio ( $D_r$ ) maintained at 2. The collected fibers were further soaked in methanol overnight to remove the solvent residues and were further dried at room temperature. Table 3.1 shows spinning conditions utilized to fabricate the blend fibers.

**Table 3.1.** Spinning conditions applied for all fibers

Spinning temperature (°C)	75	Piston speed (mm/min)	0.8
Air gap (cm)	10	Take-up speed (m/min)	64
L/D ratio of orifice	2	Draw down ratio	2
Orifice diameter (µm)	127	Coagulation bath length (m)	1.8
Coagulation liquid	Methanol	Coagulation temperature	Ambient temperature

Throughout the study, regenerated cellulose fiber is coded as CE, and the blend fibers as CESP1, CESP2, CESP3, and CESP4 with the numbers corresponding to the SPI ratio ranging from 10 to 40% in the blend fibers.

### 3.5 Characterization Techniques

The dynamic viscosity of the spinning solutions was measured in accordance with ASTM D2196 standard using a LVTDV-II-type Brookfield viscometer with a spindle rotation speed of 3 rpm. The effect of increasing protein content to the dynamic viscosity of spinning solutions at 75°C were assessed.

The total nitrogen (N %) content of the blend fibers was determined by a Perkin Elmer 2400 CHNS analyzer using total combustion method. The weight percent of protein ( $W_{pro}$ ) retained in the fibers were then computed using the equation:

$$W_{pro} = k (N - 0.14)\%$$

where  $k$  corresponds to constant of 6.65 calculated from the protein's nitrogen content,  $N$  being the nitrogen content present in the blend fibers. The nitrogen content of cellulose fiber (0.14) due to the residual solvent was deducted to reflect the true protein content in the blend fibers.

Fourier transform infrared spectroscopy (FTIR) measurements on the blend fibers were carried out by an attenuated total reflection method using a Thermo Fisher Nexus 470 FTIR,

analyzed by Omnic software. Diamond tip was used as sensor and the experiments performed in absorbance mode to record the spectra from 4000 to 700  $\text{cm}^{-1}$  over 64 scans at the resolution of 4  $\text{cm}^{-1}$ . For comparison, FTIR spectra of CE fiber and raw SPI were carried out.

Thermogravimetric analysis (TGA) was performed on a TA Q500 V20.13 TGA to analyze the mass changes that occur in fiber and control samples with increases in temperature. In this experiment, minimum 5 mg of each sample was placed on a platinum pan and a heating rate of 10°C/min was applied from 25°C to 100°C, under a dynamic nitrogen atmosphere. The temperature was held at 100 °C for 5 min in order to remove excess moisture. Then, the samples were cooled down to 30°C marking the end of the first cycle. A second cycle was performed with the same rate up to 700°C. Finally, post analysis was performed on the raw data obtained from the second cycle and the reported curves were drawn using Origin 9.1.

To determine the morphology, miscibility and compatibility of polymers in polymer-blend systems, electron microscope images were obtained by using the FEI Verios 460L field-emission scanning electron microscope (FESEM). To image the fiber cross-sections, the samples were initially frozen and fractured in liquid nitrogen, and were then mounted on carbon tape. Prior to taking images, gold/palladium was sputter coated onto the samples. Finally, micrographs were obtained at 2,500X and 10,000X magnifications and the effect of protein on the microstructure of the fibers were studied.

Wide-angle X-ray diffraction (WAXD) analyses were obtained on a Rigaku SmartLab X-ray Diffractometer equipped with a Cu X-ray tube ( $\text{CuK}_\alpha$  radiation,  $\lambda=0.1542$  nm). The operating voltage and current were set at 40 kV and 44 mA, respectively. The diffracting intensities were collected every 0.1  $2\theta^\circ$  from 5 to 40  $2\theta^\circ$ . The percent crystallinity ( $\chi_c$ ) were

then determined using a PDXL software from Rigaku (Tokyo, Japan). It was estimated from the peak areas of (10 $\bar{1}$ ), (101), and (002) planes following the equation:

$$\chi_c = \frac{I_c}{I_c + I_{am}} * 100\%$$

where  $I_c$  and  $I_{am}$  corresponds to the areas in the crystal phase and amorphous phase, respectively.

The denier of fiber specimens was measured by Vibromat ME Tester equipment based on resonating frequency. Tensile testing was carried out in accordance with ASTM D3822 procedure using an MTS Q-test/5 universal testing machine, and the data evaluated with TestWorks 4EM V4.11B software. Instron testing was conducted on cellulose and the CE/SPI blend fibers with a gauge length of 1 inch (25.4 mm) at a crosshead speed of 15 mm/min. From the instron testing, tensile properties including initial modulus and tenacity (g/den) and percentage strain at break (%) were obtained.

The refractive indices of fibers (in triplicates) were measured on a Nikon H550S Eclipse 50i polarizing optical microscope. Prior to testing, the fibers were immersed in series of mineral oils as immersion liquids, and their averaged values were reported. The birefringence ( $\Delta n$ ) of each fiber as the numerical difference between the parallel ( $n_{\parallel}$ ) and the perpendicular ( $n_{\perp}$ ) indices was calculated following the equation:  $\Delta n = n_{\parallel} - n_{\perp}$

The biodegradation test of CE, CESP2 and CESP4 fibers was studied in a compost medium with oxygen conditions [37]. A composter, Pro XE compost manufactured by Nature Mill, was used to accommodate the compost composed of food waste (~75% of mostly green, leafy vegetables), wood chips (~23%), and baking soda (~2%). After 30 days of incubation in the compost, fiber samples were removed from the compost and their mechanical properties

including peak load and elongation at peak load were measured, and compared with the untreated fibers.

## **3.6 Results and Discussion**

### **3.6.1 Dynamic viscosity of the spinning solutions**

The dissolution of cellulose and soy protein in ED/KSCN solvent system resulted in stable solutions that appeared transparent and homogenous at all compositions. The viscosity of the solutions, however, was dependent on the protein content allowing a certain degree of stretching for fiber spinning. As shown in Figure 3.2, the viscosity gradually decreased with increase in the protein content. For example, compared to the cellulose solution, replacement of 40% cellulose by SPI (CESP4) caused significant decrease (~21%) in the viscosity of the spinning solution to 31.4 Pa.S. As the solution with SPI ratio higher than 40% caused significant decrease in the viscosity with low adequate jet strength, fiber formation was not possible beyond 40% SPI at the draw ratio of 2.

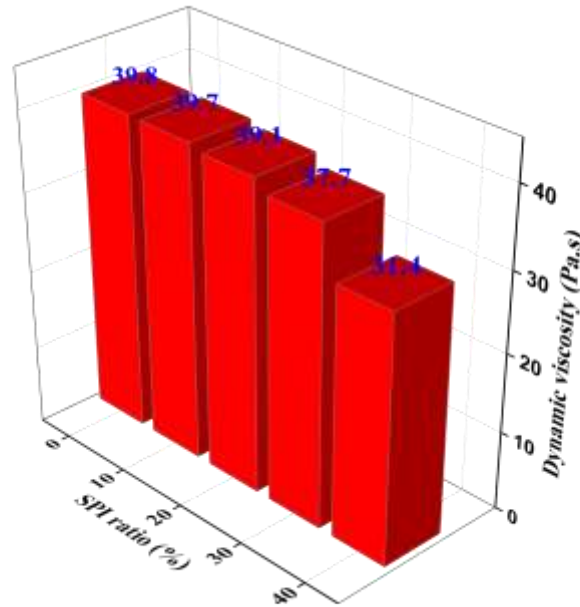


**Figure 3.2.** Dynamic viscosities of the spinning solutions with varying SPI concentrations at 75°C

### 3.6.2 Protein content

Compared to the initial added content, some of the added protein, unavoidably diffuses into the methanol during fiber coagulation, resulting in decreased content in the fiber blends. This can be attributed to enhanced solubility of the subunits present in denatured protein in the coagulant, with their precipitation into methanol from the fiber surface facilitated further by ED/KSCN solvent. A very low amount of nitrogen content was found in the cellulose fiber containing the solvent residue that was not eliminated from the calculation of the  $W_{pro}$ . Despite some loss, as seen in Table 3.2, substantial amount of the protein was retained in the blend fibers suggesting strong interactions occurred between the cellulose and soy protein through hydrogen bonding. The results correlates well with similar conclusions that have been reported in the past [38].

**Table 3.2.** Protein content ( $W_{\text{pro}}$ ) of CE, CESP fibers, and raw SPI

<b>Sample</b>	<b>N%</b>	<b><math>W_{\text{pro}}</math> (%)</b>
CE	0.14	None
CESP1	1.33	7.9
CESP2	2.15	13.4
CESP3	2.86	18.1
CESP4	3.72	23.8
SPI (raw)	14.11	93.8

### 3.6.3 Chemical structure

To investigate the interactions that occur between the cellulose and soy protein isolate phases in the fiber network, FTIR experiments were conducted on cellulose and blend fibers, and raw SPI. The results of the FTIR experiments are shown in Figure 3.3. The stretching of O–H and N–H groups present in raw SPI appeared at  $3286\text{ cm}^{-1}$ . However, after blending with cellulose and subsequent regeneration in methanol, with denatured protein likely dispersed homogeneously dispersed into cellulose network, the stretching of the mentioned functional groups is hindered. Consequently, the characteristic peaks for cellulose at  $3380\text{ cm}^{-1}$  corresponding to the stretching vibration of hydroxyl groups (OH) becomes predominant in all fibers.

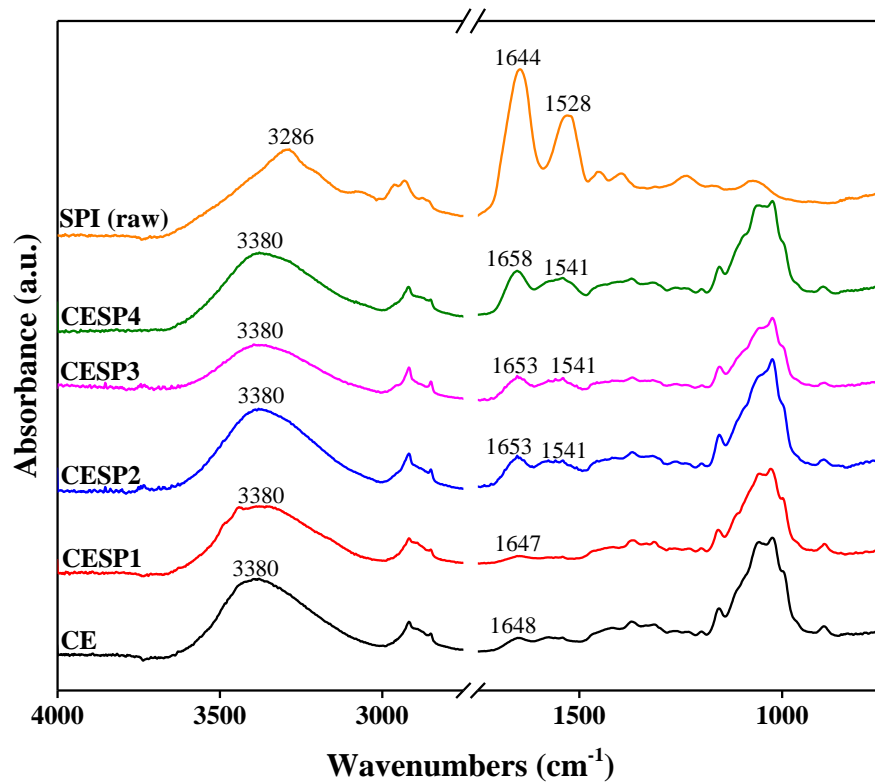


**Figure 3.3.** FTIR spectra of CE, CESP fibers and raw SPI

Some apparent peak shifts were also observed between the wavenumbers 1500 and 1700  $\text{cm}^{-1}$ . The peaks for SPI observed at 1644 and 1528  $\text{cm}^{-1}$  correspond to amide I (C=O stretching) and amide II (N–H bending) bands, respectively. In contrast, cellulose exhibited a peak at 1648  $\text{cm}^{-1}$  that can be attributed to the absorbed water [39]. After blending the polymers, at low SPI content (10%) a single evident peak at 1647  $\text{cm}^{-1}$  was observed. However, with increase in SPI content, peak shifts to higher wavenumber (1653  $\text{cm}^{-1}$ ) with emergence of a new peak at 1541  $\text{cm}^{-1}$  corresponding to amide II groups in SPI. The peak shifts corresponding to amide II groups from 1528 to 1541  $\text{cm}^{-1}$  demonstrates excellent interaction between the two phases. Likewise, with increase in SPI content, similar trend in peak shifts of amide I peaks were observed indicating the formation of intermolecular hydrogen bonds [24,26,28,31].

### 3.6.4 Thermal properties

Thermal degradation behavior of CE, CESP1, CESP2, CESP3, CESP4 fibers and raw SPI for comparison is illustrated in Figure 3.4. All samples had ~ 5% moisture which were removed in the first heating cycle. The second cycle was utilized to reveal the degradation temperatures of the fibers with and without added protein contents. Initial ( $T_i$ ) and maximum ( $T_{max}$ ) degradation temperatures of the fibers were observed to be similar; however, with increases in protein content, a concomitant decrease in the total weight loss ( $W_{Tf}$ ) was noted at the final temperature ( $T_f$ , shown by the arrow on Figure 3.4) indicating enhanced thermal stability. In other words, while the  $T_f$  of CE fiber observed at 320°C, gradually decreased to 309°C for CESP4 blend fiber. Likewise,  $W_{Tf}$  of CE was 50.8%, while for CESP4 was 43.8%. As a result, the char yield at 700°C for the fibers increased to higher level following similar trend: it increased from 29.6% for CE fiber to 33.3% for CESP4 fiber.

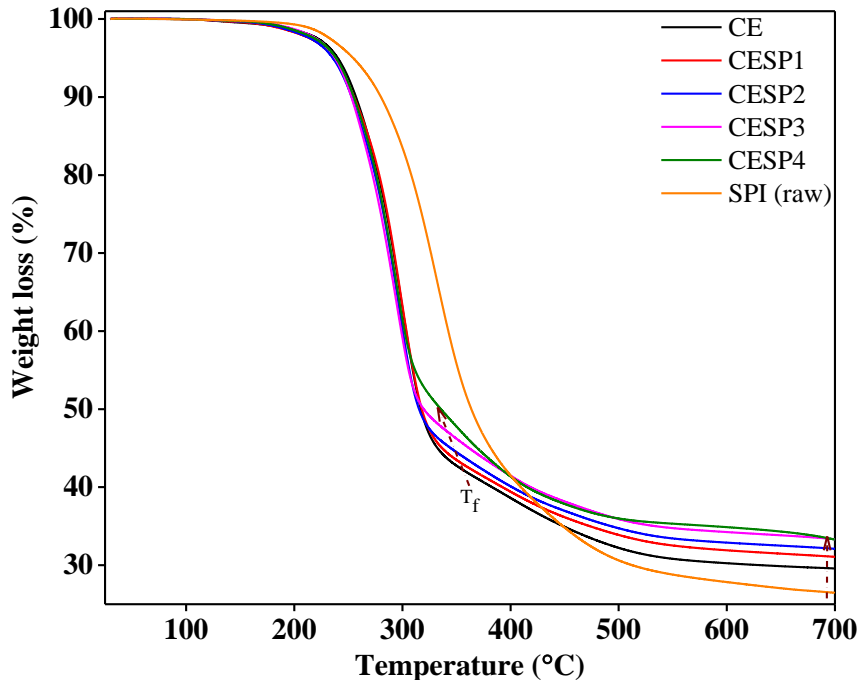


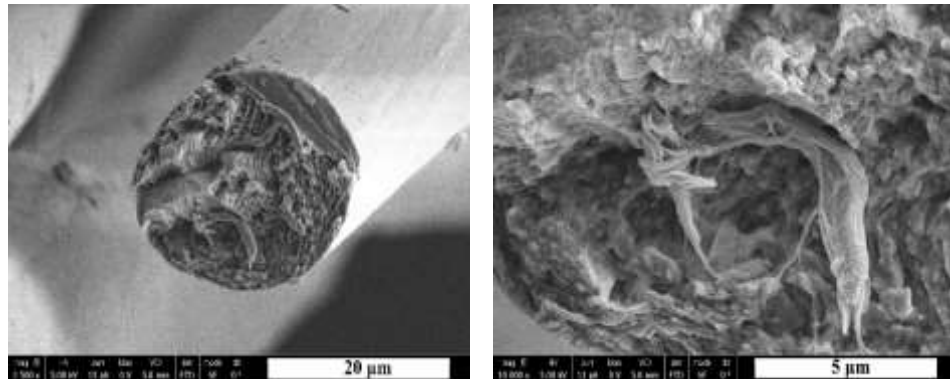
**Figure 3.4.** TGA thermograms of CE, CESP fibers and raw SPI

Additionally, the thermogram of raw SPI revealed higher decomposition temperature ( $T_{\max}=332^{\circ}\text{C}$ ) than all fibers. But, as a result of strong interactions between cellulose and soy proteins resulting in polymer blend structure, the blend fibers exhibited a higher char yield than raw SPI (26.5%). This observation suggests that the blend fibers are not mixtures of two discrete phases but are polymer blends containing strongly interacting components [36].

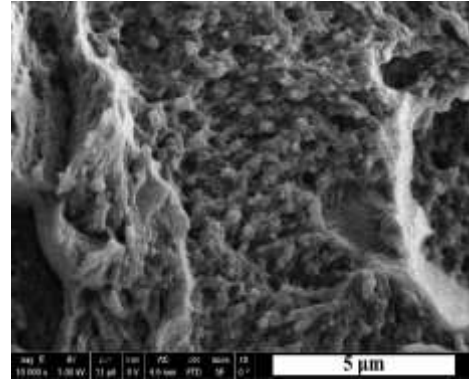
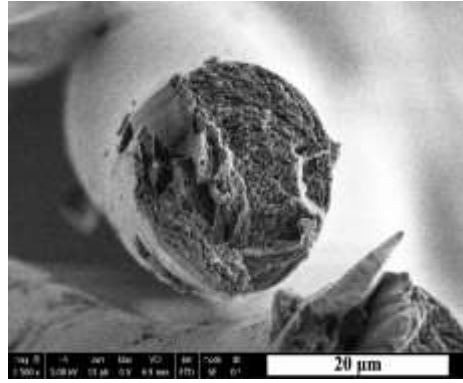
### 3.6.5 Morphology

The FESEM images obtained from the cellulose and the blend fibers are shown in Figure 3.5. All fibers had perfectly round cross-sections that were similar to melt-spun fibers. The characteristic structure of regenerated cellulose fibers with nanopores and fibrils were observed for the CE and CESP fibers, in accordance with previous report [40]. Therefore, it can be presumed that the globular structure of protein subunits was distorted or denatured due to the ED/KSNC solvent system. The unfolded structure of the protein was most likely homogeneously dispersed and thus generated rougher fibril bundle tips that are more apparent for CESP4 fiber. Compared to the reported cellulose/SPI [41] and cellulose/plant protein [42] blend fibers, microscopically large phase separation was not observed along the CESP fiber axes and the cross-sections.

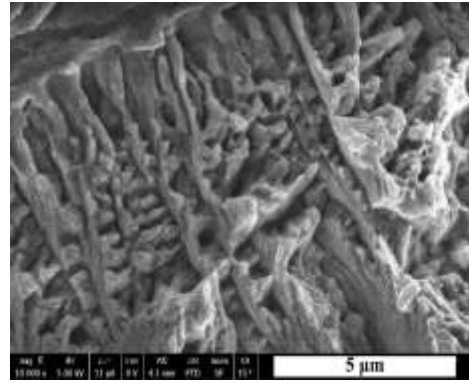
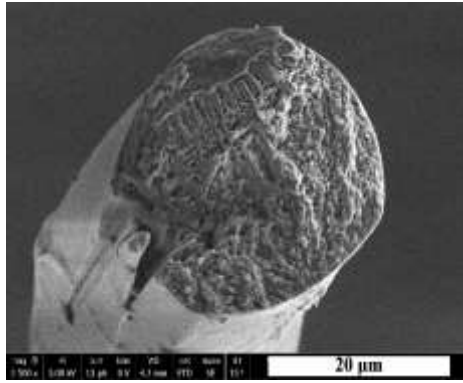
CE



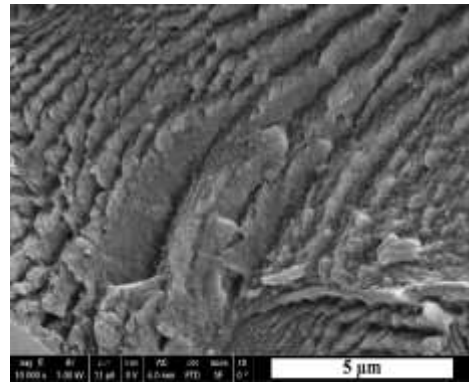
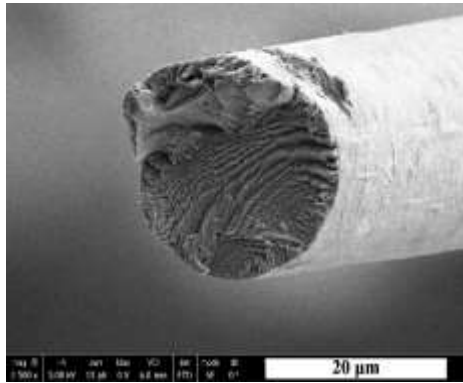
**CESP1**



**CESP2**



**CESP3**



**CESP4**

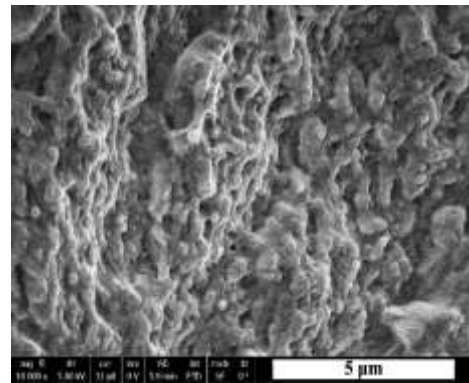
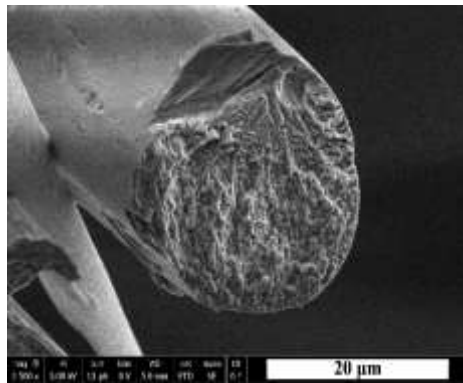


**Figure 3.5.** FESEM images of the fractured cross-sections of CE and CESP fibers

Fink et al. [40] reported the micrographs of an amine oxide-type fiber and a viscose rayon. In comparison to those fibers, the cellulose and the blend fibers regenerated from ED/KSCN system did not exhibit such a fibrillated morphology of the fiber from N-methylmorpholine N-oxide/water system. However, they resemble the rayon.

### 3.6.6 Crystalline structure

X-ray diffraction patterns of the fibers (CE, CESP1, CESP2, CESP3, and CESP4) and raw SPI are shown in Fig. 3.6. The cellulose fiber exhibits two diffraction peaks at  $2\theta = 11.7^\circ$  and  $20.8^\circ$  corresponding to typical diffraction peaks observed for the cellulose III crystal structure. This presence of this structure can be attributed to the coagulation of cellulose-amine complex in methanol or ethanol [43]. Its corresponding crystal planes are  $(10\bar{1})$  and the mixture of  $(101)$  and  $(002)$ . On the other hand, the blend fibers appear to have a transformed crystal structure exhibiting three distinct peaks associated with cellulose II crystals. The peaks of CESP1 fiber at  $2\theta = 12.2^\circ$ ,  $20.2^\circ$  and  $21.9^\circ$  slightly shifts to  $2\theta = 11.0^\circ$ ,  $19.4^\circ$  and  $21.7^\circ$  for CESP2 and remains about the same for CESP3 and CESP4 fibers. The related crystal planes of cellulose II including  $(10\bar{1})$ ,  $(101)$ , and  $(002)$  are represented on the peaks of CESP4 in Figure 3.6. Furthermore, raw SPI having mainly amorphous structure showed two broad peaks  $2\theta = 8.9^\circ$  and  $19.1^\circ$ , in accordance with the previous reports in the literature [44,45]. After the regeneration into the blend fibers, the denatured protein form predominantly random coil confirmation resulting in amorphous structure as well [46].

The transformation of crystal structure suggests that the introduction of SPI into the crystalline network rearranged the intermolecular hydrogen bonding of cellulose as a result of the interaction between the two polymers. That is to say, the crystallization of cellulose was interfered by the incorporation of SPI which is frequently referred to as a depression of polymer

crystallization in a composite. The regular folding of cellulose chains is disturbed by denatured protein chains since these two kinds of chains have close interactions and a certain level of miscibility [44].

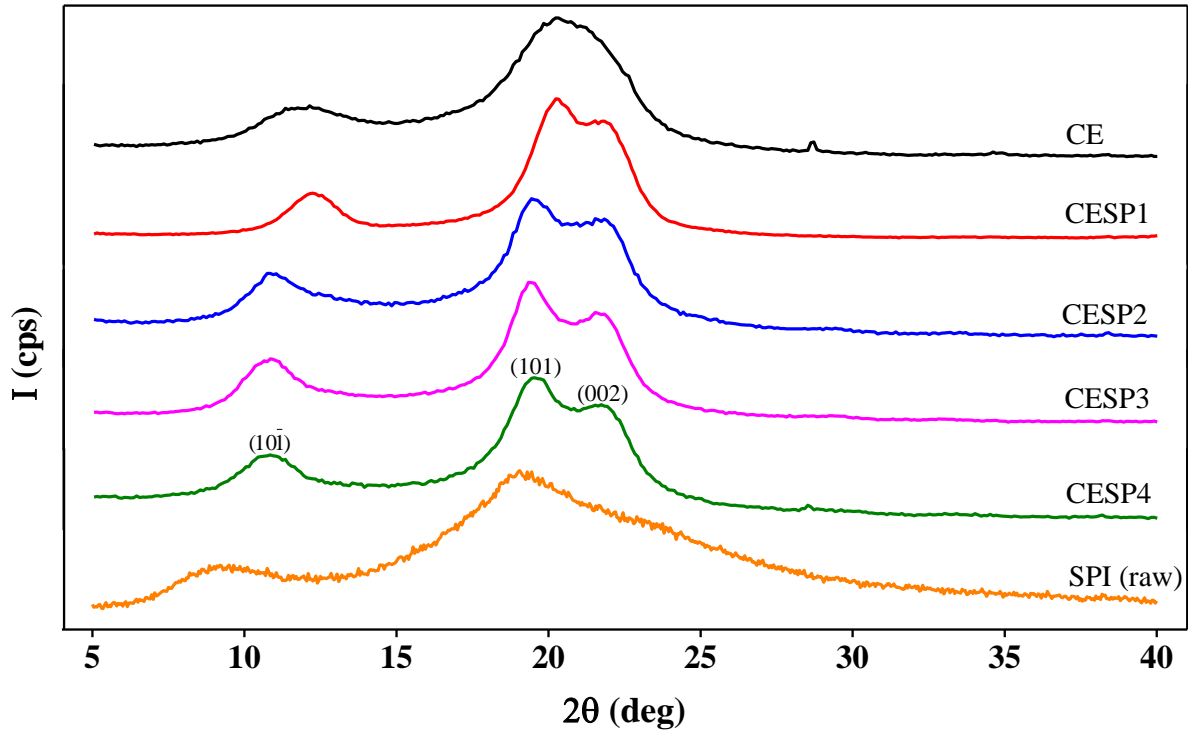


**Figure 3.6.** WAXD results of CE, CESP fibers and raw SPI

As X-ray diffraction can also be used to determine the percent crystallinity, WAXD was utilized to characterize the changes in the crystallinity with the addition of SPI. Despite their subjective nature, the crystallinity determined by this method have shown experimental uncertainty of only about 10%, the results are thus adequate for relative comparison between the cellulose and the blend fibers in this study [47]. Table 3.3 shows the percent crystallinity the fibers (CE, CESP1, CESP2, CESP3, and CESP4) and raw SPI. The CE, CESP1 and CESP2 have similar  $\chi_c$  values, but with increase in SPI content (CESP3 and CESP4 fibers), a gradual decrease in crystallinity values with up to ~20% for CESP4 were observed. In other words, up to 20% SPI content, the homogeneously dispersed protein did not have a significant effect on

the crystallinity. However, above this ratio, due to the disturbance of cellulose chains by the protein caused decreases in the crystallinity, consequently contributing to the roughness of the fibril bundle tips observed in the micrographs. Eventually, the percent crystallinity decreased from 60% for CE fiber to 49.6% for CESP4 fiber.

**Table 3.3.** The percent crystallinity of CE, CESP fibers, and raw SPI

<b>Sample</b>	<b><math>\chi_c</math> (%)</b>
CE	60.0
CESP1	58.2
CESP2	59.4
CESP3	54.6
CESP4	49.6
SPI (raw)	8.5

Compared to this report, one previously report cellulose/SPI blend fiber has showed insignificant decrease in crystallinity from their control system, but the authors related the marginal decrease in the intensity in one of two peaks to the intermolecular interaction [41]. On the other hand, in cellulose/plant protein blend fibers, crystallinity was found not to be affected with the addition of the presence of the protein, which is distinctly separated from the cellulose phase. Similarly, no change was found also for cellulose/silk fibroin fibers from LiCl/DMA solvent system [48].

### **3.6.7 Tensile properties**

As shown in Table 3.4, the initial modulus of the blend fibers is higher than the cellulose fiber indicating a correlation with the increasing protein content. It can be deduced that more protein content contributes to the overall stiffness of the fibers becoming more brittle with higher ratios of SPI and consequently decreases the elongation at break. This effect can

also be referred to the existence of larger or more microvoids in the fiber cross-sections from CE to CESP4. However, the micrographs did not show a clear difference between the fibers in terms of microvoids. In addition, the stiffness indicates strong intermolecular interaction between cellulose and SPI [48].

**Table 3.4.** Tensile properties of CE and CESP fibers

<b>Fiber</b>	<b>Initial modulus (g/den)</b>	<b>Tenacity (g/den)</b>	<b>Elongation at break (%)</b>	<b>Denier</b>
CE	91.8 ± 11.9	2.46 ± 0.1	13.2 ± 0.8	5.4 ± 0.1
CESP1	104.4 ± 7.5	2.52 ± 0.22	11.3 ± 2.3	5.3 ± 0.6
CESP2	105.5 ± 13.7	2.69 ± 0.16	12.4 ± 1.2	6.2 ± 0.5
CESP3	112.9 ± 9.1	2.39 ± 0.11	8.8 ± 1.2	5.5 ± 0.3
CESP4	115.6 ± 15.3	1.76 ± 0.12	8.5 ± 1.8	4.7 ± 0.3

The tensile property profile can be utilized to determine the compatibility of blend fibers in comparison with the pure constituent fiber [49]. To better visualize the changes in the tenacity and the elongation at break, the data from Table 3.4 were plotted versus the SPI ratio illustrated in Figure 3.7. In addition, the stress-strain curves are also shown in Figure 3.8. As seen in Figures 3.7 and 3.8, the tenacity increased with the addition of SPI (up to 20%). But at 30%, a slight decrease in the tensile strength of the composites were observed. However, with further incorporation of SPI, a significant reduction in the strength was noted. Moreover, the decrease in the elongation could be considered gradual with the exception of CESP2 fiber, which also has the highest tenacity and the percent crystallinity among the blend fibers. In other words, cellulose and SPI show the best compatibility at CESP2 fiber.

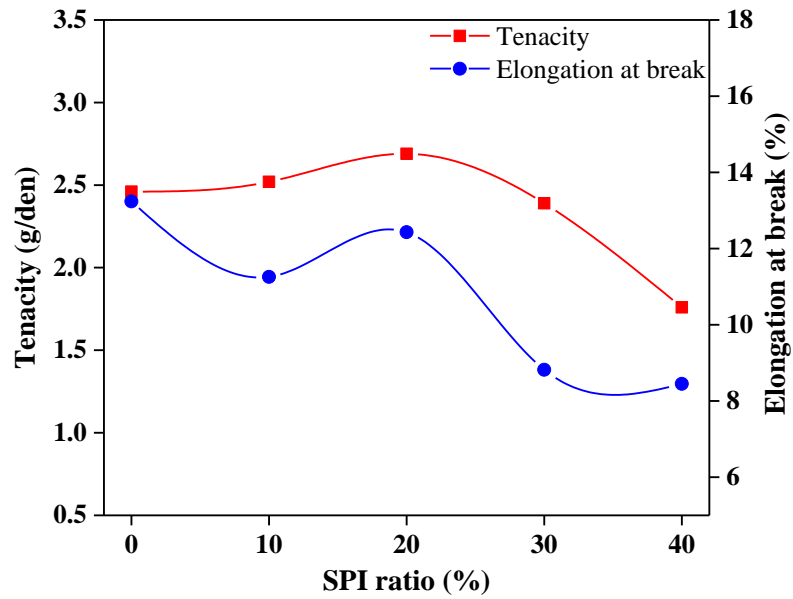


**Figure 3.7.** Effect of the SPI ratio on the tenacity and the elongation of the fibers

To summarize, when compared with the reported cellulose/SPI [41] and cellulose/plant protein [42] blend fibers, blend fibers reported in this study have superior tensile properties, which are comparable to viscose/soy protein [18] blend fiber.

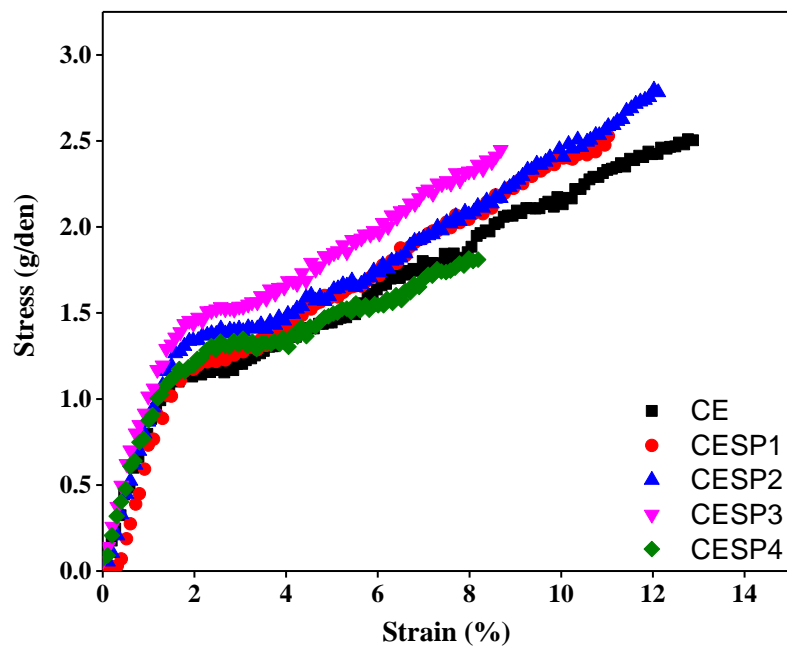


**Figure 3.8.** Stress – strain curves of the fibers

### 3.6.8 Birefringence

The correlation between the tensile properties and the molecular chain orientation of fibers can be discussed by birefringence: a parameter related closely to the degree of orientation [50]. Increasing SPI content monotonically decreased the birefringence as well as the amorphous and the crystalline orientation of the fibers. As seen in Table 3.5, the perpendicular refractive index increases constantly above 10% SPI ratio. In conjunction with the decreasing crystallinity, the blend fibers contain larger amorphous phases that are less orientated especially above the ratio of 20% SPI. Consequently, a drop in the overall orientation imparts weakness to the blend fibers with high protein content, i.e. CESP4.

**Table 3.5.** Refractive indices (RI) and birefringence of the CE and CESP fibers.

<b>Fiber</b>	$n_{\parallel}$	$n_{\perp}$	$\Delta n$
CE	1.550	1.510	0.040
CESP1	1.552	1.510	0.042
CESP2	1.552	1.512	0.040
CESP3	1.552	1.516	0.036
CESP4	1.549	1.520	0.029

It is worthwhile to report here that commercially obtained regenerated protein fibers, such as Azlon from casein and Vicara from zein, have either very low or no birefringence due to having imperfect orientation rendering the fibers isotropic [51,52]. Similar to those protein fibers, having little or no orientation from SPI hindered the overall orientation of blend fibers of CESP3 and CESP4.

### 3.6.9 Biodegradation

Composting, which is a natural means of recycling, is an effective method for testing the biodegradation of fibers, since its medium incorporates a broad range of microorganisms and moderately high temperatures. At optimum conditions, biodegradability of organic materials can be investigated and reported by measuring the mechanical properties before and after composting [37,53].

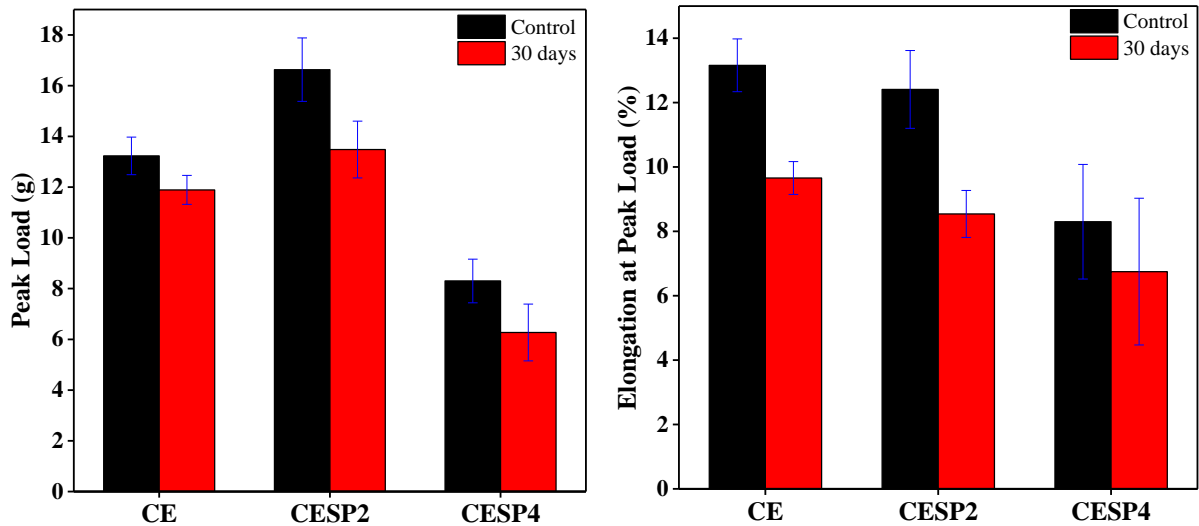


**Figure 3.9.** Peak load and elongation at peak load of the control and 30 days composted CE and CESP fibers

As shown in Figure 3.9, the cellulose fiber losing about 10% of its strength and the elongation decreasing by 27%. However, the strength loss for CESP2 fiber was 19% and a greater loss of 24%, occurred for CEPS4 fiber. Likewise, the elongation of CESP2 was reduced by 31% and in the case of CESP4, a 19% decrease with high standard deviation was observed. Overall, it can be concluded that the higher protein content hastens the biodegradation of the cellulose fibers. This can also be correlated with a decreasing percent crystallinity of the fibers with increasing SPI ratio.

### **3.7 Conclusions**

The successful incorporation of soy protein into regenerated cellulose fiber network was achieved by employing ED/KSCN a common solvent system and subsequent coagulation in methanol. Viscosity of the fiber forming solutions decreased significantly at 40% SPI ratio hindering further incorporation of protein into the fibers at the spinning conditions. The retained protein in the blend fibers gradually increased substantiating the interaction with cellulose. This was also confirmed by FTIR and WAXD results revealing the intermolecular interactions between the two polymer phases mainly through hydrogen bond formation. TGA thermograms revealed enhanced thermal stability by increasing protein content. FESEM images exhibited homogeneous dispersion of protein and no visible phase separation on the axis or the cross section of the blend fibers was observed. Although the denatured protein contributed to the fibrillar structure, its inherent amorphous morphology decreased the crystallinity of the blend fibers above 20% SPI ratio. Furthermore, the tensile properties indicated that the best compatibility of the polymers was obtained at that ratio with 2.69 g/den tenacity and 12.4% elongation. The birefringence suggests that the overall orientation is also affected by higher protein content over the 20% ratio. However, the more the protein, the faster the biodegradation of the fibers.

### **3.8 Acknowledgement**

The authors would like to acknowledge the financial support of the Turkish Ministry of National Education to Ramiz Boy during his PhD. The authors also thank Dr. Amit Naskar for the use of TGA instrument at Oak Ridge National Laboratory. Special thanks to laboratory technicians, Tri Vu, Judy D. Elson, and William Barnes, for their help. In addition, the authors

appreciate the useful advice from Dr. Samuel Hudson, Dr. Thomas Theyson, and Dr. Mohamed Bourham.

### 3.9 References

1. Narayanan G, Gupta BS, Tonelli AE (2014) Poly( $\epsilon$ -caprolactone) Nanowebs Functionalized with  $\alpha$ - and  $\gamma$ -Cyclodextrins. *Biomacromolecules* 15 (11):4122-4133
2. Narayanan G, Ormond BR, Gupta BS, Tonelli AE (2015) Efficient wound odor removal by  $\beta$ -cyclodextrin functionalized poly ( $\epsilon$ -caprolactone) nanofibers. *Journal of Applied Polymer Science* 132 (45)
3. Narayanan G, Gupta BS, Tonelli AE (2015) Enhanced mechanical properties of poly ( $\epsilon$ -caprolactone) nanofibers produced by the addition of non-stoichiometric inclusion complexes of poly ( $\epsilon$ -caprolactone) and  $\alpha$ -cyclodextrin. *Polymer* 76:321-330
4. Narayanan G, Gupta BS, Tonelli AE (2015) Estimation of the poly ( $\epsilon$ -caprolactone) [PCL] and  $\alpha$ -cyclodextrin [ $\alpha$ -CD] stoichiometric ratios in their inclusion complexes [ICs], and evaluation of porosity and fiber alignment in PCL nanofibers containing these ICs. *Data in Brief* 5:1048-1055
5. Narayanan G, Aguda R, Hartman M, Chung C-C, Boy R, Gupta BS, Tonelli AE (2016) Fabrication and Characterization of Poly( $\epsilon$ -caprolactone)/ $\alpha$ -Cyclodextrin Pseudorotaxane Nanofibers. *Biomacromolecules* 17 (1):271-279
6. Narayanan G (2014) *Electrospinning of Poly (epsilon-caprolactone) Fibers Functionalized with Cyclodextrins and their Inclusion Complexes*. North Carolina State University, Raleigh, NC, USA
7. Klemm D, Heublein B, Fink HP, Bohn A (2005) Cellulose: fascinating biopolymer and sustainable raw material. *Angew Chem Int Ed Engl* 44 (22):3358-3393

8. Yamazaki F (2001) Antibacterial Viscose Rayon and Its Production. JP Patent 2001-003223,
9. Yamazaki F (2001) Viscose Rayon Having Modified Feeling. JP Patent 2001-003224,
10. Chua JM (2009) Uniqlo's HeatTech Clothing Creates Heat From Your Sweat. <http://www.ecouterre.com/uniqlos-heattech-clothing-creates-heat-from-yoursweat/>. Accessed Oct 29, 2015
11. Yamada M, Ohshima K (2012) Method of manufacturing cellulose-gelatin composite viscose rayon filament. U.S. Patent 8,293,157,
12. Singh N, Rahatekar SS, Koziol KK, Ng TS, Patil AJ, Mann S, Hollander AP, Kafienah W (2013) Directing chondrogenesis of stem cells with specific blends of cellulose and silk. *Biomacromolecules* 14 (5):1287-1298
13. Wang J, Wei L, Ma Y, Li K, Li M, Yu Y, Wang L, Qiu H (2013) Collagen/cellulose hydrogel beads reconstituted from ionic liquid solution for Cu(II) adsorption. *Carbohydr Polym* 98 (1):736-743
14. Luo L, Gan L, Liu Y, Tian W, Tong Z, Wang X, Huselstein C, Chen Y (2015) Construction of nerve guide conduits from cellulose/soy protein composite membranes combined with Schwann cells and pyrroloquinoline quinone for the repair of peripheral nerve defect. *Biochem Biophys Res Commun* 457 (4):507-513
15. Narayanan G, Vernekar VN, Kuyinu EL, Laurencin CT (2016) Poly (lactic acid)-based biomaterials for orthopaedic regenerative engineering. *Advanced Drug Delivery Reviews*
16. Chavassieu HLJ (1910) Process of obtaining proteo-cellulosic products. US Patent,
17. Koch T (1944) Manufacture of rayon. U.S. Patent 2,345,345,
18. Nicoll WD (1950) Process for producing artificial filaments. U.S. Patent 2,515,889,

19. Kanegafuchi Spinning CL (1966) Method for producing composite protein-cellulose fibres. GB Patent GB Patent 1,025,798,
20. Woodings C (2002) Cellulose Fibers, Regenerated. In: Mark HF, Kroschwitz JI (eds) Encyclopedia of Polymer Science and Technology, vol 5. 3 edn. John Wiley & Sons, Inc, Hoboken. NJ, p 532
21. Singh P, Kumar R, Sabapathy S, Bawa A (2008) Functional and edible uses of soy protein products. *Comprehensive reviews in food science and food safety* 7 (1):14-28
22. Silva NH, Vilela C, Marrucho IM, Freire CS, Neto CP, Silvestre AJ (2014) Protein-based materials: from sources to innovative sustainable materials for biomedical applications. *Journal of Materials Chemistry B* 2 (24):3715-3740
23. Brooks M (2005) Soya bean protein fibres—past, present and future. In: R.S. B (ed) *Biodegradable and sustainable fibres*. Woodhead Publishing Ltd, Cambridge, pp 398-440
24. Chen Y, Zhang L (2004) Blend membranes prepared from cellulose and soy protein isolate in NaOH/thiourea aqueous solution. *Journal of applied polymer science* 94 (2):748-757
25. Chen Y, Zhang LN, Gu JM, Liu J (2004) Physical properties of microporous membranes prepared by hydrolyzing cellulose/soy protein blends. *Journal of Membrane Science* 241 (2):393-402
26. Luo LH, Wang XM, Zhang YF, Liu YM, Chang PR, Wang Y, Chen Y (2008) Physical properties and biocompatibility of cellulose/soy protein isolate membranes coagulated from acetic aqueous solution. *J Biomater Sci Polym Ed* 19 (4):479-496
27. Luo LH, Zhang YF, Wang XM, Wan Y, Chang PR, Anderson DP, Chen Y (2010) Preparation, characterization, and in vitro and in vivo evaluation of cellulose/soy protein isolate composite sponges. *J Biomater Appl* 24 (6):503-526

28. Wu R-L, Wang X-L, Wang Y-Z, Bian X-C, Li F (2009) Cellulose/soy protein isolate blend films prepared via room-temperature ionic liquid. *Industrial & Engineering Chemistry Research* 48 (15):7132-7136
29. Luo L, Gong W, Zhou Y, Yang L, Li D, Huselstein C, Wang X, He X, Li Y, Chen Y (2015) Cellulose/soy protein isolate composite membranes: evaluations of in vitro cytocompatibility with Schwann cells and in vivo toxicity to animals. *Biomed Mater Eng* 25:57-64
30. Tansaz S, Boccaccini AR (2015) Biomedical applications of soy protein: A brief overview. *J Biomed Mater Res A*
31. Zhang SA, Li FX, Yu JY (2011) Novel Cellulose/SPI Blend bio-fibers Prepared via Direct Dissolving Approach. *Journal of Engineered Fibers and Fabrics* 6 (1):31-37
32. Rees ED, Singer S (1956) A preliminary study of the properties of proteins in some nonaqueous solvents. *Archives of biochemistry and biophysics* 63 (1):144-159
33. Mason PE, Neilson GW, Dempsey CE, Barnes AC, Cruickshank JM (2003) The hydration structure of guanidinium and thiocyanate ions: implications for protein stability in aqueous solution. *Proc Natl Acad Sci U S A* 100 (8):4557-4561
34. Frey MW, Li L, Xiao M, Gould T (2006) Dissolution of cellulose in ethylene diamine/salt solvent systems. *Cellulose* 13 (2):147-155
35. Lee HJ (2008) Novel Cellulose Solvent System and Dry Jet Wet Spinning of Cellulose/ED/KSCN Solutions. North Carolina State University,
36. Douglass E (2010) The Development of Cellulose Blend Membranes using Cellulose and other Natural Biopolymers using a Novel Solvent System. North Carolina State University, Raleigh, NC

37. Keene BN (2012) Biodegradation of Polypropylene Nonwovens. North Carolina State University, Raleigh, NC
38. Yang QL, Lue A, Qi HS, Sun YX, Zhang XZ, Zhang LN (2009) Properties and Bioapplications of Blended Cellulose and Corn Protein Films. *Macromolecular Bioscience* 9 (9):849-856
39. Lin S, Chen L, Huang L, Cao S, Luo X, Liu K, Huang Z (2012) Preparation and characterization of chitosan/cellulose blend films using  $ZnCl_2 \cdot 3H_2O$  as a solvent. *BioResources* 7 (4):5488-5499
40. Fink HP, Weigel P, Purz HJ, Ganster J (2001) Structure formation of regenerated cellulose materials from NMMO-solutions. *Progress in Polymer Science* 26 (9):1473-1524
41. Zhang S, Li F, Yu J, Gu L (2009) Novel fibers prepared from cellulose in NaOH/thiourea/urea aqueous solution. *Fibers and Polymers* 10 (1):34-39
42. Wawro D, Stęplewski W (2010) Producing of Continuous Cellulose Fibres Modified with Plant Proteins. *Fibres & Textiles in Eastern Europe* 18 (6):83
43. Isogai A, Gilbert RD (1994) Allomorphs of cellulose and other polysaccharides. In: *Cellulosic polymers, blends and composites*. Hanser, Munich, Germany, pp 1-24
44. Xu X, Jiang L, Zhou Z, Wu X, Wang Y (2012) Preparation and properties of electrospun soy protein isolate/polyethylene oxide nanofiber membranes. *ACS Appl Mater Interfaces* 4 (8):4331-4337
45. Zhou Z, Zheng H, Wei M, Huang J, Chen Y (2008) Structure and mechanical properties of cellulose derivatives/soy protein isolate blends. *Journal of Applied Polymer Science* 107 (5):3267-3274

46. Huang FF, Rha C (1974) Protein structures and protein fibers—a review. *Polymer Engineering & Science* 14 (2):81-91
47. Xiao M, Frey MW (2009) Study of cellulose/ethylene diamine/salt systems. *Cellulose* 16 (3):381-391
48. Marsano E, Canetti M, Conio G, Corsini P, Freddi G (2007) Fibers based on cellulose–silk fibroin blend. *Journal of Applied Polymer Science* 104 (4):2187-2196
49. Robeson LM (2007) *Polymer Blends: A Comprehensive Review*. Hanser Gardner Publications, Cincinnati, OH
50. Hearle JW (2001) Physical structure and fibre properties. In: Woodings C (ed) *Regenerated Cellulose Fibres*, vol 18. Woodhead Publishing, p 199
51. Hearle JW, Morton WE (2008) *Physical properties of textile fibres*. Elsevier,
52. Brinsko KM (2010) Optical characterization of some modern "eco-friendly" fibers. *J Forensic Sci* 55 (4):915-923
53. Wrzesniewska-Tosik K, Wawro D, Ratajska M, Steplewski W (2007) Novel biocomposites with feather keratin. *Fibres & Textiles in Eastern Europe* 15 (5-6):157-162

## **Chapter 4 Novel Cellulose – Collagen Blend Biofibers Prepared from an Amine/Salt Solvent System**

Reprint of a Manuscript Submitted to International Journal of Biological Macromolecules

by Ramiz Boy, Ganesh Narayanan, Richard Kotek

Fiber & Polymer Science, College of Textiles, North Carolina State University, Raleigh, NC

**Abstract:** Cellulose/collagen biofibers were produced from ethylene diamine/ potassium thiocyanate binary solvent system, with methanol as a coagulant. The dynamic viscosity of the solutions decreased with the gradual increase in the collagen content up to 40%. The elemental analysis showed incorporation of collagen into cellulose matrix, thereby demonstrating some degree of interaction with the cellulose matrix. The chemical and thermal analysis further revealed an intermolecular interaction between cellulose and the protein and improved thermal stability, respectively. Furthermore, the electron microscopy images mostly exhibited fibrillar morphology with no visible phase separation, indicating compatibility between the two phases. Moreover, biofibers containing higher cellulose content showed higher crystallinity, tensile, and birefringence properties of the composite fibers.

### **4.1 Introduction**

Cellulose and collagen are some of the renewable polymers that are abundantly found on earth [1]. Their use has recently gained momentum due to their sustainable nature and general awareness to utilize materials of natural origin. Recently, there have been several efforts reported to utilize fibers based on materials of natural origins (oligosaccharides) for applications such as wound odor absorbance, improving mechanical properties of the composites, and for potential drug and tissue regeneration application [2-8]. Compared to these

oligosaccharides based biomaterials, being ubiquitously present in virtually all tissues laying foundation for extra cellular matrix, collagen plays a key role in proper functioning of various tissues. In addition, collagen is a material of interest in the form of tissue engineering scaffolds as collagen (type-I, type-II, etc.) is present in larger quantities in orthopedic tissues such as bone, ligaments, tendons, muscles and cartilage [9-11]. Because of their biocompatible nature and cell-adhesive properties, collagen is also widely coated onto synthetic biomaterials that do not contain surface epitopes to improve cell-biomaterial interface [11]. In addition to coatings for biomedical scaffolds, collagen is widely used in cosmetics, medical sutures, wound care, drug, and cell delivery [12, 13]. Structurally, collagen is comprised of left-handed, three parallel polypeptide chains coiled around each other to form a right-handed triple helix conformation [14].

Cellulose, on the other hand, is known for its excellent tensile properties, and is well renowned and widely used in diverse applications, including textiles [15, 16]. Solution blending of cellulose with collagen could thus be a practical method to enhance the functionality of the final product, thereby opening new horizons and make them suitable for unexplored applications [17-19]. In addition, regenerated collagen has been evaluated by combining the collagen with cellulose, thereby overcoming the brittleness that is typically encountered by processing collagen, thus making them suitable for various applications in the form of film, fiber and gels [20]. But significant challenges lay ahead in fabricating these systems such as suitable solvent systems that are not only practically viable but also that causes minimal environmental concerns. Other challenges include, phase compatibility between collagen and cellulose. One approach to fabricate phase compatible cellulose/collagen blend

is by using ethyl-3-methylimidazolium acetate as a solvent demonstrated an entanglement effect between the two polymers in solution [21].

Initial knowledge about combining collagen and viscose rayon (modified cellulose) was demonstrated by a Japanese patent, that showed enhancements in the light fastness and the dyeing characteristics [22]. Followed by this study, another study reported successful preparation of collagen from N-methylmorpholine- N-oxide (NMMO) monohydrate for edible food casing and cartilage tissue regeneration [23]. However, both the studies showed significant disadvantages either by posing environmental issues (former study) [24, 25], or the requirement for a high process temperature (later study) [25, 26], alongside poor and limited dissolution of the protein [27]. To overcome poor solubility issue, more recently, cellulose/collagen blend films were produced by solubilizing in imidazolium based ionic liquids (ILs) [21, 28-30]. Although this type of solvents can dissolve the protein [20, 31], the regeneration into an intact form with cellulose might also be possible, but toxicity of these ILs is a major concern, along with their high cost for regeneration of natural polymers [32].

One feasible option is to utilize synthetically modified polymer, which provides better processing opportunities and also possess similar thermomechanical, and physical characteristics of cellulose. One recent study by Thanikaivelan et al. evaluated the blends of hydroxyethyl cellulose (a cellulose derivative) and collagen to obtain the so-called “hybrid films” with improved mechanical properties, better biostability, and enhanced cell growth compared to the protein film [33]. They further extended this research to produce hybrid fibers that had less than 1 g/den tenacity making them practically applicable as bioresorbable materials for wound healing applications [34]. Prior to this work, an amine/salt solvent system

have also been applied to dissolve cellulose [35] and soy protein [36-38] phases at elevated temperatures for relatively short time to obtain stable solution for fiber spinning.

As can be seen from the current technical literature, fabrication of composite fibers of cellulose and protein faces significant challenges, such as chemical toxicity, polymer solubility or cost. In addition, even if such composite fibers are fabricated, there is a dearth in thermomechanical, morphological, optical, and crystallographic knowledge of these materials. In this paper, we demonstrate successful preparation of cellulose/ collagen fibers from a mixture of ethylene diamine/potassium thiocyanate (ED/KSCN). In addition, we provide a thorough understanding of the thermomechanical, optical, and morphological behavior of these materials. With better understanding of their behavior, we anticipate successful application of these cellulose/collagen blend biofibers for variety of applications, including biomedical applications.

## **4.2 Materials**

The solvent system used in this study consisted of 65 wt% ethylenediamine (ED\_ and 35 wt% KSCN both reagent grade obtained from Sigma-Aldrich, St. Louis, MO. Prior to spinning, the salt was dried to eliminate the water present in the solvent system. The ED/KSCN mixture was stirred on a hot plate with little heat applied to expedite the dissolution. Once the salt was completely solubilized, the solvent was kept at room temperature to equilibrate.

Cellulose used for this research was Buckeye VFC (degree of polymerization~ 600) received in the form of thick sheets made from acetate grade, pressed, refined, and bleached wood pulp. The sheets were cut into small pieces and ground to facilitate dissolution. Collagen, obtained as peptide obtained from fish scale origin with a molecular weight (Mn) of 900~1500, was kindly donated by JNC America and, directly utilized for dissolution in solvents. Before

the solution preparation, cellulose and collagen were kept at least 12 hours in a vacuum oven at 60°C to remove absorbed moisture. ACS reagent grade methanol was obtained from BDH Industries Ltd, and was used for coagulant to precipitate the spun fibers.

### **4.3 Solution preparation**

A concentration ( $C_p$ ) of 7 wt% cellulose-collagen-ED/KSCN solution was prepared for all compositions by varying the weight ratio of cellulose to collagen with 10% increase up to a total 40% collagen content: CECOL1 (with 10% collagen), CECOL2 (with 20% collagen), CECOL3 (with 30% collagen), CECOL4 (with 40% collagen). The spinning dopes were obtained by mixing at 90°C for 2-3 hours to ensure complete dissolution. As fibers with the collagen ratio above 40% could only be used as-spun fibers without any applied stretching, those were not included in the study, as they are beyond the scope of this study. To verify complete dissolution of the two phases, an optical microscope (Nikon H550S Eclipse 50i) was used to examine the dissolution of cellulose and collagen. By examining a small amount of solution on a microscope slide with a coverslip, samples were observed under the cross-polarized view of optical microscope, once solutions emerged dark, complete dissolution of the two phases were confirmed.

#### 4.4 Fiber Formation

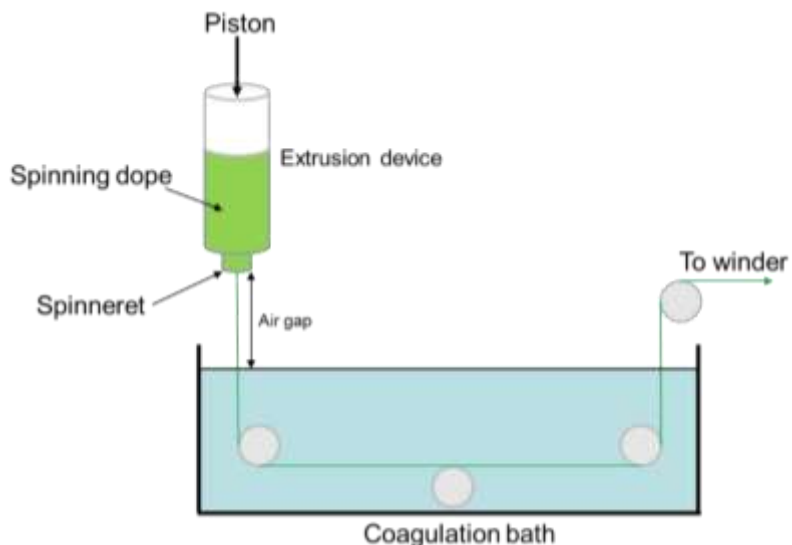


**Figure 4.1.** An illustration of dry-jet wet spinning system [38]

The fibers were spun in a laboratory scale dry-jet wet spinning line (Figure 4.1) which comprised of a piston spinning unit, a spinneret pack with stainless steel barrel containing two filters and four Teflon® O-rings, a 1.8 m long coagulation bath and a take-up winder to collect the fibers. The spinneret pack was covered with a braided heating tape to maintain the spinning temperature (75°C). Once the dope was poured into the barrel, the piston was pushed at a speed of 0.8 mm/min. The dope then passed through the filters and a single-hole spinneret ( $\phi=0.005$  inch and length/diameter=2). By travelling through an air gap of 1 inch from the spinneret into the methanol bath at room temperature, the fluid jet formed by the dope was coagulated by removal of the solvent. The obtained fiber was then wound up on a plastic bobbin via a take-up winder. The draw down ratio ( $D_r$ ) of all fibers were 2 with the exception of CECOL4 fiber that had a  $D_r$  of 1.6, which was necessary because of the viscosity decrease in the solution, caused by addition of collagen at higher amounts. The collected fiber was then aged overnight in methanol to eliminate the solvent residues, and was finally left to dry at ambient temperature. The fiber spinning conditions utilized in this study are included in Table 4.1.

**Table 4.1.** Fiber spinning conditions [38]

Spinning temperature (°C)	75	Piston speed (mm/min)	0.8
Air gap (inch)	1	Take-up speed (m/min)	64
L/D ratio of orifice	2	Draw down ratio ( $D_r$ )	2
Orifice diameter ( $\mu\text{m}$ )	127	Coagulation bath length (m)	1.8
Coagulation liquid	Methanol	Coagulation temperature	Ambient temperature

Note:  $D_r$  of CECOL4 was 1.6 so the take-up speed was 52 mm/min.

#### 4.5 Characterization Techniques

The dynamic viscosity measurement of the spinning solutions was performed according to ASTM D-2196 standard, on a LVTDV-II-type Brookfield viscometer, at spindle rotation speed of 3 rpm. The effect of collagen on the dynamic viscosity of solutions at 75°C, with collagen to cellulose ratios of 10:90, 20:80, 30:70, and 40:60, was evaluated in this study. The weight percent of protein ( $W_{\text{pro}}$ ) in the blend fibers was calculated from the total nitrogen ( $N\%$ ) content obtained using a Perkin Elmer 2400 CHNS analyzer, using the equation:  $W_{\text{pro}} = k(N-0.14)\%$ , where  $k$  and  $N$  are constant of 5.87 calculated from the protein's nitrogen content, and total nitrogen content, respectively. 0.14, the nitrogen content of cellulose fiber containing residual solvent is subtracted in order to evaluate only the content of protein.

Fourier transform infrared spectroscopic (FTIR) studies on the fibers were performed on a Perkin Elmer FTIR using an attenuated total reflection (ATR) technique which typically results in evanescent wave. A total of 64 scans at the resolution of 4  $\text{cm}^{-1}$  scans on each samples conducted between 4000 and 500  $\text{cm}^{-1}$  wavenumbers in absorbance mode. The obtained raw data was then plotted using OriginPro 9.1.

The thermal properties of fibers and raw materials were analyzed on a TA Q500 V20.13 thermogravimetric analyzer (TGA) using a heat-cool-heat cycle, with nitrogen gas used as purge gas throughout the experiments. The samples (~5 mg) were initially heated to 100 °C and, maintained at 100 °C for 5 min to remove any adsorbed moisture. The samples were then cooled down to 30°C, followed by which a heat cycle applied from 30 to 700 °C at 10°C per minute. The raw data was then exported to plot the degradation behavior of the samples on Origin 9.1.

The cross-sectional morphology of the biofibers were examined by a FEI Verios 460L field-emission scanning electron microscope (FESEM). Prior to SEM examination, the samples were freeze-fractured in liquid nitrogen and, then placed on adhesive carbon tape. A thin layer (~10 nm) of gold/palladium was sputter-coated for 45 s using EmTech Turbo EM Sputter Coater to make the samples electrically conductive for SEM examination. The SEM micrographs of the samples were obtained at 2,500X and 10,000X magnifications to evaluate the changes in the microstructures of the fibers caused by the protein content.

The X-ray diffraction patterns of the biofibers were acquired using a Rigaku SmartLab X-ray Diffractometer containing a Cu X-ray tube (CuK<sub>α</sub> radiation, λ=0.1542 nm). An X-ray beam with operating voltage of 40 kV and current of 44 mA was applied perpendicular to the fiber bundle wrapped around the sample holder. The intensity of diffraction at every 0.05 2θ° (diffraction angle) were obtained between from 5 and 40 2θ°. The percent crystallinity (χ<sub>c</sub>) was calculated on PDXL software using the peak area technique:

$$\chi_c = \frac{I_c}{I_c + I_{am}} * 100\%$$

where  $I_c$ ,  $I_{am}$ , and  $\chi_c$  being the crystal and amorphous phase area of the fibers, and % crystallinity, respectively.

Based on vibration frequencies, a Vibromat ME Tester was utilized to measure the linear mass density (denier) of all biofiber specimens, which were subsequently used for the tensile testing performed according to ASTM D3822 standard. A universal testing instrument (MTS Q-test/5) calibrated with 5 lbs. load cell was programmed with a gauge length of 25.4 mm and a crosshead speed of 15 mm/min. Tensile properties such as initial modulus, tenacity and strain at break, were computed based on the force-elongation curves for all fibers.

The birefringence values were obtained from the refractive index measurements carried out on the cross-polarizing optical microscope (Nikon H550S Eclipse 50i). Three specimens of each fiber was observed under the microscope, after immersing the fibers into a series of mineral oils. The mean values of the parallel ( $n_{\parallel}$ ) and the perpendicular ( $n_{\perp}$ ) index were then calculated, and finally birefringence values calculated using the following equation:

$$\Delta n = n_{\parallel} - n_{\perp} ,$$

where  $\Delta n$ ,  $n_{\parallel}$ ,  $n_{\perp}$  are birefringence, parallel and perpendicular index, respectively.

## **4.6 Results and Discussion**

### **4.6.1 Dynamic viscosity of the spinning solutions**

Besides the dissolution effect, heat and KSCN are known factors that can cause denaturing of the collagen. As the collagen undergoes denaturing, fiber forming capability of the protein is typically lost [39, 40]. However, by having cellulose as the matrix, regeneration of collagen is facilitated in the biofiber blend. Thus, dynamic viscosity plays a key role in determining the possibility of fiber spinning collagen or other proteins with a polysaccharide such as cellulose. The effect of collagen on the blend solution's dynamic viscosity is shown in Figure 4.2, where an increase in the collagen content is seen to adversely affect the dynamic

viscosity of spinning solutions. With even inclusion of 10% collagen resulted in considerable decrease in the viscosity. However, the viscosity of 20% collagen solution increases and has values similar to that of the protein free solution, indicating some intermolecular interactions and entanglement effects with the cellulose matrix. With the further increase in collagen content (30%), the dynamic viscosity further decreased, and beyond this concentration, spinning of blend biofibers was not feasible at  $Dr = 2$ .

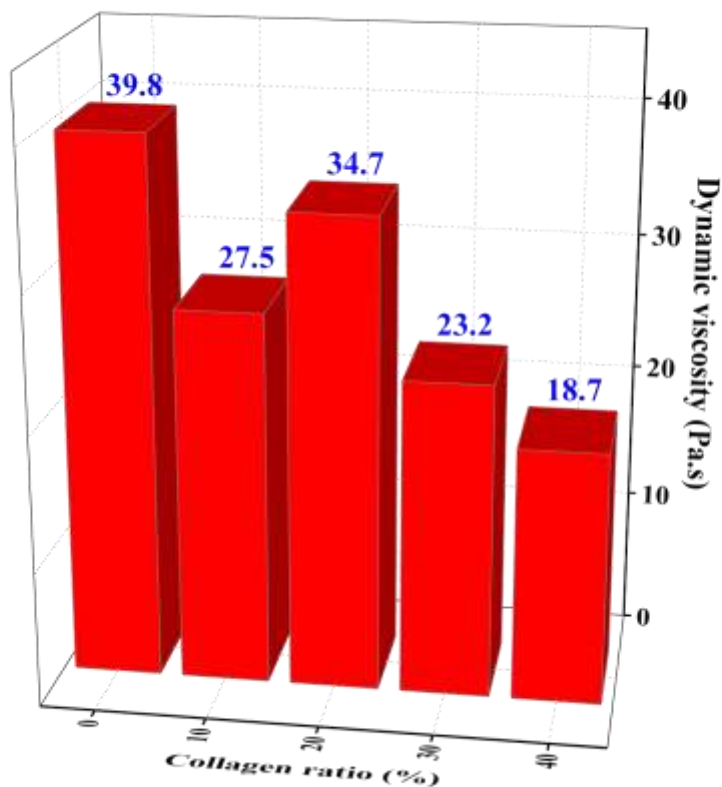


**Figure 4.2.** Dynamic viscosity of the dope solutions measured at 75°C

#### 4.6.2 Protein content

As the degree of interaction between the polysaccharide and the denatured protein could potentially play a significant role on the resultant protein content of the blend fibers, protein content analysis was performed on the biofibers, and the results are shown in Table 4.2. As expected, cellulose being a non-nitrogen containing polysaccharide, does not possess any nitrogen. Conversely, collagen being a protein elicits a nitrogen content of more than 90%.

With the addition of collagen to the cellulose matrix, at low collagen concentration (10 and 20%), protein analysis indicates roughly 50% of the added collagen is retained in the biofibers, after the coagulation process. However, when the collagen content is raised in the blend (30% and 40%), the resulting fibers contain only 13.2% and 16.3% protein content, respectively. These values correlate to 46 and 40% of the added collagen content, respectively. In other words, the diffusion of more collagen out of the fiber during coagulation was inevitable. Nevertheless, the remaining protein in the blend fibers indicates a certain degree of interaction between cellulose and collagen.

**Table 4.2.** Protein content of CE [38], CECOL fibers, and raw collagen

<b>Sample</b>	<b>N%</b>	<b>W<sub>pro</sub> (%)</b>
CE	0.14	None
CECOL1	1.07	5.5
CECOL2	2.07	11.3
CECOL3	2.38	13.2
CECOL4	2.92	16.3
Collagen (raw)	15.33	90.0

### 4.6.3 Chemical structure

To further investigate the intermolecular interaction between the two phases (collagen and cellulose), FTIR experiments were conducted on all fiber samples, with neat collagen and cellulose acting as controls. The FTIR spectra of the fibers and the raw collagen in the wavenumber range of 3750-2750  $\text{cm}^{-1}$  and 1750 – 700  $\text{cm}^{-1}$  are shown in Figure 4.3. The peaks for collagen at 1643 and 1528  $\text{cm}^{-1}$  denote amide I (C=O stretching) and amide II (N–H bending) bands, respectively [41]. The blend fibers show characteristic IR peaks, similar to those observed in cellulose fibers. In the blend fibers, the peaks corresponding to hydroxyl

groups (OH) of cellulose at  $3360\text{ cm}^{-1}$  shifted towards  $3290\text{ cm}^{-1}$  coinciding with amide A (N-H stretching) group of collagen resulting in a broad peak in the blend fibers, indicating hydrogen bonding between the protein and cellulose phases. Likewise, amide B band, a weaker absorbance of amide A, at  $3080\text{ cm}^{-1}$  appears as a slight shoulder on the CECOL4 spectrum due to the intermolecular interaction between the two phases [42]. Also, the absorbance of the amide I in helical form increased with increasing collagen concentration. On the other hand, cellulose exhibited a weak peak for carbonyl group at  $1648\text{ cm}^{-1}$ . Moreover, the amide II band in random coil at  $1531\text{ cm}^{-1}$  appeared at a higher wavenumber on the spectrum of CECOL4, most likely due to the hydrogen bonding. Thus FTIR spectra indicate the possibility of intermolecular interaction between the two phases in the biofibers at all concentrations (10 to 40% collagen content in cellulose/collagen fibers).

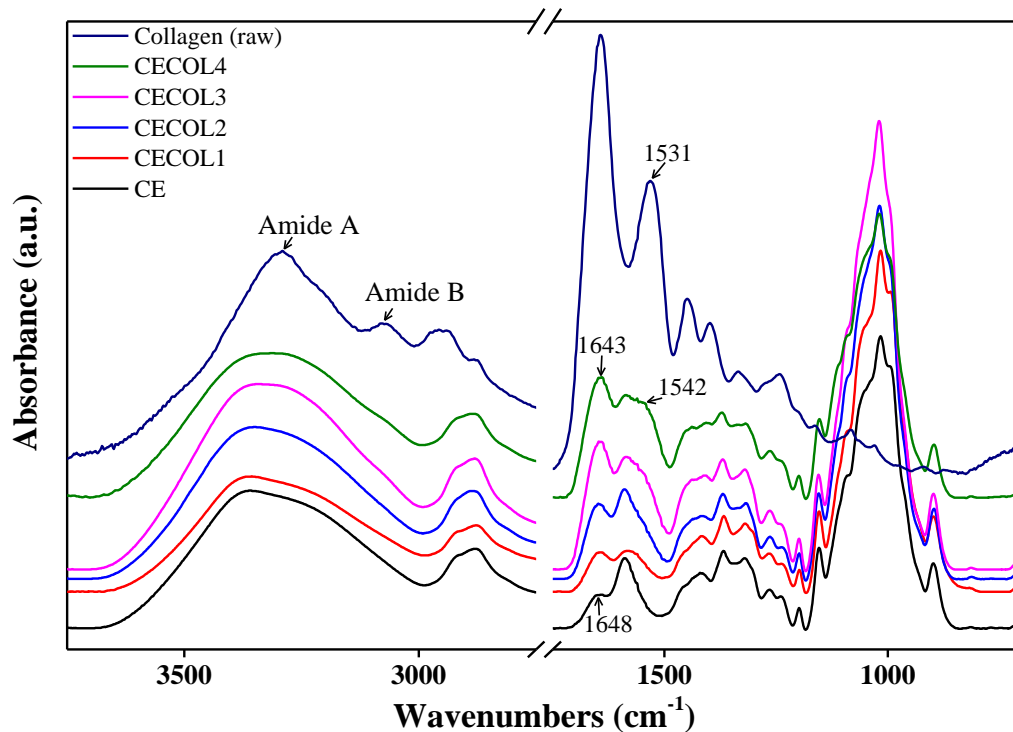


**Figure 4.3.** FTIR spectra of CE [38], CECOL fibers and raw collagen

#### 4.6.4 Thermal properties

The thermal degradation patterns of collagen, cellulose, and their blend in biofiber samples are shown in Figure 4.4. While, the first heating cycle aided in the removal of 5% excess moisture, the second heating cycle provided basic information about the initial ( $T_i$ ), maximum ( $T_{max}$ ) and final ( $T_f$ ) degradation temperatures of the samples, with  $T_f$  being shown by an arrow in the Figure 4.4. The thermogram of raw collagen indicate a slightly higher degradation temperature  $T_{max}$  (313°C), but also slightly lower  $T_i$  (238°C) than other fibers. While comparatively, neat cellulose had both lower  $T_i$  and  $T_{max}$ , whereas in the blend fibers  $T_i$  was in very close proximity to each other, however higher  $T_{max}$  was observed in CECOL3 and CECOL4 fibers which showed shift towards higher temperatures indicating improved thermal stability. Furthermore,  $T_f$  of the blend fibers, i.e. 325°C for CECOL4 fiber, were slightly greater than even the cellulose fiber ( $T_{f(CE)} = 320^\circ\text{C}$ ).

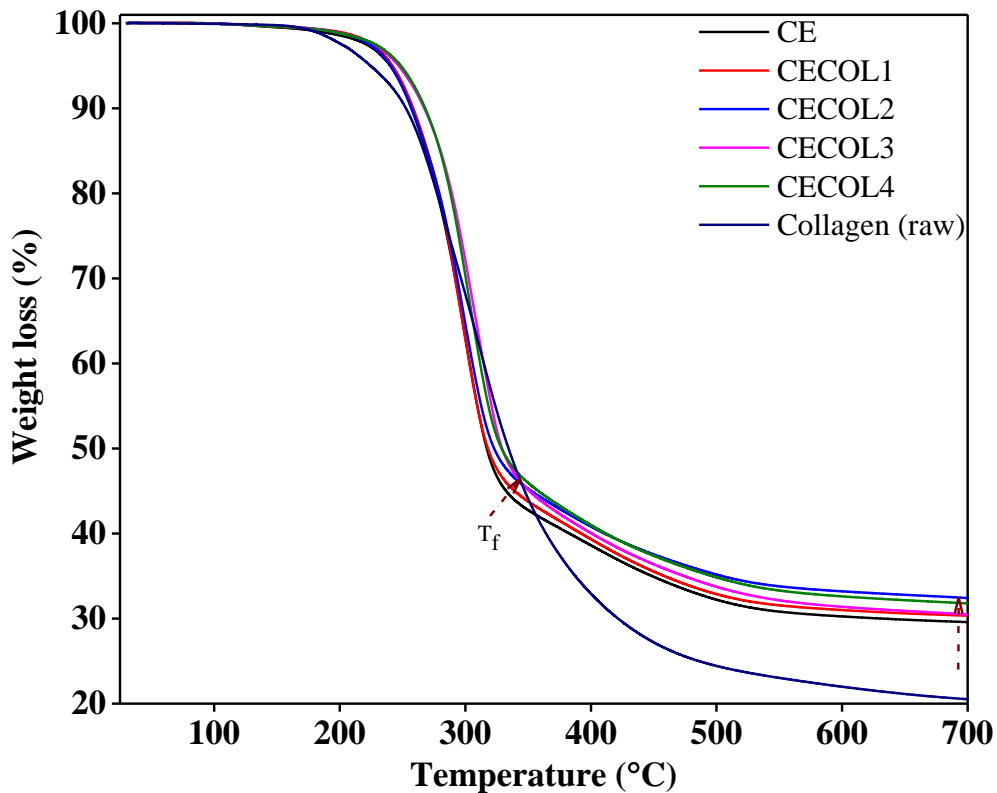


**Figure 4.4.** TGA thermographs of CE [38], CECOL fibers and raw collagen

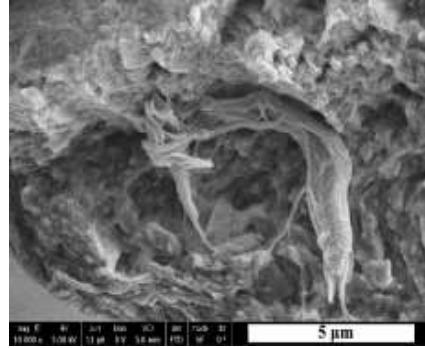
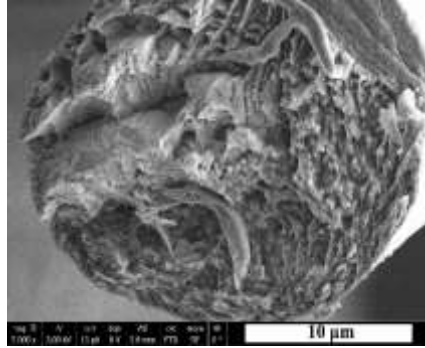
In a simple physical mixture, such improved thermal stabilities are typically not seen, while, presence of an intermolecular interaction lead to a higher thermal stability in the composites. Therefore, higher thermal stabilities seen in CECOL3 and CECOL4 systems indicate presence of such intermolecular interaction between the phases. This argument is further augmented by analyzing the total weight loss ( $W_{Tf}$ ) of the fibers and control samples. It can be noted that that at the final temperature ( $T_f$ ) of CE fibers  $W_{Tf}$  increased from 49.2 to 53%, with the 40% collagen content. Following a similar trend, the char yield at 700°C for the blend fibers was also higher than the control fiber (indicated by an arrow close to 700°C). Despite this, the synergistic effect between cellulose and collagen contributed to the enhancements in the thermal stability of the blend fibers, leaving more char yield than raw collagen (20.5%). This argument on thermal stability is further proven based on our recent report on cellulose/soy protein fibers [38], that showed thermal degradation at elevated temperatures due to intermolecular interaction between the cellulose/soy protein blend fibers.

#### **4.6.5 Morphology**

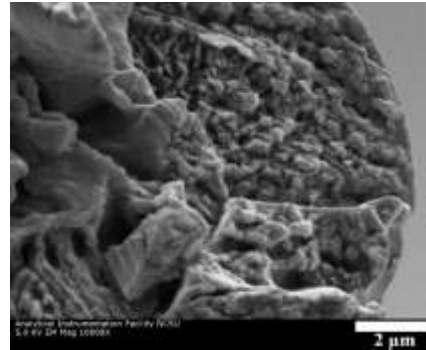
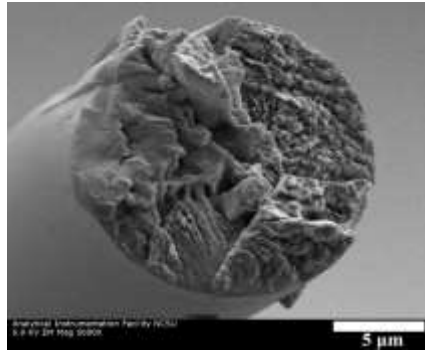
The electron micrographs of the cellulose and blend biofibers with collagen obtained from the FESEM are shown in Figure 4.5. The cellulose fibers exhibit circular cross sections with uniform dimensions along the fiber axis, with their morphology consisting of fibrillar and nano-porous structure, similar to the previous report that showed similar morphology in regenerated cellulose fibers [26]. Although the fibrillar structure also demonstrated similar morphology in the blend fibers, with increases in the protein content, an emerging trend in morphology with granular structures was observed. In addition, the images shown in Figure 4.5 did not elicit any clear evidence of phase separation in the blend fibers. Therefore, it can

be suggested that the denatured collagen was homogeneously dispersed in the cellulose matrix indicating compatibility between the two phases.

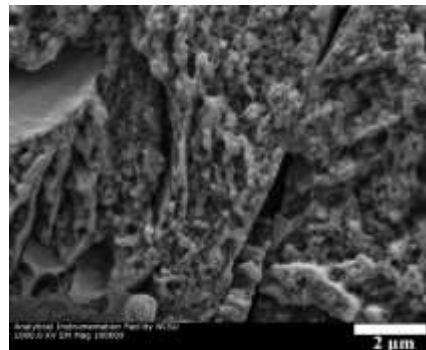
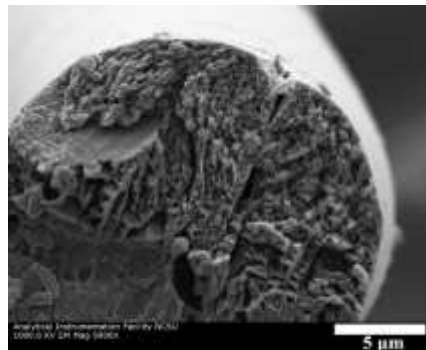
**CE**



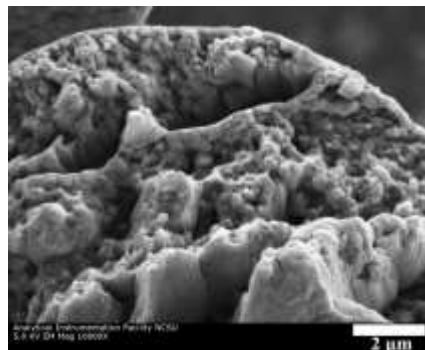
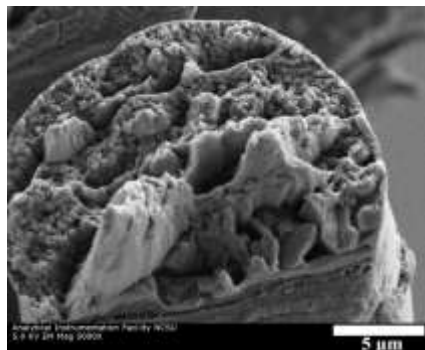
**CECOL1**



**CECOL2**



**CECOL3**



**CECOL4**

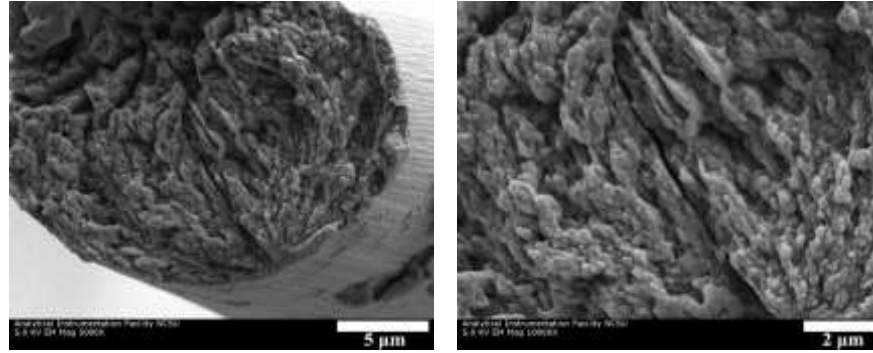


**Figure 4.5.** FESEM micrographs of CE [38] and CECOL fibers' cross-sections at 5000X (left) and 10000X magnifications (right)

Interestingly, Marsano et al. [43] also observed the granular morphology in the cross sections of cellulose/silk fibroin fibers, and have hypothesized the structures to have a compatibility between the phases. Similar observations were also made in other modified cellulose/collagen structures that showed more uniform and smooth surface in blend fibers produced by wet spinning method [34]. Additionally, another study on viscose/gelatin fiber blends obtained by the similar method, albeit with an additional crosslinking agent, showed a common surface morphology with enhanced dimensional stability, similar to the blend fibers that we report in this study [44]. Thus based on the electron micrographs that is shown in Figure 4.5, which illustrate a similar behavior that has been seen in the past, we can conclude a compatible nature existing between the collagen and cellulose phases.

#### **4.6.6 Crystalline structure**

One of the most commonly used method to study interfacial compatibility and interactions in solid structures have been by employing the wide angle X-ray diffraction analyses. The characteristic WAXD patterns of the raw collagen, regenerated cellulose and biofiber blends of collagen cellulose are shown in Figure 4.6. The WAXD analysis of the raw collagen contained mostly amorphous structure appeared with a broad peak around  $2\theta = 20^\circ$

on the X-ray diffraction pattern. The WAXD analysis of the cellulose fibers, however, illustrate two reflection peaks at  $2\theta = 11.7$  and  $20.8^\circ$ , that can be ascribed to the cellulose type-III polymorph. This well-known crystal structure is a result of coagulation of the cellulose-amine complex solution in an alcohol solvent such as methanol or ethanol [38, 45]. All the blend fibers also showed the same patterns except CECOL1 fiber, which showed an additional polymorph of cellulose II. Both cellulose II and III share the crystal planes of  $(10\bar{1})$ ,  $(101)$ , and  $(002)$  that are marked on Figure 4.6 at the top of the peaks of CECOL1 fiber. However, cellulose III peak is formed by a mixture of  $(101)$ , and  $(002)$  planes, resulting in a single peak. The amorphous nature of the collagen thus restricts our capability to infer further information about the crystal structures formed in the biofibers. However, WAXD also can provide further information the crystallinity observed in the fibers.

The percent crystallinity ( $\chi_c$ ) of CE, CECOL (10, 20, 30, and 40%) fibers and raw collagen were calculated to be 60, 46.7, 54.9, 53.3, 50.1 and 9.9%, respectively. With the exception of CECOL1,  $\chi_c$  tended to diminish with the increase in  $W_{\text{pro}}$ . A major decrease in  $\chi_c$  was seen with the biofiber containing 10% collagen, which can be attributed to the transformation in their crystal structure resulting in the formation of microvoids and microfractures. This could consequently be also related to the microbubbles generated in the solution that resulted in a lower dynamic viscosity compared to the solution containing 20% collagen. Furthermore, regardless of its lower  $D_r$ , the polymorphs seen in CECOL4 fiber was cellulose III and, its crystallinity did not differ significantly from the CECOL2 and CECOL3 fibers. Overall, more replacement of cellulose with protein enlarged the amorphous regions of the fibers contributing to the granulation of the fibrillar morphology observed in Figure 4.5.

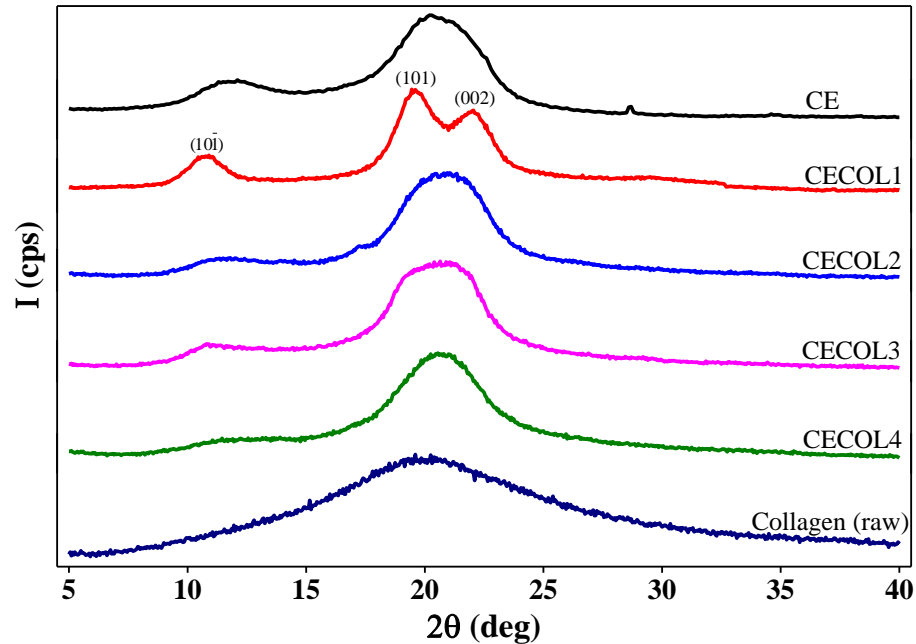


**Figure 4.6.** WAXD plot of CE [38], CECOL fibers and raw collagen

Such a decrease in  $\chi_c$  with an increase in collagen loading is not unique as Zhang et al. and Pei et al. have shown such decreases in  $\chi_c$  with concomitant increases in the protein content for the cellulose/collagen and the cellulose/collagen hydrolysate films, respectively [19, 29]. Although the cellulose/collagen blend films were cast and regenerated without any stretching or annealing, the reported values of  $\chi_c$  were still higher than the blend fibers. In addition, analogous to the effect of collagen, the incorporation of silk fibroin has also been shown to lower the crystallinity of cellulose fibers [43, 46].

#### 4.6.7 Tensile properties

To correlate the intermolecular interaction and the crystal structure transformation, quasi-static tensile measurements of cellulose and cellulose/collagen fibers were conducted and, are summarized in Table 4.3. Additionally, initial modulus and tenacity were plotted against increasing collagen content in the biofibers and, are shown in Figure 4.7. The initial

modulus of the blend fibers was lower than the cellulose fiber and, the trend stayed till the content of collagen was 40%. This trend was unlike our recently reported study on the cellulose/soy protein fibers, where addition of collagen did not significantly affect the stiffness of the composite fibers [38]. Even though an intermolecular interaction was confirmed by chemical and thermal analyses, the decreasing modulus can be partially attributed to the increasing loss of collagen content in comparison with its initial ratio in the cellulose/collagen blend solution.

**Table 4.3.** Tensile properties of CE [38] and CECOL fibers

<b>Fiber</b>	<b>Denier</b>	<b>Initial modulus (g/den)</b>	<b>Tenacity (g/den)</b>	<b>Elongation at break (%)</b>
CE	5.4 ± 0.1	91.8 ± 11.9	2.46 ± 0.1	13.2 ± 0.8
CECOL1	6.1 ± 0.2	71.1 ± 7.9	1.44 ± 0.11	11.4 ± 1.4
CECOL2	5.3 ± 0.3	62.6 ± 12.7	2.02 ± 0.24	13.0 ± 1.9
CECOL3	4.9 ± 0.2	62.5 ± 10.2	1.97 ± 0.07	15.5 ± 1.3
CECOL4	5.5 ± 0.2	62.2 ± 7.03	1.81 ± 0.18	10.7 ± 2.2

As indicated by the FESEM micrographs, the protein was homogeneously distributed through the cellulose matrix, which is the continuous phase and the backbone of the blend fibers. Therefore, the increasing ratio of cellulose increased the tenacity of all fibers, except CECOL1, which was made from solution with low dynamic viscosity compared to CE and CECOL2. Also, it can be recalled that the polymorphs of CECOL1 seen in WAXD analyses was distinct from the other biofibers, and also had the lowest crystallinity. Thus low tenacity of the CECOL1 fibers can be attributed to the unique and distant crystal structure. However, above 20% collagen ratio, the tenacity did not dramatically change indicating certain degree of compatibility irrespective of some protein loss. Our recent report on cellulose/ soy protein

blend fibers demonstrated higher modulus and lower elongation than the cellulose/collagen fibers the current study [38]. This comparison suggests that random coil conformations from respective globular and fibrillar proteins resulted in reversing alterations in the microstructure of cellulose fiber.

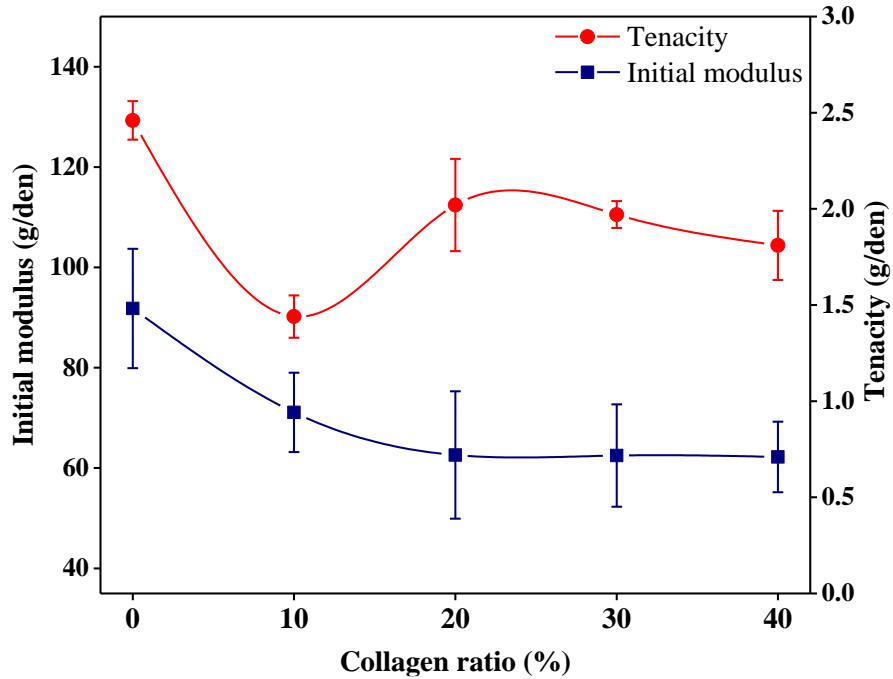


**Figure 4.7.** Dependence of initial modulus and tenacity of CE [38] and CECOL fibers on the collagen content

#### 4.6.8 Birefringence

One way to evaluate the degree of orientation of the polymer chains along the c-axis of the fibers is by evaluating the birefringence obtained from the refractive indices, along the parallel and the perpendicular axis to the fibers [47]. Birefringence values of CE and CECOL fibers are summarized in Table 4.4. As  $W_{pro}$  increases, the birefringence ( $\Delta n$ ) values of the composite biofibers decreases, and thus the overall orientation of the polymer chains along the fiber axis. As seen from Table 4.4, the perpendicular refractive indices ( $n_{\perp}$ ) increases slightly for composite fibers containing 20% collagen, with further increase when the collagen content

was 40%. With no similar concomitant increase in the parallel indices, indicate the amorphous area most likely affected the orientation resulting in both lower crystallinity and modulus for the blend fibers. Consequently,  $\Delta n$  dwindled to 0.036 inducing reduced strength to the blend fibers compared to the cellulose fiber. As a comparison, commercially produced regenerated fibers from proteins, such as casein (Azlon) and zein (Vicara), have  $\Delta n$  from 0.000 to 0.006 due to their non-crystalline nature and overall low orientation [48, 49]. In comparison, lack of orientation in random coil confirmation of the collagen chains also resulted in the decrease of the birefringence, which is still higher than viscose rayon ( $\Delta n = 0.020 - 0.028$ ) [49].

**Table 4.4.** Refractive indices (RI) and birefringence of the CE [38] and CECOL fibers

<b>Fiber</b>	$n_{\parallel}$	$n_{\perp}$	$\Delta n$
CE	1.550	1.510	0.040
CECOL1	1.550	1.510	0.040
CECOL2	1.550	1.512	0.038
CECOL3	1.550	1.512	0.038
CECOL4	1.550	1.514	0.036

#### 4.7 Conclusions

Cellulose and collagen were mixed effectively and dissolved in a binary solvent mixture of ED/KSCN in order to reconstitute blend biofibers in methanol. The dynamic viscosity of the fiber forming solution dropped below 20 Pa.s, when 40% collagen was added that prevented applying the same draw down ratio as with other blend fibers made from dope containing lower collagen content. Although some of collagen diffused into the coagulation bath in conjunction with the solvent, the  $W_{pro}$  of blend fiber ensured certain degree of interaction with cellulose. The chemical analysis indicated the likely interaction is via the formation of hydrogen bonding between cellulose and the protein. The thermogravimetric

analysis further revealed blend fibers to have higher thermal stability evidenced by a higher  $T_{\max}$  than the cellulose fiber and raw collagen. Because no clear phase separation was observed in SEM micrographs, collagen can be presumed to have been homogeneously distributed, thereby increasing the granular structure of fibrillar morphology in the blend fibers. Furthermore, the cellulose fiber and the blend fibers, excluding CECOL1 fiber, exhibited cellulose III crystal structure. However, the crystallinity of the fibers was affected by increasing collagen content due to its intrinsic amorphous structure. While both initial modulus and tenacity decreased with an increasing protein content, tenacity of blend fibers with 20 and 30% collagen ratio was about 2 g/den. Likewise, the birefringence and tensile modulus values followed the same trend. Thus, we demonstrated here the successful preparation of cellulose-collagen biofibers with a compatible phase. A compatible interface in cellulose/collagen biofibers with good mechanical, optical, and thermomechanical characteristics thus opens newer horizons for these materials to be applied where tunable properties are desired.

#### **4.8 Acknowledgement**

The authors would like to acknowledge the sponsorship of Turkish Ministry of National Education for Ramiz Boy for his PhD studies. Also, we would like to express our special thanks to Dr. Amit Naskar of Oak Ridge National Laboratory for the use of FTIR and TGA instrument. The authors appreciate the help from the College of Textiles, NC State University laboratory technicians, Tri Vu and Judy D. Elson for their help in designing and executing experiments. Finally, the authors are thankful for the valuable advice from Drs Samuel Hudson, Mohamed Bourham and Thomas Theyson.

#### 4.9 References

- [1] Fratzl P. Cellulose and collagen: from fibres to tissues. *Current Opinion in Colloid & Interface Science*. 2003;8:32-9.
- [2] Narayanan G, Gupta BS, Tonelli AE. Poly( $\epsilon$ -caprolactone) Nanowebs Functionalized with  $\alpha$ - and  $\gamma$ -Cyclodextrins. *Biomacromolecules*. 2014;15:4122-33.
- [3] Narayanan G, Ormond BR, Gupta BS, Tonelli AE. Efficient wound odor removal by  $\beta$ -cyclodextrin functionalized poly ( $\epsilon$ -caprolactone) nanofibers. *Journal of Applied Polymer Science*. 2015, DOI: 10.1002/app.42782;132.
- [4] Narayanan G, Gupta BS, Tonelli AE. Enhanced mechanical properties of poly ( $\epsilon$ -caprolactone) nanofibers produced by the addition of non-stoichiometric inclusion complexes of poly ( $\epsilon$ -caprolactone) and  $\alpha$ -cyclodextrin. *Polymer*. 2015;76:321-30.
- [5] Narayanan G, Gupta BS, Tonelli AE. Estimation of the poly ( $\epsilon$ -caprolactone) [PCL] and  $\alpha$ -cyclodextrin [ $\alpha$ -CD] stoichiometric ratios in their inclusion complexes [ICs], and evaluation of porosity and fiber alignment in PCL nanofibers containing these ICs. *Data in Brief*. 2015;5:1048-55.
- [6] Narayanan G, Aguda R, Hartman M, Chung C-C, Boy R, Gupta BS, et al. Fabrication and Characterization of Poly( $\epsilon$ -caprolactone)/ $\alpha$ -Cyclodextrin Pseudorotaxane Nanofibers. *Biomacromolecules*. 2016;17:271-9.
- [7] Narayanan G, Chung C-C, Aguda R, Boy R, Hartman M, Mehraban N, et al. Correlation of the stoichiometries of poly ( $\epsilon$ -caprolactone) and  $\alpha$ -cyclodextrin pseudorotaxanes with their solution rheology and the molecular orientation, crystallite size, and thermomechanical properties of their nanofibers. *Biomacromolecules*. 2016.

- [8] Narayanan G, Boy R, Gupta BS, Tonelli AE. Functional Nanofibers Containing Cyclodextrins. In: Ayoub AS, Lucia LA, editors. Polysaccharide fiber processing. Raleigh, NC: Springer briefs; 2016.
- [9] Huang FF, Rha C. Protein structures and protein fibers—a review. *Polymer Engineering & Science*. 1974;14:81-91.
- [10] Shoulders MD, Raines RT. Collagen Structure and Stability. *Annual Review of Biochemistry*. Palo Alto: Annual Reviews; 2009. p. 929-58.
- [11] Narayanan G, Vernekar VN, Kuyinu EL, Laurencin CT. Poly (Lactic Acid)-Based Biomaterials for Orthopaedic Regenerative Engineering. *Advanced Drug Delivery Reviews*. 2016, <http://dx.doi.org/10.1016/j.addr.2016.04.015>.
- [12] Lee CH, Singla A, Lee Y. Biomedical applications of collagen. *International Journal of Pharmaceutics*. 2001;221:1-22.
- [13] Cen L, Liu W, Cui L, Zhang WJ, Cao YL. Collagen tissue engineering: Development of novel biomaterials and applications. *Pediatric Research*. 2008;63:492-6.
- [14] Annual R. ANNUAL REVIEW OF BIOCHEMISTRY. *Annual Review of Biochemistry*. Palo Alto: Annual Reviews; 2009. p. 1-1056.
- [15] Klemm D, Heublein B, Fink HP, Bohn A. Cellulose: fascinating biopolymer and sustainable raw material. *Angew Chem Int Ed Engl*. 2005;44:3358-93.
- [16] Bledzki AK, Gassan J. Composites reinforced with cellulose based fibres. *Progress in Polymer Science*. 1999;24:221-74.
- [17] Zhang M, Ding CC, Chen LH, Huang LL. Preparation of Tannin-immobilized Collagen/Cellulose Bead for Pb(II) Adsorption in Aqueous Solutions. *Bioresources*. 2015;10:1773-89.

- [18] Wang J, Wei L, Ma Y, Li K, Li M, Yu Y, et al. Collagen/cellulose hydrogel beads reconstituted from ionic liquid solution for Cu(II) adsorption. *Carbohydr Polym.* 2013;98:736-43.
- [19] Pei Y, Yang J, Liu P, Xu M, Zhang XZ, Zhang LN. Fabrication, properties and bioapplications of cellulose/collagen hydrolysate composite films. *Carbohydr Polym.* 2013;92:1752-60.
- [20] Meng Z, Zheng X, Tang K, Liu J, Ma Z, Zhao Q. Dissolution and regeneration of collagen fibers using ionic liquid. *Int J Biol Macromol.* 2012;51:440-8.
- [21] Zhang M, Ding CC, Huang LL, Chen LH, Yang HY. Interactions of collagen and cellulose in their blends with 1-ethyl-3-methylimidazolium acetate as solvent. *Cellulose.* 2014;21:3311-22.
- [22] Ikeda M, Mukoyama H. Excellent regenerated cellulose fiber and a method of manufacturing the same dyeability. JP1997.
- [23] Gord H, Hammer KD, Melle J. Collagen-based shaped body. WO2006.
- [24] Hattori K, Abe E, Yoshida T, Cuculo JA. New solvents for cellulose. II. Ethylenediamine/thiocyanate salt system. *Polymer Journal.* 2004;36:123-30.
- [25] Kotek R. Regenerated cellulose fibers. In: Lewin M, editor. *Handbook of fibre chemistry.* 3 ed. Boca Raton, FL: CRC Press; 2002. p. 667-771.
- [26] Fink HP, Weigel P, Purz HJ, Ganster J. Structure formation of regenerated cellulose materials from NMMO-solutions. *Prog Polym Sci.* 2001;26:1473-524.
- [27] Weigel P, Fink HP, Doss M, Beckers S, Hendrikx R. Tubular films formed from cellulose/protein blends. US2003.

- [28] Wang HF, Lv HN, Feng J, Wang ZK. Novel Blend Films Prepared from Solution of Collagen and Cellulose in 1-Allyl-3-methylimidazolium Chloride Ionic Liquid. In: Liu XH, Jiang Z, Han JT, editors. *Materials Processing Technology, Pts 1-3*. Stafa-Zurich: Trans Tech Publications Ltd; 2012. p. 30-3.
- [29] Zhang M, Ding CC, Chen LH, Huang LL. The Preparation of Cellulose/Collagen Composite Films using 1-Ethyl-3-Methylimidazolium Acetate as a Solvent. *Bioresources*. 2014;9:756-71.
- [30] Wang GW, Guo JR, Zhuang LH, Wang Y, Xu B. Dissolution and regeneration of hide powder/cellulose composite in Gemini imidazolium ionic liquid. *International Journal of Biological Macromolecules*. 2015;76:70-9.
- [31] Hu Y, Liu L, Dan W, Dan N, Gu Z. Evaluation of 1-ethyl-3-methylimidazolium acetate based ionic liquid systems as a suitable solvent for collagen. *J Appl Polym Sci*. 2013;130:2245-56.
- [32] Wood N, Stephens G. Accelerating the discovery of biocompatible ionic liquids. *Physical Chemistry Chemical Physics*. 2010;12:1670-4.
- [33] Anumary A, Thanikaivelan P, Ashokkumar M, Kumar R, Sehgal PK, Chandrasekaran B. Synthesis and Characterization of Hybrid Biodegradable Films From Bovine Hide Collagen and Cellulose Derivatives for Biomedical Applications. *Soft Materials*. 2013;11:181-94.
- [34] Amsaveni M, Anumary A, Ashokkumar M, Chandrasekaran B, Thanikaivelan P. Green synthesis and characterization of hybrid collagen–cellulose–albumin biofibers from skin waste. *Appl Biochem Biotechnol*. 2013;171:1500-12.
- [35] Lee HJ. *Novel Cellulose Solvent System and Dry Jet Wet Spinning of Cellulose/ED/KSCN Solutions*: North Carolina State University; 2008.

- [36] Zhu YD, Douglass E, Theyson T, Hogan R, Kotek R. Cellulose and Soy Proteins Based Membrane Networks. *Macromolecular Symposia*. 2013;329:70-86.
- [37] Douglass E. The Development of Cellulose Blend Membranes using Cellulose and other Natural Biopolymers using a Novel Solvent System. Raleigh, NC: North Carolina State University; 2010.
- [38] Boy R, Kotek R. Properties of Cellulose – Soy Protein Blend Biofibers Regenerated from an Amine/Salt Solvent System. accepted for *Cellulose*, 2016.
- [39] Nishihara T. Method for colloidally dispersing collagen. US1964.
- [40] Boedtker H, Doty P. The native and denatured states of soluble collagen. *Journal of the American Chemical Society*. 1956;78:4267-80.
- [41] Rabotyagova ES, Cebe P, Kaplan DL. Collagen structural hierarchy and susceptibility to degradation by ultraviolet radiation. *Materials Science & Engineering C-Biomimetic and Supramolecular Systems*. 2008;28:1420-9.
- [42] Barth A. Infrared spectroscopy of proteins. *Biochimica Et Biophysica Acta-Bioenergetics*. 2007;1767:1073-101.
- [43] Marsano E, Corsini P, Canetti M, Freddi G. Regenerated cellulose-silk fibroin blends fibers. *Int J Biol Macromol*. 2008;43:106-14.
- [44] Yamada M, Ohshima K. Method of manufacturing cellulose-gelatin composite viscose rayon filament. US2009.
- [45] Isogai A. Allomorphs of cellulose and other polysaccharides. In: Gilbert RD, editor. *Cellulosic polymers, blends and composites*. Munich, Germany: Hanser; 1994. p. 1-24.

[46] Yao Y, Zhang E, Xia X, Yu J, Wu K, Zhang Y, et al. Morphology and properties of cellulose/silk fibroin blend fiber prepared with 1-butyl-3-methylimidazolium chloride as solvent. *Cellulose*. 2015;22:625-35.

[47] Hearle JW. Physical structure and fibre properties. In: Woodings C, editor. *Regenerated Cellulose Fibres*: Woodhead Publishing; 2001. p. 199.

[48] Hearle JW, Morton WE. *Physical properties of textile fibres*: Elsevier; 2008.

[49] Brinsko KM. Optical characterization of some modern "eco-friendly" fibers. *J Forensic Sci*. 2010;55:915-23.

## Chapter 5 Properties of Cellulose – Keratin Blend Biofibers Regenerated from an Amine/Salt Solvent System

### 5.1 Introduction

Keratin is a fibrous protein extracted from wool, hair, fingernails and horns. It prevalently contains  $\alpha$ -helical structure that helps to extend wool at high elongations [1]. Its alkali solution was blended with cellulose xanthate to enhance the acid dye affinity for resulting rayon [2-5]. A derivative of the protein, cyclotriphosphazenekeratin, rendered the rayon flame retardant [6]. Alkali blend solution of biologically modified cellulose and feather keratin was regenerated in sulfuric acid and sodium sulfate forming composite biofiber. It exhibited improved wettability and moisture absorption than the cellulose fiber [7].

Xie et al. [8] utilized 1-butyl-3-methylimidazolium chloride ([BMIm]Cl) to dissolve 11 wt% wool keratin fibers (cleaned and defatted form of wool fiber) at 130°C in 10 h. The keratin regenerated by precipitating in methanol had slightly lower thermal stability than natural wool fiber. WAXS crystallinity analysis revealed that  $\alpha$ -helix crystalline structure of wool was not present in the regenerated wool keratin. The initially produced membrane from the protein was very brittle. Consequently, the polymer was blended with cellulose to attain enhanced mechanical properties. Their report included only SEM images indicating the possibility of preparing cellulose/keratin (5/1 w/w) solution in order to produce blended membrane and fiber. A further study by Hameed and Guo [9] showed that the blend films have higher thermostability and strain at break compared to their single components. Interestingly, the dissolution of human hair keratin in the same solvent was also investigated to prepare blend films incorporating cellulose [10]. The obtained results were comparable to the previous study.

Furthermore, a tri-component film from cellulose, chitosan and keratin was investigated for drug release applications [11].

The objective of this study is similar to what was intended in the previous chapters. The difference is just the type of protein; namely, keratin. The same solvent system was utilized to produce the blend fiber from cellulose and keratin by regenerating in methanol. Unlike previously reported fibers, our cellulose/keratin blend fiber contains up to 40% keratin.

## **5.2 Materials**

The solvent system consists of 65 wt% ED and 35 wt% KSCN that are both reagent grade and obtained from Sigma-Aldrich. The salt was dried to eliminate water in the solvent system for mixing with the amine. The ED/KSCN mixture was stirred on a hot plate with a little heat applied. After the salt was completely solubilized, the solvent was kept at room temperature to equilibrate.

Cellulose used for this research was Buckeye VFC (DP of around 600) received in the form of thick sheets made from acetate grade, pressed, refined, and bleached wood pulp. The sheets were cut into small pieces and ground before dissolution to facilitate dissolution. Keratin was kindly donated by Nacalai Tesque, Inc. (Kyoto, Japan). Before the solution preparation, cellulose and keratin were kept at least 12 hours in a vacuum oven at 60°C to remove absorbed moisture. In addition, methanol with ACS reagent grade was obtained from BDH Industries Ltd to use a coagulant.

## **5.3 Preparation of Spinning Solutions**

A total concentration ( $C_p$ ) of 7 wt% cellulose-keratin-ED/KSCN solution was prepared for all compositions by varying the weight ratio of cellulose to keratin with 10% increase: CEKER1 (10% keratin), CEKER2 (20% keratin), CEKER3 (30% keratin), CEKER4 (40%

keratin). The spinning dopes were obtained by mixing at 90°C for 2-3 hours to ensure complete dissolution. The keratin ratio above 40% could only be used as-spun fibers without any stretching applied that is not in the objective of this study.

An optical microscope was used to examine the dissolution of cellulose and keratin. A small amount of each solution was poured on a microscope slide and a coverslip was placed on the sample carefully to avoid any bubble formation. Then, the sample was observed under the cross-polarized view of Nikon H550S Eclipse 50i optical microscope. The solutions emerged dark under the microscope as a result of complete dissolution.

#### 5.4 Fiber Formation

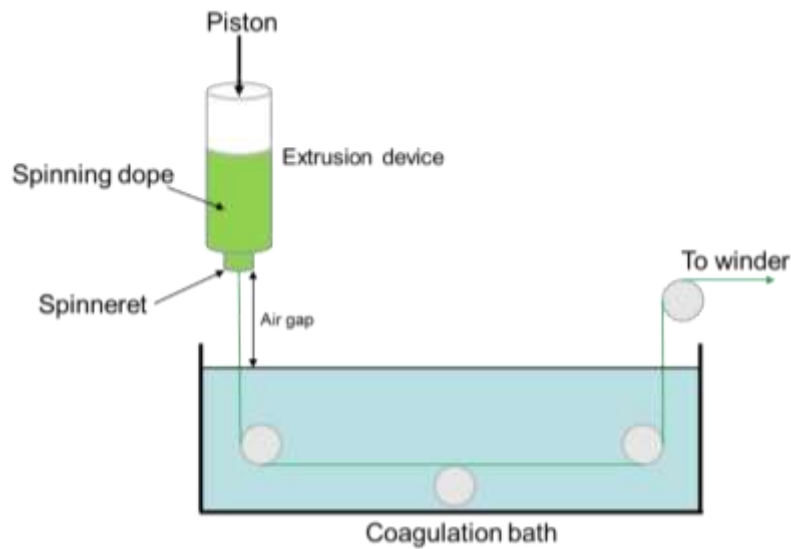


**Figure 5.1.** An illustration of dry-jet wet spinning system

The fibers were spun via a laboratory scale dry-jet wet spinning line (Figure 5.1) composed of a piston spinning unit, a spinneret pack with stainless steel barrel containing two filters and four Teflon® O-rings, a 1.8 m long coagulation bath and a take-up winder. The spinneret pack was covered with braided heating tape in order to maintain the spinning temperature at 75°C. After the dope was poured into the barrel, the piston was pushed at a speed of 0.8 mm/min. The dope passed through the filters and a single-hole spinneret ( $\phi=0.005$

inch and Length/Diameter=2). Travelling an air gap of 1 inch from the spinneret to the methanol bath at room temperature, the fluid jet formed by the dope was coagulated by removing the solvent. The obtained fiber was then wound up on a plastic bobbin by a take-up winder. The draw down ratio ( $D_r$ ) of all blend fibers were 1.6. The collected fiber was aged overnight in methanol to eliminate the solvent residues. They were finally left to dry at ambient temperature. All fiber spinning conditions were included in Table 5.1.

**Table 5.1.** Spinning conditions applied for all fibers

Spinning temperature (°C)	75	Piston speed (mm/min)	0.8
Air gap (inch)	1	Take-up speed (m/min)	52
L/D ratio of orifice	2	Draw down ratio	1.6
Orifice diameter (μm)	127	Coagulation bath length (m)	1.8
Coagulation liquid	Methanol	Coagulation temperature	Ambient temperature

Compared to the cellulose/soy protein and cellulose/collagen blend solutions, cellulose/keratin had relatively lower viscosities that prevented applying the same draw down ratio as the cellulose fiber, which had the ratio of 2.

## 5.5 Characterization Techniques

Fourier transform infrared spectroscopy (FTIR) of all fibers was measured with a Perkin Elmer FTIR using attenuated total reflection (ATR) method. FTIR spectrum of each fiber was obtained between 4000 and 500  $\text{cm}^{-1}$  wavenumbers in absorbance mode over 64 scans at the resolution of 4  $\text{cm}^{-1}$ . The obtained raw data was plotted using OriginPro 9.1, an analysis and graphing software.

The thermal properties of all fibers and raw materials were analyzed with at least 5 mg of each sample using a TA Q500 V20.13 thermogravimetric analyzer (TGA). The samples were first heated to 100°C and kept there for 5 min to eliminate the absorbed moisture. After cooling down to 30°C, each sample was heated at 10°C per minute up to 700°C. Nitrogen gas was purged throughout the experiment and the raw data was exported to plot the degradation behavior of the samples on Origin 9.1.

A FEI Verios 460L field-emission scanning electron microscope (FESEM) was utilized to examine the cross-section morphology of all fibers. The samples were first freeze-fractured in liquid nitrogen and then placed on adhesive carbon tape. A thin layer of gold/palladium was sputter-coated onto the samples. The micrograph of each sample at 2,500X and 10,000X magnifications were captured to evaluate the change in the microstructure of the fibers due to the varying protein content.

The X-ray diffraction patterns of all fibers were acquired by using Rigaku SmartLab X-ray Diffractometer containing a Cu X-ray tube (CuK $\alpha$  radiation,  $\lambda=0.1542$  nm). An X-ray beam with operating voltage of 40 kV and current of 44 mA was applied perpendicular to the fiber bundle wrapped around the sample holder. The intensity of diffraction at every 0.05  $2\theta^\circ$  (diffraction angle) were obtained between from 5 and 40  $2\theta^\circ$ . The percent crystallinity ( $\chi_c$ ) was calculated on PDXL software that uses the peak area technique:

$$\chi_c = \frac{I_c}{I_c + I_{am}} * 100\%$$

Where  $I_c$  and  $I_{am}$  are respectively the crystal phase area and amorphous phase area.

Vibromat ME Tester was utilized to measure the linear mass density (denier) of all tested fiber specimens based on vibration frequency. The obtained values were used for the tensile testing performed according to ASTM D3822 standard. A universal testing instrument

(MTS Q-test/5) calibrated with 5 lbs. load cell were programmed with a gauge length of 25.4 mm and constant crosshead speed of 15 mm/min. The tensile properties, such as initial modulus, tenacity and strain at break, were measured for all fibers.

## 5.6 Results and Discussion

### 5.6.1 Chemical structure

The blend fibers exhibited similar absorption peaks to the cellulose fiber. Figure 5.2 represents the FTIR spectra of all fibers and the raw keratin in the wavenumber range of 3750-2750  $\text{cm}^{-1}$  and 1750 – 700  $\text{cm}^{-1}$ . The stretching vibration of hydroxyl groups (OH) for cellulose at 3360  $\text{cm}^{-1}$  was predominant for all fibers. The corresponding peak for keratin was less intense thus showed no effect on the spectra of the blend fibers.

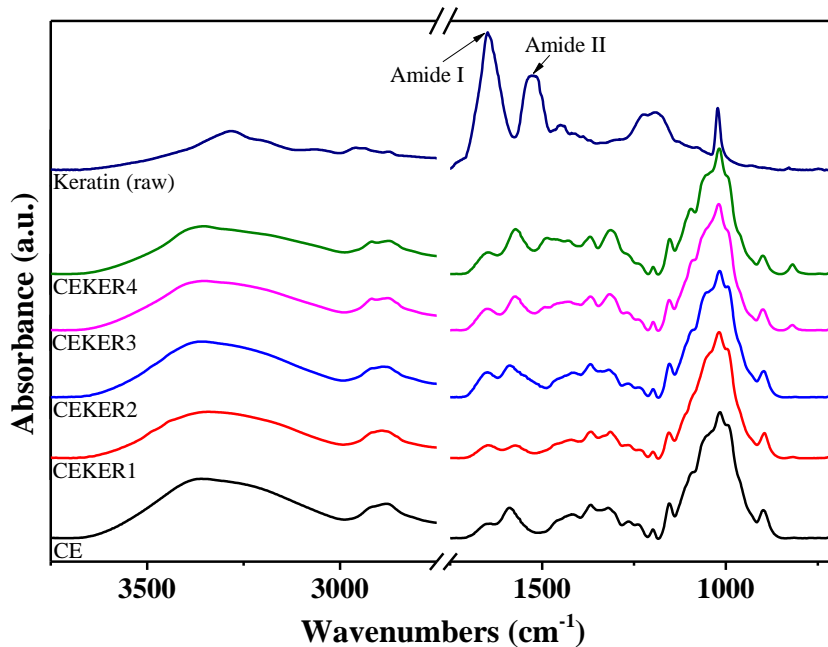


**Figure 5.2.** FTIR spectra of CE [12], CEKER fibers and raw keratin

The peaks at 1648 and 1526  $\text{cm}^{-1}$  for keratin indicated by arrows are amide I (C=O stretching) and amide II (N–H bending) bands, respectively. These peaks did not appear on the

spectra of the blend fibers and no significant shift occurred from the peaks of cellulose fiber. It is evident that the addition of keratin had little impact on the examined chemical structure of cellulose. Comparable FTIR analysis was also reported for viscose/wool powder fibers [5].

### 5.6.2 Thermal properties

The thermal degradation of all samples is shown in Figure 5.3. The first heating cycle helped to remove 5% excess moisture. Through the second heating cycle, initial ( $T_i$ ) and maximum ( $T_{max}$ ) temperatures of the main degradation stage were revealed. All blend fibers had lower  $T_i$  and  $T_{max}$  than CE fiber. It can be clearly observed from the derivative thermogravimetric (DTG) thermograms that  $T_{max}$  decreased by increasing protein content. At 40% keratin content, the fiber had  $T_{max}$  at 236°C which is close to the first  $T_{max}$  (232°C) of three major degradation stages of raw keratin. The first stage is related to the melting or denaturation of  $\alpha$ -helix structure in the protein's microfibrils. Upon regeneration and drawing, the helical component transforms to  $\beta$ -sheet structure [13]. The blend fibers with up to 30% keratin ratio also exhibited a slight shoulder of this stage. Moreover, the other two stages of keratin decomposition are due to disrupted disulfide bond and degraded polypeptide chains [14,15]. The regenerated keratin contained in the blend fibers did not show the other stages of the raw keratin. In other words, the thermal stability of keratin became superior upon regeneration. On the other hand, the thermal stability of blend fibers was improved by increasing cellulose content. Similar findings were also reported for cellulose/keratin blend films [9,10].

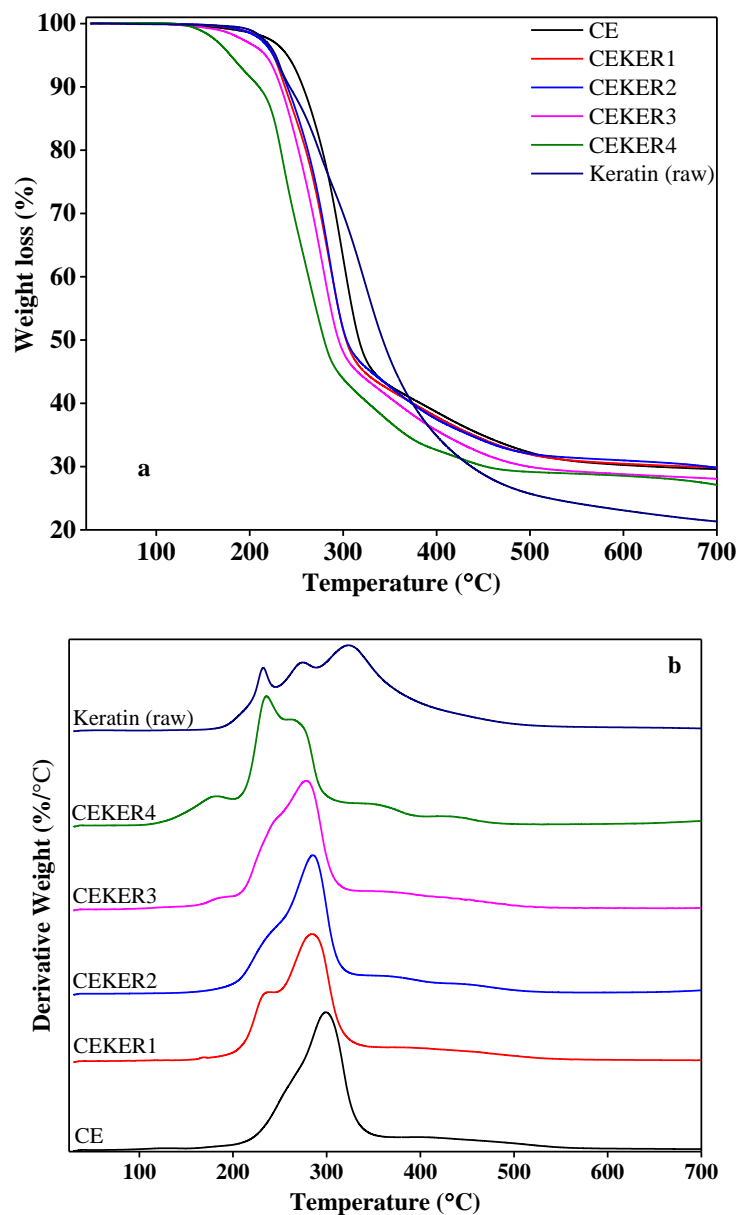


**Figure 5.3.** TGA (a) and DTG (b) thermographs of CE [12], CEKER fibers and raw keratin

### 5.6.3 Morphology

The micrographs of the fibers obtained from the FESEM are included in Figure 5.4. The round shape of fibers' cross section did not alter with 10 and 20% keratin ratio. However, further incorporation of the protein generated slight grooves along the fiber axis hence distorted the circular form. Compared to the cellulose fiber with the nano-porous and fibrillar morphology, the blend fibers revealed much denser and compact structure. In addition, the



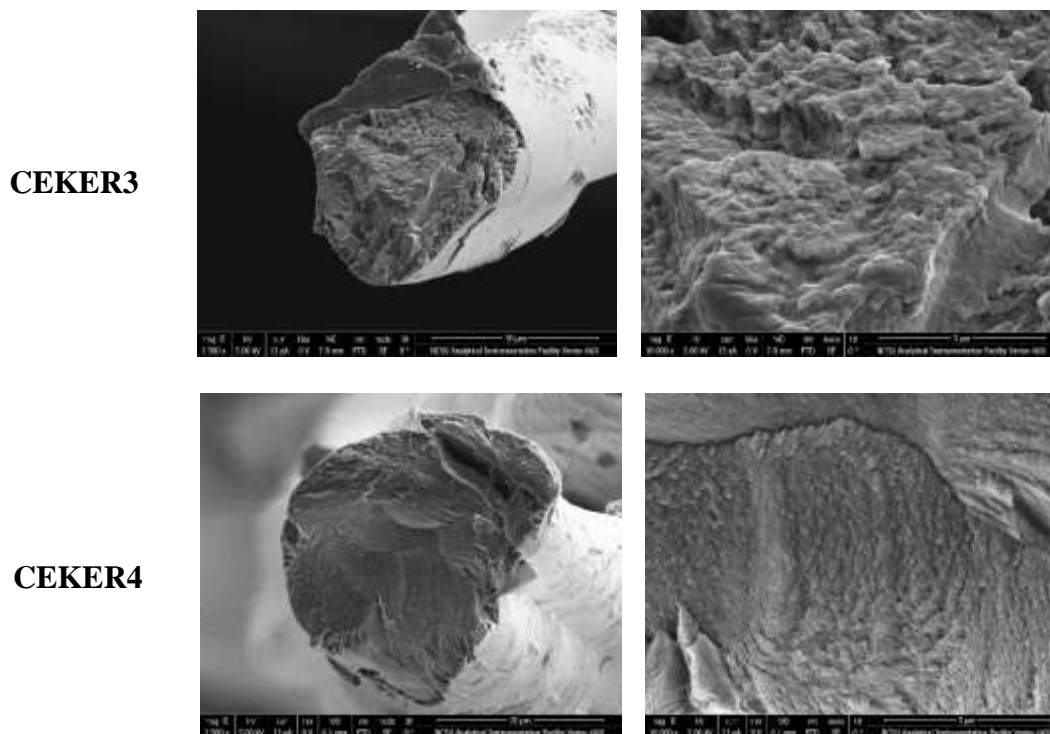


**Figure 5.4.** FESEM images of the fractured cross-sections of CE [12] and CEKER fibers

In comparison with our cellulose/keratin fibers, the biomodified cellulose/feather keratin fibers reported by Wrześniewska-Tosik et al. [7] showed evident phase separation between the two polymer domains. Moreover, the viscose/wool powder fibers produced by Li et al. [5] contained sputtered particles of the powder on the fiber surface.

#### 5.6.4 Crystalline structure

The characteristic WAXD patterns of the fibers and raw keratin are illustrated in Figure 5.5. The profile of the cellulose fiber contains two reflection peaks of cellulose III crystal structure at  $2\theta = 11.7^\circ$  and  $20.8^\circ$ . The structure is a well-known result of the cellulose-amine complex solution coagulated in an alcohol, such as methanol and ethanol [12,16]. However, the crystal structure of blend fibers converted to cellulose II exhibiting three separate peaks. Both cellulose II and III contain the crystal planes of  $(10\bar{1})$ ,  $(101)$ , and  $(002)$  that are shown above the peaks of CEKER1 fiber. Cellulose III, though, is a mixture of  $(101)$ , and  $(002)$  planes

and characterized by a single peak. Furthermore, the typical diffraction peaks of raw keratin appeared at  $2\theta = 9.6^\circ$  and  $20.3^\circ$  indexing with  $\alpha$ -helix and  $\beta$ -sheet structures, respectively.

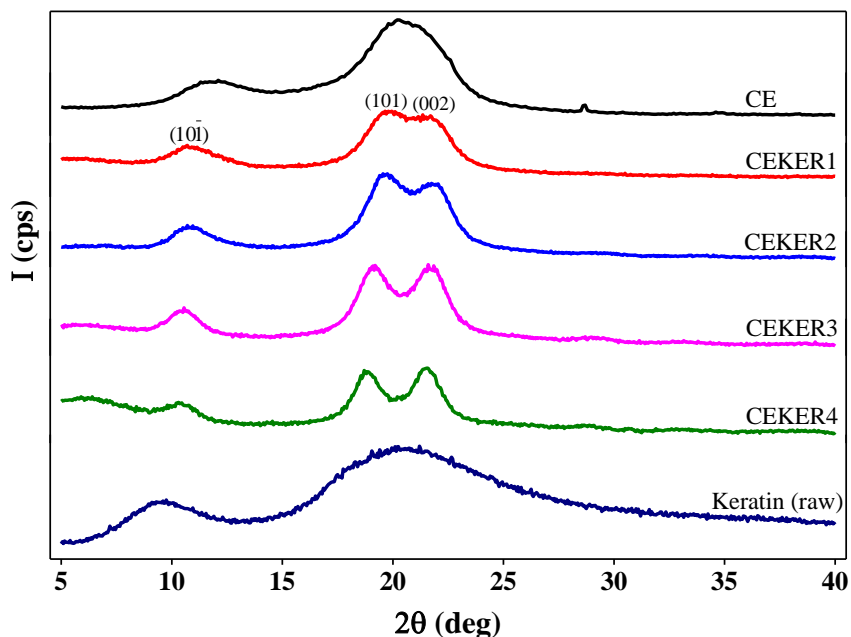


**Figure 5.5.** WAXD results of CE [12], CEKER fibers and raw keratin

The aforementioned TGA results indicated a likely existence of  $\beta$ -sheet structure in the blend fibers. However, the diffraction patterns did not indicate such characteristics of the protein. Interestingly, (101) and (002) crystal planes of the blend fibers became slightly separated by more protein content suggesting an interruption throughout the cellulose matrix. This can also be referred to the intermolecular interaction between the two polymer phases. Comparable to our blend fibers, the viscose/wool powder also did not show any peak shift due to the incorporation of protein [5].

### 5.6.5 Tensile properties

The tensile properties of cellulose/keratin fibers are shown in Table 5.2. The initial modulus and tenacity are also plotted against increasing keratin ratio in Figure 5.6. Both the

initial modulus and the tenacity showed a sudden drop with CEKER1 fiber. This result is expected since the applied  $D_r$  ratio of blend fibers was lower than the cellulose fiber.

**Table 5.2.** Tensile properties of CE [12] and CEKER fibers

Fiber	Initial modulus (g/den)	Tenacity (g/den)	Elongation at break (%)	Denier
CE	91.8 ± 11.9	2.46 ± 0.1	13.2 ± 0.8	5.4 ± 0.1
CEKER1	71.3 ± 9.3	1.40 ± 0.07	9.3 ± 0.7	6.6 ± 0.2
CEKER2	63.4 ± 10.4	1.14 ± 0.08	9.8 ± 1.9	7.2 ± 0.3
CEKER3	56.1 ± 16.4	1.02 ± 0.14	11.0 ± 1.8	8.2 ± 0.9
CEKER4	34.8 ± 15.0	0.69 ± 0.06	14.4 ± 2.8	10.8 ± 1.5

The modulus and the tenacity of blend fibers decreased gradually by increasing protein content. However, the elongation was reversely affected thus increased from 9.3 to 14.4% at 40% keratin ratio. In addition, the fiber denier became larger with more protein content.

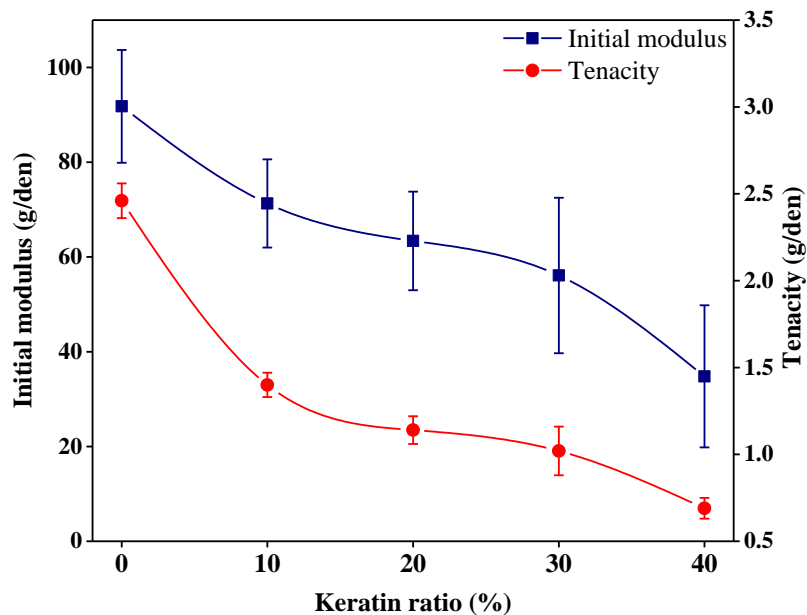


**Figure 5.6.** Effect of the keratin ratio on the initial modulus and the tenacity of CE [12] and CEKER fibers

Our blend fibers are stronger than the cellulose/keratin composite fibers [7] but weaker than the viscose/wool powder fibers [5], stemming from the difference in spinning conditions.

## **5.7 Conclusions**

Solution blends of cellulose with up to 40% keratin were effectively reconstituted into fibers by using ED/KSCN as a co-solvent and methanol as coagulant. Although FTIR spectra hindered the chemical structure of the regenerated protein in the blend fibers, TGA thermograms confirmed the substantial blending of the two polymers. The thermal stability was enhanced by increasing cellulose content. Furthermore, the electron microscopy images did not exhibit two phase morphology indicating compatible blends between cellulose and keratin. Upon adding the protein, the crystal structure transformed from cellulose III to cellulose II. The diffraction peaks of cellulose II became more distinct with more protein content due most likely to the enlarging network of intermolecular interaction between the polymer phases. While the modulus and the tenacity diminished, the elongation at break for the blend fibers improved with an increasing keratin ratio.

## **5.8 References**

1. Bettelheim FA, Brown WH, Campbell MK, Farrell SO, Torres OJ (2012) Introduction to general organic and biochemistry. 10 edn. Brooks/Cole Cengage Learning, Belmont, CA
2. Yamada M, Ohshima K, Arimochi M, Nakajima K (2004) Spinning dope for cellulose/protein compound fiber and cellulose/protein compound fiber. JP Patent 2004-149953, 24 May 2004
3. Ikeda M, Mukoyama H (1997) Regenerated Cellulosic Fiber Excellent in Dyeability and Its Production. JP Patent 09-241920,
4. Saleh MS (2014) Fibrous protein processing method. US Patent 20140326165, 6 Nov 2014

5. Li W, Ke G, Li G, Xu W (2015) Study on the structure and properties of viscose/wool powder blended fibre. *Fibres Text East Eur* 23 (1 (109)):26-29
6. Zhou Z, Weiren B, Youbo D, Jinming D (2015) Preparation and characterization of cyclotriphosphazene/keratin/viscose fibers. *Fiber Polym* 16 (3):560-564
7. Wrzesniewska-Tosik K, Wawro D, Ratajska M, Stepkowski W (2007) Novel biocomposites with feather keratin. *Fibres Text East Eur* 15 (5-6):157-162
8. Xie H, Li S, Zhang S (2005) Ionic liquids as novel solvents for the dissolution and blending of wool keratin fibers. *Green Chem* 7 (8):606-608
9. Hameed N, Guo QP (2010) Blend films of natural wool and cellulose prepared from an ionic liquid. *Cellulose* 17 (4):803-813.
10. Wang M, Zhao T, Wang GH, Zhou JL (2014) Blend films of human hair and cellulose prepared from an ionic liquid. *Textile Research Journal* 84 (12):1315-1324.
11. Tran CD, Mututuvvari TM (2015) Cellulose, Chitosan, and Keratin Composite Materials. Controlled Drug Release. *Langmuir* 31 (4):1516-1526.
12. R. B, Kotek R (2016) Properties of Cellulose – Soy Protein Blend Biofibers Regenerated from an Amine/Salt Solvent System.
13. Spei M, Holzem R Thermoanalytical investigations of extended and annealed keratins. *Colloid and Polymer Science* 265 (11):965-970.
14. Idris A, Vijayaraghavan R, Patti AF, MacFarlane DR (2014) Distillable Protic Ionic Liquids for Keratin Dissolution and Recovery. *ACS Sustainable Chemistry & Engineering* 2 (7):1888-1894.
15. Li R, Wang D (2013) Preparation of Regenerated Wool Keratin Films from Wool Keratin-Ionic Liquid Solutions. *Journal of Applied Polymer Science* 127 (4):2648-2653.

16. Isogai A, Gilbert RD (1994) Allomorphs of cellulose and other polysaccharides. In: Cellulosic polymers, blends and composites. Hanser, Munich, Germany, pp 1-24

## **Chapter 6 Blend Biofilms Prepared from Gamma Irradiated Solutions**

### **6.1 Introduction**

The two common methods to process blended polysaccharides and proteins into films and membranes are solution casting and thermal processing. Since the focus in this research is to produce highly miscible blends with strong interactions between cellulose and proteins, the latter is applied by employing a cosolvent, ED/KSCN. Because it is very effective and practical, the commonly adopted method to make films is to manually spread dilute film solutions (typically 5-10 wt% concentration) of biopolymers on an appropriate platform. Then, depending on the solvent, either coagulation before drying or directly drying under controlled conditions takes place. With technologic equipment, wide and long films with a given thickness can be mechanically produced [1].

The quality of blend films is governed by the composition of film forming solution, casting conditions including post and/or pretreatments, and drying method. For instance, the composition of biopolymers in solution strongly affects the cellulose-protein interaction and their miscibility and thus the properties of resulting film [1]. In solution casting by coagulation, gel sheet formed by spreading the solution must have a fixed casting thickness. The composition and temperature of coagulant must be the same for every gel sheet. Drying conditions, such as the substrate on which the films dry, drying time, ambient temperature, airflow, must be constant in order to obtain reproducible results.

Tailoring films by beginning from a blend of proteins, polysaccharides and/or lipids is a useful approach to take advantage of the functional properties of each component. In blend films, proteins significantly contribute to tensile properties by functioning as binder for structural integrity [1]. However, proteinaceous films could be poor water resistance and thus

lose their integrity upon exposing to water. In particular, globular proteins and water-soluble proteins including collagen hydrolysate and gelatin are the proteins showing such a weakness. Modification of these proteins by chemical, enzymatic and physical methods has been applied to enhance primarily their stability in water as well as their tensile strength.

The chemical modification has included crosslinking agents from aldehyde family (Figure 6.1), especially formaldehyde (also mentioned for the plastics of casein and soy protein), glutaraldehyde and glyoxal as the common ones. The enzymatic modification has mainly focused on an enzyme called transglutaminase for its ability to crosslink proteins. The enzyme and glyoxal chemical treatments were effective in improving the stability of proteins in water but not the tensile properties. Although formaldehyde and glutaraldehyde were found to be efficient for enhancing such properties, their toxicity must pose the problem of the aldehyde residues remaining in final applications, i.e. food [2] and biomedical [3]. In contrast to these treatments,  $\gamma$ -irradiation could be an alternative method for crosslinking proteins [4].

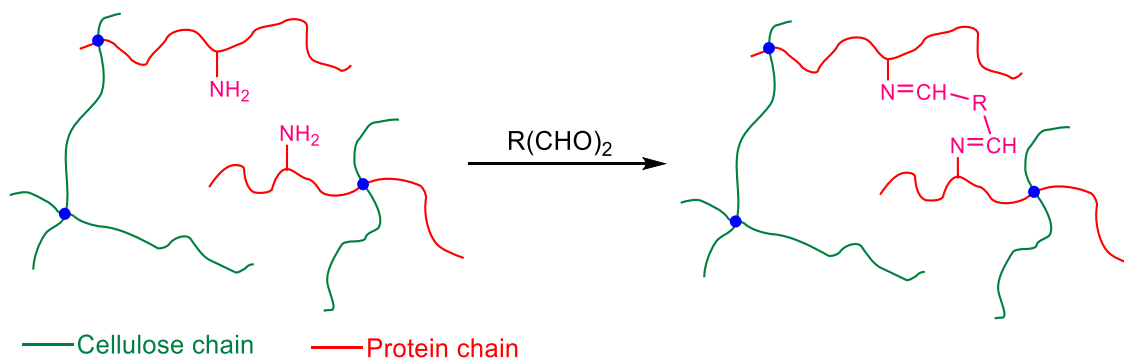


**Figure 6.1.** Illustrated crosslinking of protein network to form network structure via dialdehyde mediated interchain crosslinking (redrawn and modified) [1]

Yidan Zhu [5], in Dr. Kotek's research group, continued the research of Douglass to improve the functional properties of cellulose/soy protein concentrate (SPC) films. Even though expected results from crosslinking the films were achieved in terms of the stability of

the films in water and the mechanical properties, the appearance and size of the films were severely affected.

### **6.1.1 Gamma ( $\gamma$ )–Irradiation**

Gamma-irradiation alters the conformation of proteins, oxidize the amino acids, disrupt the covalent bonds and generate protein free radicals. Crosslinking, aggregation, fragmentation, and oxidation by oxygen radicals formed in the radiolysis of water are confirmed chemical changes in irradiated proteins. In a film forming solution, the irradiation activates  $\text{OH}^-$  and  $\text{O}_2^-$  radicals that could react with molecules of proteins. As a result, covalent cross-linkages are formed in the solution causing functional and structural changes in proteinic films [6-9].

Exposure to radiation was a useful way of creating crosslinks in edible films from soy, casein and whey proteins. Their protein structure was moderately altered to a more stable and more ordered form [10]. Ouattara et al. [11] reported that gamma-irradiation increased the concentration of milk proteins with high molecular weight in the film forming solution. The authors also suggested two hypotheses to explain the effect of the irradiation: (1) more amino acids from proteins with different physicochemical properties participate in intermolecular interactions (2) covalent crosslinks in and between the polymer chains are formed in the film forming solution.

Lee et al. studied the effect of  $\gamma$ -irradiation on SPI. Irradiation doses up to 50 kGy were applied to the film forming solution of SPI. The water vapor permeability of resulting films decreased about 10% at 4 kGy dose and the tensile strength was doubled at 50 kGy [9]. Xu et al. [12] added starch solution into SPI solution both of which were modified with similar  $\gamma$ -irradiation doses. The water absorption capacity of the resulting blend films decreased almost

linearly with increasing irradiation doses. It was concluded that the viscosity of blend solution did not decrease more above 30 kGy due to crosslinking of the proteins/starch and aggregation of the polypeptide chains. This resulted in an increase in water resistance and tensile strength and a surface that was more glossy and smoother.

The effect of gamma-irradiation on cellulose is of interest in our research since the blends that will be produced are all cellulose-based. The irradiation on the polymer generates cellulosic substrates by degradation [13]. While high doses degraded cellulose thereby decreasing the DP and the crystallinity, crosslinking was observed at low doses of radiation ( $10 < \text{kGy}$ ) [14]. At any extent, this could highly affect the structure and the reactivity and thus the physical and chemical properties [15]. As a result, properties, such as low elasticity, low wet strength, low adhesive capacity to some materials, and low shape stability, can be improved [14].

The objective of this study is to prepare blend biofilms from cellulose and globular proteins, particularly soy protein, by utilizing gamma irradiation to stabilize the resulting films. The treatment at various doses is applied to the film forming solution that contains the both polymers at the same composition. The physicochemical properties of the films will be analyzed and compared in order to understand the effect of the gamma radiation. The blend biofilms that are produced by solution casting method can be used for food packaging and biomedical applications.

## **6.2 Materials**

The amine/salt system is composed of 65 wt% ethylenediamine (ED) and 35 wt% potassium thiocyanate (KSCN), both are reagent grade and purchased from Sigma-Aldrich. KSCN was first dried overnight in a vacuum oven at  $60^{\circ}\text{C}$  to remove excess moisture. A known

weight of that was slowly added into the corresponding weight of ED while mixing. Then, the mixture of ED and KSCN were stirred by slightly heating until the salt was completely dissolved. Finally, the solvent was left to cool and to equilibrate.

Cellulose was received from Buckeye Technologies Inc. as sheets of dissolving wood pulp that was an acetate grade, pressed, refined and bleached. The sheets were shredded in a grinder forming cellulose crumbs. The obtained cellulose was coded as Buckeye VFC cellulose by the company and it has a DP of ca. 400. Soy protein isolate (PRO-FAM 955<sup>®</sup>) containing 93.8% dry basis protein was provided by ADM Specialty Products-Oilseeds. Table 2.1 provides the details about the protein. Prior to dissolution, the cellulose and the soy protein (SPI) were dried overnight in a vacuum oven at 60°C to eliminate undesired moisture.

Methanol used as a coagulant was ACS reagent grade and provided by BDH Industries Ltd. The tools for film casting were polyester transparent PET films, Teflon films, a glass casting board, and a stainless steel bar with 5 – 50 mil casting thickness that were all obtained from Byk-Gardner.

### **6.3 Preparation of Film Forming Solution**

3.6 g of ground cellulose, 2.4 g of SPI, and 94 g of ED/KSCN were all added into a three-necked round bottom flask to obtain a solution with 40% protein content. The center neck of the flask held a glass stirring rod with a Teflon<sup>®</sup> blade inside the flask. The other ending of the glass rod was attached to an electric motor for stirring. One of the side necks was attached to a water-cooled condenser with nitrogen flowing inside to prevent the evaporation of ED from the solvent. The other side neck was simply plugged with a glass stopper.

The flask was kept in an oil bath at 90°C and the cellulose-SPI-ED/KSCN mixture was stirred for 2 – 3 hrs until complete dissolution. The obtained blend solution was allowed to

cool down to room temperature, and then heated back to the same temperature to transfer into a glass jar. A total of four jars of solution were prepared for exposing to gamma radiation.

#### **6.4 Gamma Irradiation**

The jars were placed in the  $^{60}\text{Co}$  gamma radiation chamber of Nuclear Engineering Department in our University. The blend solution in four jars was irradiated at the doses from 5 – 20 kGy with a 5 kGy increment. The dose rate was 0.71 kGy/day and the irradiation was performed at ambient conditions.

#### **6.5 Film Casting**

Each jar with the irradiated solution was heated to ensure a steady flow. A little irradiated solution was poured onto a PET film that was held on a glass casting board. Then, the solution was dragged by using the casting bar with 25 mil casting thickness to obtain gel sheets, a form of film prior to coagulation. These sheets handled with the PET films were immediately transferred into a methanol bath. The coagulation of the sheets could be observed within several seconds turning into wet films.

The wet films were kept in the first coagulation bath for at least 15 min. Subsequently, they were soaked into a fresh coagulation bath for no less than 20 min. This coagulation step was repeated 3 times total to remove all residues of the ED/KSCN solvent. After the last coagulation bath, the films were stacked and separated by Teflon films between two flat rectangular glasses. A brick was placed on top applying an even pressure to obtain uniform films. This stack of films with the applied pressure were left to dry in a vacuum oven for 24 hrs at ambient temperature. Two additional days of drying between 40 and 50°C was also applied producing completely dry and uniform films. The resulting films were coded as CS0,

CS5, CS10, CS15, CS20. The numbers in the codes represent the radiation doses to which the film forming solutions were exposed.

## **6.6 Characterization Techniques**

Fourier transform infrared spectroscopy (FTIR) of all films was measured with a Thermo Electron Nexus 470 FTIR with OMNIC software analysis. FTIR spectrum of each film was obtained between 4000 and 500  $\text{cm}^{-1}$  wavenumbers in absorbance mode over 64 scans at the resolution of 4  $\text{cm}^{-1}$ . The obtained raw data was plotted using OriginPro 9.1, an analysis and graphing software.

For accurate tensile data, we opted to test 5 films from each composition. To condition the films, they were left overnight in the testing facility. The thickness of each film to be tested was measured 10 times with the Thwing-Albert Electronic Thickness Tester. Following this, each individual film was cut into 4 strips with the same width (1/2 inch) and taped on both ends 5 cm apart. This produced 20 strips for each composition, resulting in a total of 100 strips to be tested.

The tensile testing was carried out using the MTS Q-test Tensile Testing Machine and performed in accordance with ASTM D882: Tensile Testing of Thin Plastic Sheeting. Testing used the 250 lb. load cell, 50 mm gauge length, and 10 mm/min initial speed.

Thermo-gravimetric analysis (TGA) was utilized to study the changes of mass of the investigated polymer systems against increasing temperature. It was performed on the Perkin Elmer TGA under a dynamic nitrogen atmosphere at a heating rate of 20°C/min from 20°C to 550°C using ca. 5 mg samples of each material. Post analysis was performed using the raw data on Origin 8.5, a data analysis and graphing software.

Light transmission test was performed on a Varian Cary 3 UV-Vis Spectrophotometer between the wavelength of 360 and 700 nm. A small area of each film was secured onto the wall of the sample holder. Transparency was assessed from the light transmitted through the films relative to air.

Water absorption capacity of the films were examined to determine the amount of water absorbed over a 24 h period. Each film was pre-weighed, soaked in deionized water for 24 h, and then weighed again to calculate the increase of mass in percentage.

## **6.7 Results and Discussion**

### **6.7.1 Chemical structure**

The blend films from irradiated solutions exhibited similar absorption peaks to the control film. Figure 6.2 represents the FTIR spectra of all films in the wavenumber range of 3750–2750  $\text{cm}^{-1}$  and 1750–750  $\text{cm}^{-1}$ . The stretching vibration of hydroxyl groups (OH) at 3370  $\text{cm}^{-1}$  was predominant for all films. The peaks at 1649 and 1543  $\text{cm}^{-1}$  for the control film indicated on the spectrum are amide I (C=O stretching) and amide II (N–H bending) bands, respectively. Although there is no shift occurred for the amide I peak, its intensity gradually decreased by increasing irradiation dose. In addition, the amide II band shifted to higher wavenumber due to the gamma irradiation. Both changes of amide peaks are a result of the reorganization of the interaction between the two polymers, the blend solution of which were exposed to the irradiation.

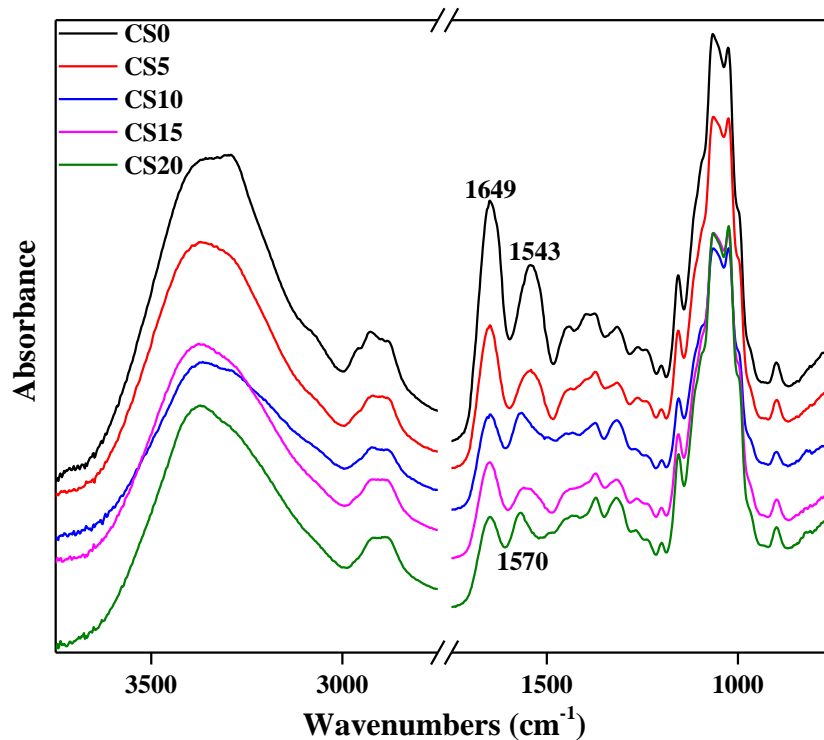


**Figure 6.2.** FTIR spectra of all blend films

### 6.7.2 Thermal properties

Figure 6.3 shows the percent weight changes of the irradiated blend films by increasing temperature. The maximum degradation temperature of non-irradiated films somewhat decreased by increasing irradiation dose. Although it was not significant, the thermal stability of the films was influenced by the film forming solution exposed to gamma radiation. Unlike chemical crosslinking, this result is expected from  $\gamma$ -irradiation, which causes polymer degradation.

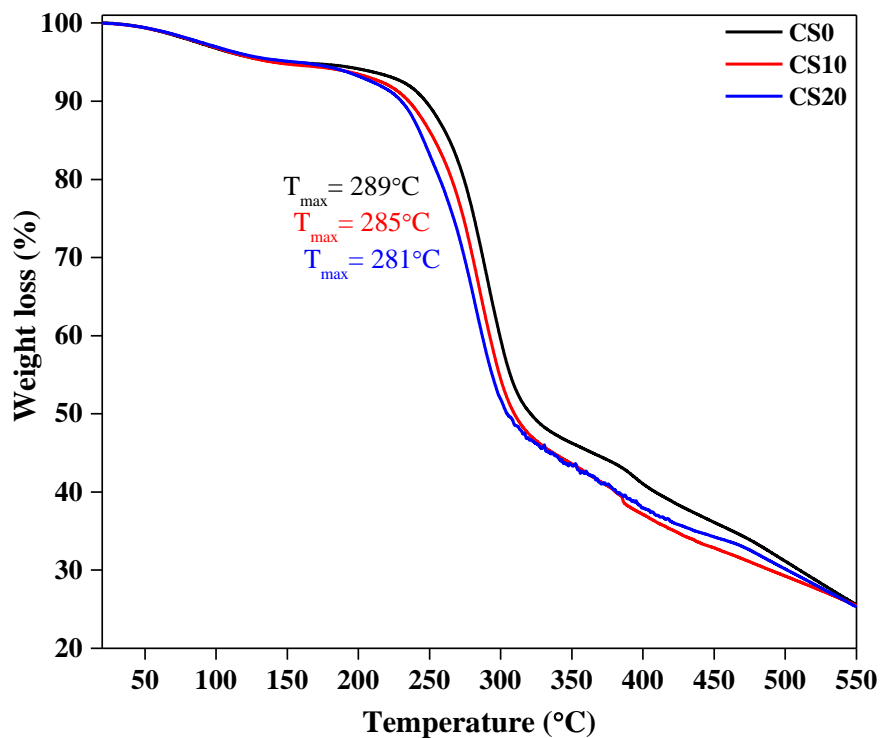


**Figure 6.3.** TGA thermograms of the films from irradiated control solutions

### 6.7.3 Tensile properties

The thicknesses of blend films were not significantly different from each other as the same casting thickness was applied to every film forming solution. The tensile properties of blend films shown in Table 6.1 had diverse changes for each parameter upon increasing the irradiation dose.

**Table 6.1.** The tensile properties of all films

Films	Modulus (GPa)	Tensile strength (MPa)	Elongation (%)	Thickness (mm)
CS0	2.86 ± 0.23	55.7 ± 7.8	14.5 ± 8.5	0.028 ± 0.001
CS5	2.91 ± 0.27	56.2 ± 6.9	20.6 ± 7.2	0.028 ± 0.002
CS10	2.46 ± 0.26	56.4 ± 6.9	25.9 ± 7.4	0.027 ± 0.003
CS15	2.93 ± 0.23	49.8 ± 5.9	11.9 ± 7.5	0.027 ± 0.002
CS20	2.12 ± 0.14	34.2 ± 3.9	13.7 ± 7.1	0.033 ± 0.001

The effect of gamma irradiation dose on tensile strength and the elongation at break is demonstrated by Figure 6.4, which is a plot of the data from Table 6.1. As indicated in the figure, the tensile strength showed a very subtle increase whereas the percent elongation almost doubled at 10 kGy dose. According to Pruzinec et al. [14], crosslinking was observed below such dose for cellulose thus improving the elasticity of the film network. The protein in the same network also participated in the crosslinking. As already mentioned, the irradiation yields polymer radicals in proteins that can associate with two hydrogen atoms. It is likely that alkyl radicals in the irradiated blend solution reacted with one another through hydrogen-bonding crosslinks. They could also interact with the free radicals of the end of polymer chain to form terminal-crosslinks [12]. Hypothetically, more amino acids participating in intermolecular interactions [11] with cellulose contributed to the increase in both the tensile strength and the percent elongation. Furthermore, above 10 kGy doses, the films lost significant strength and elasticity as expected due to the degradation of cellulose.

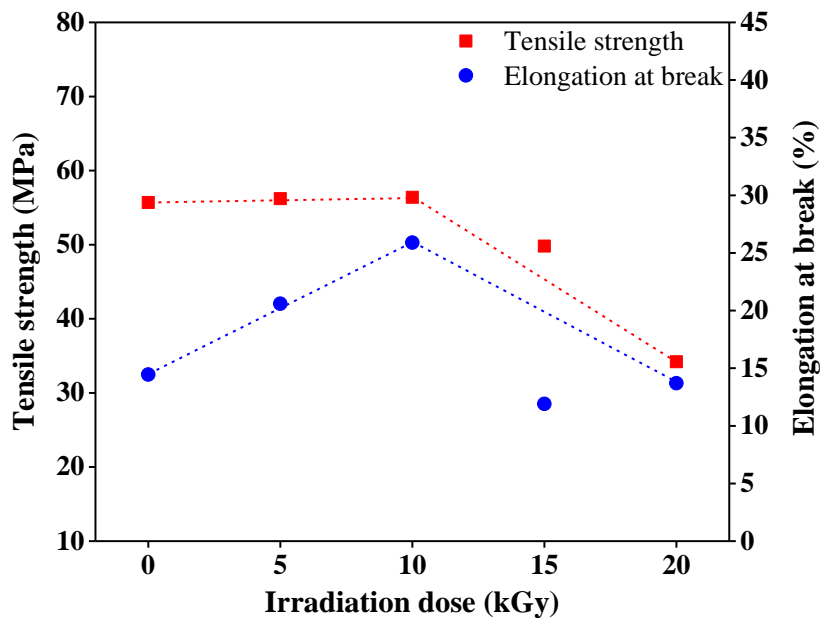


**Figure 6.4.** Effect of  $\gamma$ -radiation dose on tensile strength and elongation of the blend film with 40% SPI

### 6.7.4 Transparency

The light transmission provides information about the transparency of the films in the visible light spectrum from 400–700 nm wavelength. As plotted in Figure 6.5, the transmission decreases with a decreasing wavelength.

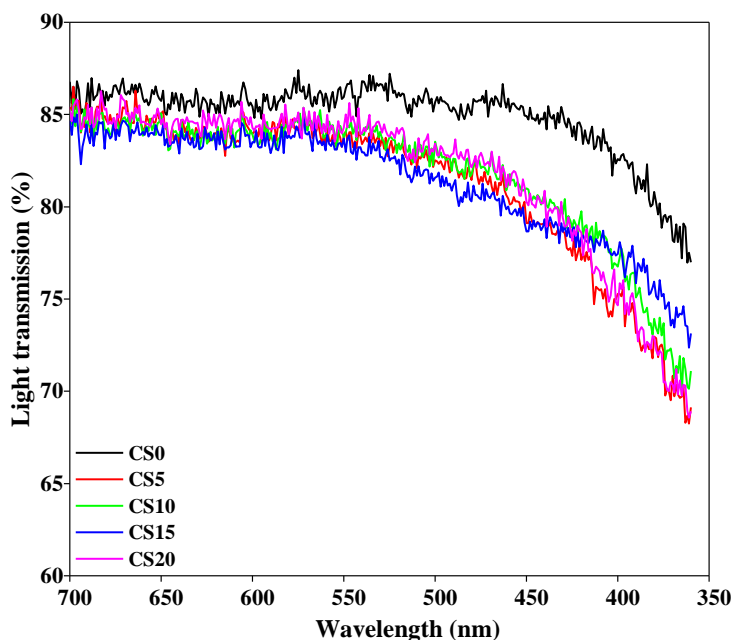


**Figure 6.5.** Effect of  $\gamma$ -irradiation on the light transmission of the blend film

The control film had around 87% light transmission at 700 nm and remained about the same through 500 nm. On the other hand, the gamma irradiation treated samples were clearly showed a lower light transmission for the same region. Therefore, the visibly observed transparency change was also confirmed by the light transmission indicating the effect of irradiation.

### 6.7.5 Water absorption

Figure 6.6 illustrates the changes in water absorption capacity of the film by increasing irradiation dose. The control cellulose film absorbed about 62% water that dropped to 46% after exposing to 10 kGy dose of irradiation indicating certain degree of crosslinking between

the cellulose and soy protein isolate. Increasing the irradiation dose above that point did not show significant influence in the capacity.

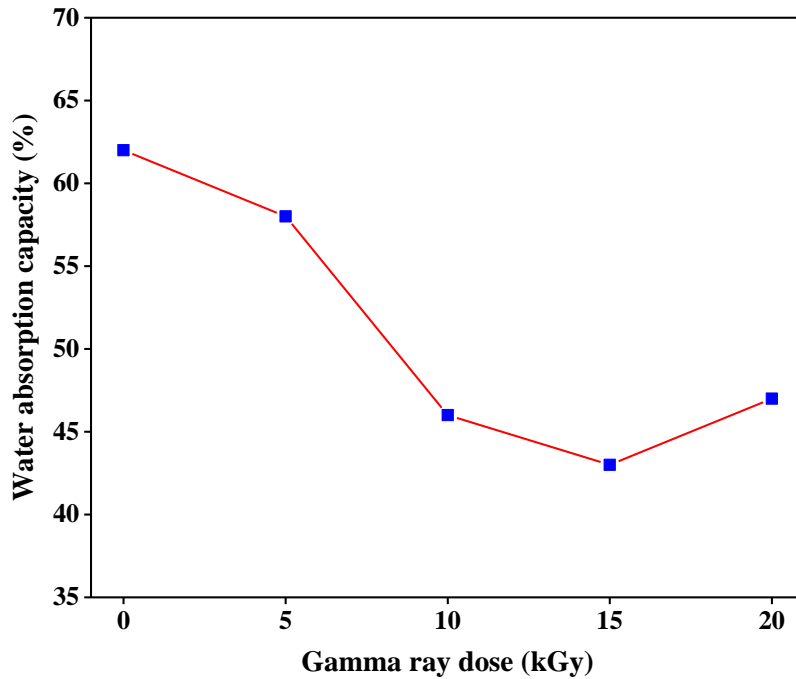


**Figure 6.6.** Influence of  $\gamma$ -irradiation on the water absorption capacity of the blend film

The chemical crosslinking with glutaraldehyde also resulted in reduced water absorption capacity for cellulose/soy protein concentrate films [5]. Furthermore, Xu et al. [12] reported gradual decrease in the water absorption by increasing irradiation dose for SPI-based films.

## 6.8 Conclusions

Uniform and strong cellulose/soy protein isolate films were produced using the ED/KSCN solvent system. Gamma irradiation was applied to the film forming solutions to stabilize the molecular network structure of the blend films. The interaction between cellulose and soy protein, exhibited by FTIR spectra, was rearranged after exposure to the irradiation. The TGA analysis revealed insignificant changes in the thermal stability. The irradiation up to

10 kGy led to higher elongation at in the resulting film. Moreover, the transparency of the film somewhat decreased. However, the water absorption capacity significantly decreased.

## 6.9 References

1. Song Y, Zheng Q (2014) Ecomaterials Based on Food Proteins and Polysaccharides. *Polymer Reviews* 54 (3):514-571.
2. Gord H, Hammer KD, Neeff R, Berghof K, Eilers M, Taeger E, Buerger H (2004) Chewable film containing cellulose. US Patent 20040166209, 26 Aug 2004
3. Buerger H, Taeger E, Eilers M, Berghof K (2004) Protein shaped body and method for the production thereof according to the NMMO method. US Patent 20040046277, 11 Mar 2004
4. Bourtoom T (2009) Edible protein films: properties enhancement. *International Food Research Journal* 16 (1):1-9
5. Zhu Y (2012) The Development of Membranes Made with Blends of Soy Protein and Other Natural Biopolymers using a Novel Solvent System and Stabilized with Glutaraldehyde. North Carolina State University, Raleigh, NC
6. Schuessler H, Schilling K (1984) Oxygen Effect in the Radiolysis of Proteins: Part 2 Bovine Serum Albumin. *International Journal of Radiation Biology* 45 (3):267-281.
7. Cheftel JC, Cuq JL, Lorient D (1985) Amino acids, peptides, and proteins. In: Fennema OR (ed) *Food chemistry*, vol 2. Marcel Dekker, New York, pp 245-369
8. Garrison WM (1987) Reaction mechanisms in the radiolysis of peptides, polypeptides, and proteins. *Chemical Reviews* 87 (2):381-398.
9. Lee M, Lee S, Song KB (2005) Effect of  $\gamma$ -irradiation on the physicochemical properties of soy protein isolate films. *Radiation Physics and Chemistry* 72 (1):35-40.

10. Lacroix M, Le TC, Ouattara B, Yu H, Letendre M, Sabato SF, Mateescu MA, Patterson G (2002) Use of  $\gamma$ -irradiation to produce films from whey, casein and soya proteins: structure and functional characteristics. *Radiation Physics and Chemistry* 63 (3–6):827-832.
11. Ouattara B, Canh LT, Vachon C, Mateescu MA, Lacroix M (2002) Use of  $\gamma$ -irradiation cross-linking to improve the water vapor permeability and the chemical stability of milk protein films. *Radiation Physics and Chemistry* 63 (3–6):821-825.
12. Xu W, Liu B, Yang H, Liu K, Jia S, Chen F (2014) Effect of  $\gamma$ -irradiation on the physicochemical properties of mixed soy protein isolate/starch material. *African Journal of Biotechnology* 11 (28):7238-7246
13. Krässig HA (1993) *Cellulose: Structure, Accessibility, and Reactivity*. Gordon and Breach Science,
14. Pruzinec J, Kadlecik J, Varga S, Pivovarnicek F (1981) Study of the effects of high-energy radiation on cellulose. *Radiochemical and Radioanalytical Letters* 49 (6):395-404
15. Ciechańska D, Wesołowska E, Wawro D (2009) An introduction to cellulose fibres. In: Eichhorn SJ, Hearle JWS, Jaffe M, Kikutani T (eds) *Handbook of textile fibre structure*, vol 2. Woodhead Publishing, Cambridge, England, pp 3-61